



Government of **Western Australia**  
Department of **Mines, Industry Regulation and Safety**

RECORD 2018/2

# GSWA 2018 EXTENDED ABSTRACTS

## Promoting the prospectivity of Western Australia



Geological Survey of Western Australia



Government of **Western Australia**  
Department of **Mines, Industry Regulation and Safety**

**Record 2018/2**

# **GSWA 2018 EXTENDED ABSTRACTS**

## **Promoting the prospectivity of Western Australia**

**February 2018**

**Perth 2018**



**Geological Survey of  
Western Australia**

**MINISTER FOR MINES AND PETROLEUM**  
**Hon Bill Johnston MLA**

**DIRECTOR GENERAL, DEPARTMENT OF MINES, INDUSTRY REGULATION AND SAFETY**  
**David Smith**

**EXECUTIVE DIRECTOR, GEOSCIENCE AND RESOURCE STRATEGY**  
**Jeff Haworth**

#### REFERENCE

**The recommended reference for this publication is:**

- (a) For reference to an individual contribution:  
Smithies, RH, Lu, Y-J, Gessner, K, Ivanic, TJ, Wyche, S, Lowrey, JR, Morris, PA and Champion, DC 2018, New approaches in understanding the Yilgarn Craton, *in* GSWA 2018 extended abstracts: Geological Survey of Western Australia, Record 2018/2, p. 1–3.
- (b) For reference to the publication:  
Geological Survey of Western Australia 2018, GSWA 2018 extended abstracts: promoting the prospectivity of Western Australia: Geological Survey of Western Australia, Record 2018/2, 49p.

ISBN 978-1-74168-805-4 (print); 978-1-74168-804-7 (PDF)

#### Disclaimer

This product was produced using information from various sources. The Department of Mines, Industry Regulation and Safety (DMIRS) and the State cannot guarantee the accuracy, currency or completeness of the information. Neither the department nor the State of Western Australia nor any employee or agent of the department shall be responsible or liable for any loss, damage or injury arising from the use of or reliance on any information, data or advice (including incomplete, out of date, incorrect, inaccurate or misleading information, data or advice) expressed or implied in, or coming from, this publication or incorporated into it by reference, by any person whatsoever.



**Published 2018 by the Geological Survey of Western Australia**

This Record is published in digital format (PDF) and is available online at <[www.dmp.wa.gov.au/GSWApublications](http://www.dmp.wa.gov.au/GSWApublications)>.



© State of Western Australia (Department of Mines, Industry Regulation and Safety) 2018

With the exception of the Western Australian Coat of Arms and other logos, and where otherwise noted, these data are provided under a Creative Commons Attribution 4.0 International Licence. (<http://creativecommons.org/licenses/by/4.0/legalcode>)

**Further details of geological products and maps produced by the Geological Survey of Western Australia are available from:**

Information Centre  
Department of Mines and Petroleum  
100 Plain Street  
EAST PERTH WESTERN AUSTRALIA 6004  
Telephone: +61 8 9222 3459 Facsimile: +61 8 9222 3444  
[www.dmp.wa.gov.au/GSWApublications](http://www.dmp.wa.gov.au/GSWApublications)

**Cover image:** Elongate salt lake on the Yilgarn Craton — part of the Moore–Monger paleovalley — here viewed from the top of Wownaminia Hill, 20 km southeast of Yalgoo, Murchison Goldfields. Photograph by I Zibra for the Geological Survey of Western Australia.



## GSWA 2018 program — 23 February 2018, Fremantle

**8.15 – 8.45**     **REGISTRATION**

**8.45 – 9.00**     Welcome and opening remarks

Hon Bill Johnston MLA,  
Minister for Mines and Petroleum

### **SESSION 1**     *Chair: Charlotte Hall*

**9.00 – 9.35**     New approaches in understanding the Yilgarn Craton



Hugh Smithies

**9.35 – 10.00**     The tectono-magmatic evolution of the Yilgarn orogen: in search of a model

Ivan Zibra

### *Morning tea 10.00 – 11.00*

### **SESSION 2**     *Chair: Jeff Haworth*

**11.00 – 11.25**     De Grey Superbasin and Fortescue Basin in the Pilbara: can they be compared with the Witwatersrand Basin?

Ian Tyler

**11.25 – 11.50**     Focusing on the Fortescue and Hamersley Basins



Heather Howard

**11.50 – 12.15**     Zircon composition as a fertility indicator of Archean granites



Yongjun Lu

### *Lunch 12.15 – 1.35*

### **SESSION 3**     *Chair: Don Flint*

**1.35 – 2.00**     Putting the horse in front of the cart: why exploration geoscience needs drilling

Professor David Giles  
University of South Australia

**2.00 – 2.25**     Compatibility of ground and airborne gravity data in the Western Australia 'Generation 2' reconnaissance gravity mapping project



David Howard

**2.25 – 2.50**     Looking beneath the Canning Basin: new insights from geochronology, seismic and potential-field data



Peter Haines

### *Afternoon tea 2.50 – 3.15*

### **SESSION 4**     *Chair: Ian Tyler*

**3.15 – 3.40**     Western Australia: a battery metal powerhouse

Trevor Beardsmore

**3.40 – 4.05**     Provenance fingerprinting of gold nuggets from the Kurnalpi Goldfield

Lena Hancock

**4.05 – 4.30**     Diamond prospectivity of Western Australia: a major synthesis and review



Don Flint

### *Sundowner 4.30 – 5.30*





## Contents

New approaches in understanding the Yilgarn Craton .....	1
<i>by RH Smithies, Y-J Lu, K Gessner, TJ Ivanic, S Wyche, JR Lowrey, PA Morris and DC Champion</i>	
The tectono-magmatic evolution of the Yilgarn Orogen: in search of a model.....	4
<i>by I Zibra</i>	
De Grey Superbasin and Fortescue Basin in the Pilbara: can they be compared with the Witerwatersrand Basin? .....	8
<i>by IM Tyler, RH Smithies and MTD Wingate</i>	
Focusing on the Fortescue and Hamersley Basins .....	14
<i>by HM Howard and DMcB Martin</i>	
Zircon composition as a fertility indicator of Archean granites .....	18
<i>by Y-J Lu, RH Smithies, MTD Wingate, NJ Evans, PA Morris, DC Champion and TC McCuaig</i>	
Putting the horse in front of the cart: why exploration geoscience needs drilling .....	24
<i>by D Giles</i>	
Compatibility of ground and airborne gravity data in the Western Australia ‘Generation 2’ reconnaissance gravity mapping project .....	27
<i>by SHD Howard</i>	
Looking beneath the Canning Basin: new insights from geochronology, seismic and potential-field data.....	30
<i>by PW Haines, MTD Wingate, Y Zhan and DW Maidment</i>	
Western Australia: a battery metal powerhouse .....	34
<i>by TJ Beardsmore</i>	
Provenance fingerprinting of gold nuggets from the Kurnalpi Goldfield .....	40
<i>by EA Hancock and TJ Beardsmore</i>	
Diamond prospectivity of Western Australia: a major synthesis and review.....	44
<i>by MT Hutchison and DJ Flint</i>	





# New approaches in understanding the Yilgarn Craton

by

RH Smithies, Y-J Lu, K Gessner, TJ Ivanic, S Wyche, JR Lowrey<sup>1</sup>, PA Morris and DC Champion<sup>2</sup>

The integration of ongoing detailed surface mapping with continuously expanding and increasingly refined geophysical, geochemical and geochronological datasets allows us to test and expand our understanding of how the lithospheric architecture of the Yilgarn Craton has evolved. Future work by the Geological Survey of Western Australia (GSWA) will continue to update and improve detailed surface mapping with the aim of a craton-wide 1:100 000 scale interpreted bedrock map, but will increasingly concentrate on the collection and interpretation of datasets that allow us to map lithospheric volumes through time. Two recent projects utilizing current whole-rock geochemical datasets to provide new insights into the geological evolution of the craton are discussed. The recently initiated ‘greenstone geochemical barcoding’ project is also described. This project promises to provide a significant aid to mineral explorers throughout the Eastern Goldfields Superterrane (EGST) by developing geochemically well-constrained volcanic stratigraphies for all greenstone belts.

## Two distinct origins for Archean greenstone belts

Opinion is divided on whether Archean greenstones reflect plume or subduction tectonics. One approach to assessing any potential role of subduction processes in greenstone evolution has been to compare the geochemistry of basaltic and intermediate rocks in greenstone belts to geochemical proxies of modern subduction processes. Whereas many such proxies identify a ‘crustal’ signature in the bulk source of many Archean magmas, they cannot uniquely identify whether crustal components were added to a mantle source region prior to melting, or were later acquired by mantle-derived magmas during their emplacement within the crust. The Th/Yb vs Nb/Yb plot of Pearce (2008) offers a simple diagnostic means of interpreting how mantle-derived magmas and crust may have interacted. Using ~2200 high-quality,

stratigraphically and geographically constrained analyses, the Th/Yb vs Nb/Yb plot (Fig. 1) shows that individual volcanic sequences of the Yilgarn Craton evolved through one of two distinct processes reflecting different modes of crust–mantle interaction. The BIF-rich, komatiite-poor, volcanic stratigraphy of the 2.99 – 2.71 Ga Youanmi Terrane, and of rare pre-2.73 Ga stratigraphic components of the EGST, evolved through processes leading to Th/Yb vs Nb/Yb trends with a narrow range of Th/Nb (‘constant-Th/Nb’ greenstones). In contrast, the younger, more widespread 2.71 – 2.66 Ga volcanic stratigraphy of the EGST evolved through processes leading to Th/Yb vs Nb/Yb trends showing a continuous range in Th/Nb (‘variable-Th/Nb’ greenstones).

Constant-Th/Nb greenstones are very rare worldwide, and may reflect derivation from a mantle source already with a high and constant Th/Nb ratio. This, and a lithological association including boninite-like lavas and calc-alkaline andesites, all within a narrow Th/Nb range, resembles compositions typical of modern-style subduction settings. The similarities between the Youanmi greenstones and the older greenstone components of the EGST suggest a once continuous terrain.

Variable-Th/Nb trends dominate greenstone sequences in Australia and worldwide. These greenstones are typically accompanied in the early stages by komatiite. They are also temporally associated with peaks in granite magmatism. The increasing Th/Nb in basaltic rock (Fig. 1) correlates with decreasing  $\epsilon_{\text{Nd}}$ , reflecting variable amounts of crustal assimilation during emplacement of mantle-derived magmas. Their Th/Nb trends are very difficult to reconcile with modern-style subduction processes, but strong links with komatiite probably implicates plume tectonics. The simplest interpretation of these data is that the EGST developed as plume-related rift over existing granite–greenstone crust — in this case the Youanmi Terrane. A corollary is that the dominant north-northwest structural trend of the Yilgarn Craton might not be relevant to pre-2.71 Ga crustal evolution.

The scarcity of constant-Th/Nb trends suggests either that processes forming them never dominated Archean greenstone evolution, or that such greenstones simply were rarely preserved. Formation of granite promotes crustal preservation and so Youanmi greenstones were probably only preserved because of the 2.71 Ga ‘EGST event’.

<sup>1</sup> School of Geosciences, The University of Sydney, NSW 2006, Australia

<sup>2</sup> Geoscience Australia, GPO Box 378, Canberra, ACT 2601, Australia

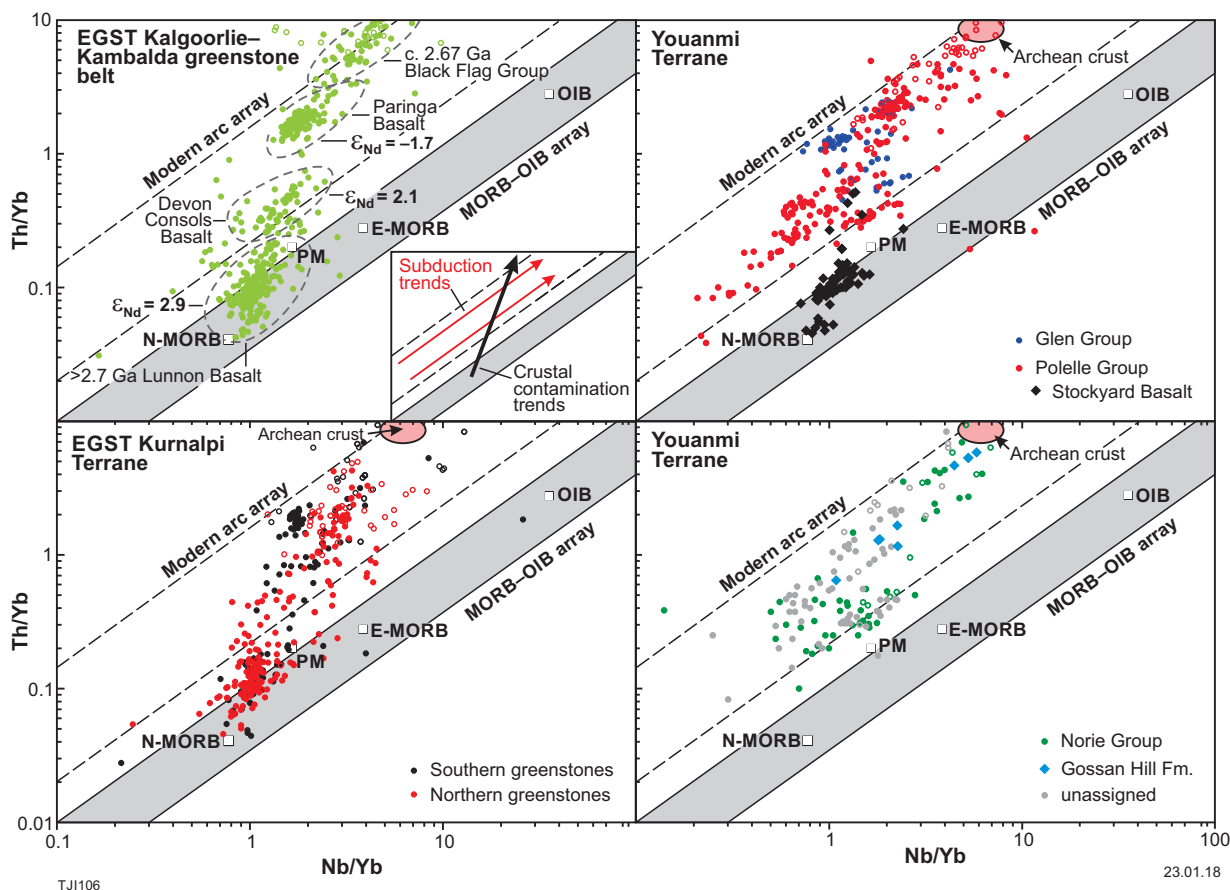


**Figure 1.** The Th/Yb vs Nb/Yb plot of Pearce (2008). Values for various mantle reservoirs are from Sun and McDonough (1989) and the field for Archean crust encompasses Archean felsic average from Pearce (2008) and average Yilgarn Craton granite. Inset in the top, left-hand diagram shows compositional vectors expected for magma series derived from a subduction-enriched mantle source (red arrows), or from contamination of a magma derived from an unmodified mantle source (as in the case of MORB) that subsequently undergoes variable degrees of contamination (assimilation) by crust with a composition typical of average Archean felsic crust (black arrow)

## Imaging the southwest Yilgarn basement through granite geochemistry

A new dataset of ~250 new whole-rock geochemical analyses of granitic rocks has been compiled to better constrain the geological evolution of the poorly understood South West Terrane. Of particular interest was the insight these data might provide into the origins of a lower-crustal density anomaly (Fig. 2) that follows the southern and western margins of the South West Terrane, and which has been attributed to eclogite residuum from Archean crustal differentiation. In addition, these data are used to test the (craton-wide) assumption that basement terranes (i.e. granite source regions) parallel the late north-northwest structural trend of the Yilgarn Craton.

The dataset has been simplified into three groups. Group 1 comprises granitic rocks of dominantly high-Ca composition, with low  $K_2O/Na_2O$  (average 0.6) and high Sr, Sr/Y, La/Yb and Nb/Ta, reflecting true high-Al TTG derived through high-pressure melting of a sodic, mafic source. Group 2 comprises high- and low-Ca granitic rocks, with a wide compositional range but generally higher  $K_2O/Na_2O$  (average 1.0), and lower Sr, Sr/Y,

La/Yb and Nb/Ta, reflecting lower-pressure melting of a less homogeneous source. Group 3 also comprises high- and low-Ca granitic rocks (dominantly low-Ca). Their compositions are mainly similar to group 2 but lie within the upper range of group 2 in terms of  $K_2O/Na_2O$  (average 1.16) and La/Yb, and within the lower range in terms of Sr and Sr/Y. However, they have distinctly higher Nb/Ta and typically higher Dy/Yb, perhaps reflecting melting, over a range of pressures, of an inhomogeneous, hornblende-rich source that locally included high-Al TTG components from which high La/Yb and Nb/Ta signals were inherited.

Extraction of felsic magma, leaving a dense crustal residuum of garnet-rich, or eclogitic, mineralogy imparts distinctively high Sr/Y, La/Yb and Nb/Ta characteristics on those magmas. Variation in such melting-pressure proxies shows no spatial relationship with the high density (gravity) anomaly identified in the lower crust of the southern and western parts of the region (Fig. 2). This anomaly does not appear to be directly related to Archean felsic magmatism, but more likely relates to the Proterozoic evolution of the craton margin.

In addition, the geographical distribution of the three granite groups defines northeast trends (Fig. 2) that truncate the north-northwest trends that characterize

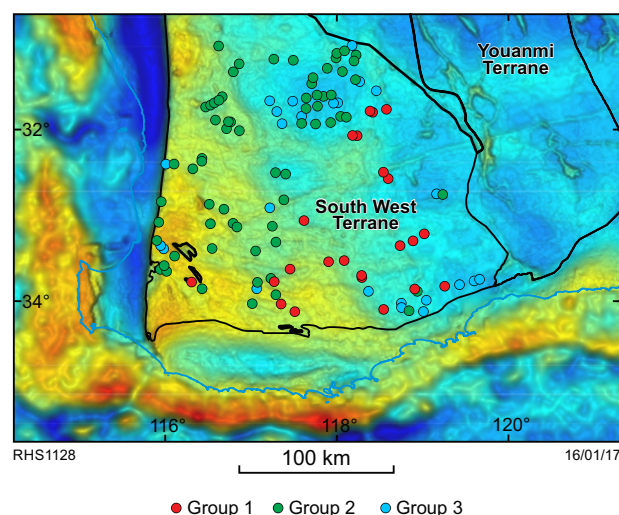


**Figure 2.** Gravity image of the southwestern part of the Yilgarn Craton showing the distribution of new granite samples

the more obvious structural trend of the Yilgarn Craton, including terrane boundaries. The northeast trends in granite composition potentially reflect similar trends in basement source domains; i.e. northeast-trending belts of either compositionally distinct crust or of crust undergoing melting at specific conditions, or both. Preliminary data further suggest that these northeasterly basement trends may extend across the entire craton. The idea that the Yilgarn Craton evolved through processes leading to northeast domain trends that were later overprinted by (intracratonic?) north-northwest trends perhaps deserves further consideration.

## Greenstone geochemical barcoding project

Establishing a stratigraphy is the most fundamental step in geological understanding. In a region of poor outcrop that stubbornly resists yielding any helpful information, geochemistry is well suited in terms of constraining stratigraphy. The greenstone geochemical barcoding project was designed to add geochemical credence to the EGST lithostratigraphy and 1:100 000 scale interpreted bedrock mapping projects, and will ultimately provide a detailed geochemical characterization of individual greenstone sequences throughout the EGST.

A relatively simple, basalt–komatiite–basalt–basalt–felsic-volcanic or volcanoclastic stratigraphy has long been recognized within the Kalgoorlie Terrane of the EGST, but equally well established is that the detail within that stratigraphy is often poorly known, extremely complex, and highly variable within and between individual greenstone belts. Moreover, the long-recognized <2.72 Ga stratigraphy does not take into account the local existence of older greenstone stratigraphies (i.e. basement). Nor is it clear if any of the Kalgoorlie Terrane stratigraphy is relevant to the east, in the adjoining Kurnalpi Terrane, except, perhaps, for a common c. 2.71 Ga komatiite event marker.

Hence, in a craton where geological context is often particularly difficult to establish, and where limited drillcore or rock-chip intervals might provide the only samples, the geochemical barcoding project aims to determine to what extent stratigraphic correlation can be established both within and between greenstone belts. In particular, this project aims to establish geochemical protocols or proxies that will allow the matching of limited stratigraphic intervals against an established chemical stratigraphy for any particular area.

The success of this project depends on the collection of high-quality major and trace element whole-rock geochemical data from a very large number of representative samples from all regions where a volcanic stratigraphy can already be established or reasonably inferred. The amount of existing, publicly available, high-quality whole-rock geochemical data from EGST greenstones is remarkably low. Over the past year, the amount of available data has almost doubled, through the addition of a further ~1800 new analyses, mainly from diamond drillcore samples of greenstones in the region between Kalgoorlie and Norseman. All samples have been analysed using a common analytical approach at a single laboratory to ensure internal consistency of data. The success of this project critically depends on the willingness of companies to provide access to stratigraphic drillcore.

## References

- Pearce, J 2008, Geochemical fingerprinting of oceanic basalts with applications to ophiolite classification and the search for Archean oceanic crust: *Lithos*, v. 100, p. 14–48.
- Sun, S-S and McDonough, WF 1989, Chemical and isotopic systematics of oceanic basalts: implications for mantle compositions and processes, in *Magmatism in ocean basins edited by AD Saunders and MJ Norry*: Geological Society London, Special Publications, v. 42, p. 313–345.



# The tectono-magmatic evolution of the Yilgarn orogen: in search of a model

by

I Zibra

Secular changes in fundamental physical parameters, such as mantle temperature and density (Labrosse and Jaupart, 2007), imply that the mechanical behaviour of the continental lithosphere has changed through time. Since the geological record becomes progressively more fragmented as we go back in time, there is a general lack of consensus about Archean geodynamics (van Hunen and Moyen, 2012). Moreover, given that the association of granites with volcano-sedimentary supracrustal sequences has no clear Phanerozoic counterparts, the tectonic setting of Archean granite–greenstone terranes is highly debated (Bédard, 2010). The two end-member processes that have been proposed for Archean tectonics are generally referred to as ‘horizontal tectonism’ and ‘vertical tectonism’, reflecting the view that Archean geodynamics was dominated by uniformitarian (i.e. plate tectonics-like) or non-uniformitarian processes, respectively (e.g. Van Kranendonk et al., 2004). Although some plate tectonic features (such as subduction–accretion) probably occurred sporadically in the Mesoarchean geological record (e.g. Smithies et al., 2005), several lines of evidence indicate that the transition from episodic–overturn/stagnant-lid regime (a form of vertical tectonism) to modern-style plate tectonics occurred progressively throughout Neoproterozoic times. The Neoproterozoic transition in global geodynamics primarily reflects a significant increase in recycling of crustal material into the mantle, and is therefore interpreted as evidence for the widespread occurrence of complete Wilson cycles.

The Neoproterozoic Yilgarn orogen of Western Australia (Fig. 1; Zibra et al., 2017a) contains many typical traits of ancient-type orogens, such as negligible topography and the occurrence of long-lasting and widespread synorogenic magmatism (Van Kranendonk et al., 2013), features that are generally thought characteristic of hot Precambrian orogens. However, the Yilgarn orogen contains regional-scale synorogenic clastic deposits (Figs 1b, 2) that developed during major tectonic episodes of crustal shortening, at the onset of the orogeny (Zibra et al., 2017a), and the late-orogenic, orogen-wide transpressional event associated with the exhumation of high-grade greenstones (Zibra et al., 2017b). These features imply that the Neoproterozoic Yilgarn orogenic lithosphere was stiff enough to allow tectonic processes analogous to those that dominate modern-style orogenic belts, such as strain localization, development of significant regional topography and, consequently, focused erosion. Such tectonic styles might represent an intermediate stage between Archean-type and modern-type orogens.

The bulk east–west horizontal shortening recorded during most of the tectonic evolution of the Yilgarn Orogen is commonly ascribed to a series of accretion episodes that led to amalgamation of the Eastern Goldfields Superterrane (EGST), and the Narryer and South West Terranes, onto an older foreland represented by the Youanmi Terrane (Myers, 1995; Wilde et al., 1996; Krapež and Barley, 2008). The Ida Fault is regarded as the suture between the EGST and the Youanmi Terrane (Myers, 1995), a scenario that is consistent with the existence of a 2736–2724 Ma volcanic arc setting now preserved in the hangingwall of the Ida Fault (de Joux et al., 2014), together with the occurrence of high-grade greenstones along this major structure (Zibra et al., 2017b). Alternatively, the various terranes could have once been part of a Mesoarchean ‘proto-Yilgarn’ continent, subsequently rifted into a series of ribbon continents during possible extensional events within the 2960–2750 Ma time slice, and in turn amalgamated again by inversion tectonics during the Neoproterozoic Yilgarn Orogeny (autochthonous models; Czarnota et al., 2010; Pawley et al., 2012; Van Kranendonk et al., 2013). Autochthonous models mainly hinge on the geochronological and isotopic evidence of broadly contemporaneous crust-forming events throughout the various terranes from at least c. 3100 Ma (Wyche et al., 2012; Mole et al., 2015). However, given that the Precambrian Earth recorded a series of global tectono-magmatic events, broadly contemporaneous crust-forming events would also be expected if the terranes now assembled into the Yilgarn Craton were not in physical contact. In summary, available datasets allow for both end-member geodynamic models (accretion of an allochthonous EGST or inversion of an autochthonous ensialic rift) and both models may account for the tectono-magmatic and sedimentary evolution of the Yilgarn continent. Thus, many of the fundamental questions about Archean tectonics that have been raised since the 1970s (e.g. van Hunen and Moyen, 2012) remain unanswered.

Recent structural work has documented that several of the transpressional, crustal-scale shear zones exposed in the Yilgarn Craton accommodated the synorogenic emplacement of syntectonic plutons (Zibra et al., 2014). Shearing along these major structures was intimately connected with the development of syntectonic clastic deposits and with exhumation of high-grade greenstones along the Ida Fault (Zibra et al., 2017b). Structural and geochronological evidence indicate that each episode of pluton emplacement induced a deformation event that

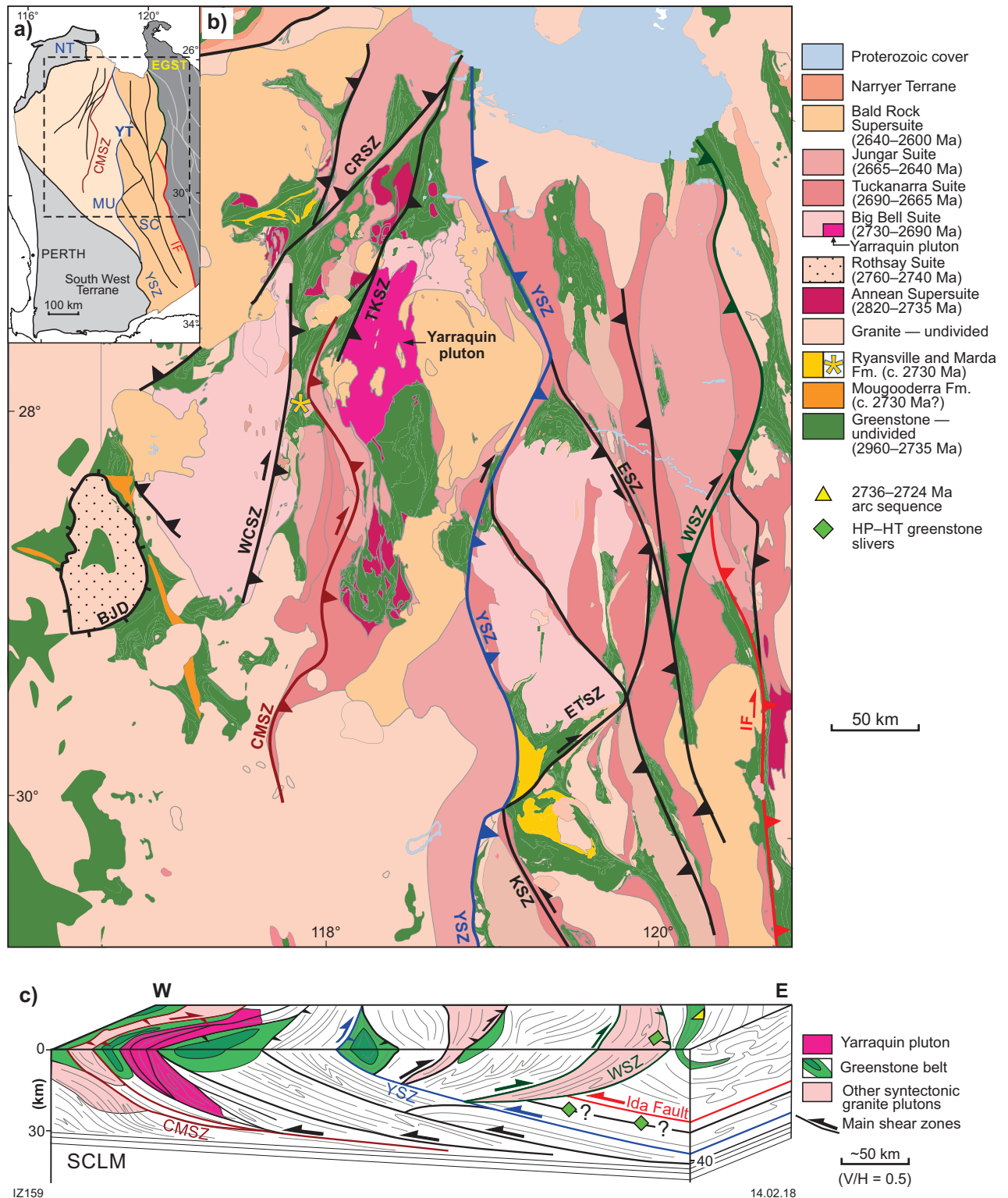


**Figure 1.** a) Simplified map of the main geological subdivisions and shear zones of the western portion of the Yilgarn Craton, showing the main terranes and the network of craton-scale shear zones. EGST, Eastern Goldfields Superterrane; NT, Narryer Terrane. In the western half of the craton, the Youanmi Terrane (YT) is subdivided into Murchison (MU) and Southern Cross (SC) domains. Main shear zones are colour-coded: IF, Ida Fault; YSZ, Youanmi Shear Zone; CMSZ, Cundimurra Shear Zone. Rectangle shows the location of (b); b) interpreted geological map of the central portion of the Youanmi Terrane. Abbreviations for the shear zones not shown in (a): CRSZ, Chunderloo Shear Zone; ESZ, Edale Shear Zone; ETSZ, Evanston Shear Zone; KSZ, Koolyanobbing Shear Zone; TKSZ, Tuckabianna Shear Zone; WSZ, Waroonga Shear Zone; WCSZ, Wattle Creek Shear Zone; BJD, Badja Decollement. Location of HP–HT greenstone slivers and the 2736–2724 Ma arc sequence are from (Zibra et al., 2017b) and de Joux et al. (2014), respectively; c) block diagram summarizing the crustal architecture of the western portion of the Yilgarn Craton, as reconstructed by merging the results of seismic traverses. The Moho discontinuity and the highly reflective middle to lower crust overlie a seismically transparent subcontinental lithospheric mantle (SCLM)

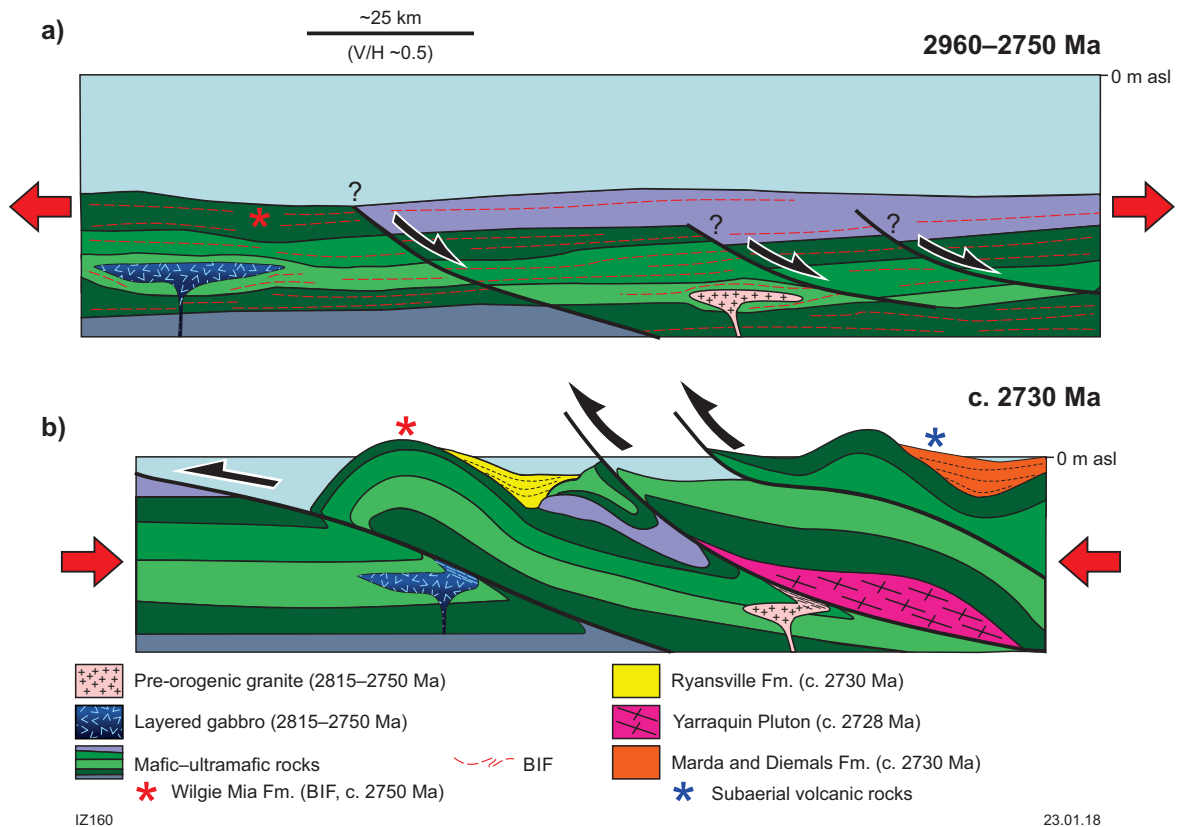


**Figure 2.** Cartoon outlining the pre- to early-orogenic evolution of the western part of the Yilgarn orogen: a) 2960–2750 Ma accumulation of a thick greenstone pile dominated by mafic-ultramafic volcanic rocks interlayered with BIF, the latter devoid of any clastic input. It is likely that events of lithospheric extension during this period were accommodated by large-scale shear zones with normal kinematics; b) at c. 2730 Ma, the onset of the Neoarchean orogeny is marked by shearing along large-scale, E-dipping contractional structures, exhumation of the 2960–2750 Ma succession to subaerial conditions, and proximal, high-energy sedimentary basins developed above a regional unconformity. At the same time, the Yarraquin pluton was emplaced along part of the wide network of east-dipping, contractional shear zones

was mostly localized within the pluton itself and within the crustal-scale channel that allowed its emplacement, leaving only a minor structural signature in the adjacent areas. The overall orogenic cycle produced adjacent high-strain belts showing comparable geometry and kinematics, but whose ages span from c. 2730 to 2660 Ma, covering most of the duration of the Neoarchean Yilgarn Orogeny. These results indicate that the concept of regional deformation in Archean granite-greenstone systems needs to be reassessed.

One way to investigate the tectonic evolution of the Yilgarn Orogen is to compare the tectono-magmatic evolution of the two main terranes juxtaposed by the Ida Fault. This approach focuses on two historically contentious issues: 1) the nature of the greenstone basement (oceanic vs continental?), and 2) the significance of terrane boundaries (sutures vs intracontinental weaknesses?). A synthesis of recently published work and in-progress data indicates that greenstones belonging to both the Youanmi Terrane and the EGST developed on older sialic crust, and therefore the nature of the Archean

oceanic crust remains elusive. In fact, the 2820–2800 Ma time slice is characterized, in the Youanmi Terrane, by the development of a thick greenstone sequence developed in a distal, deep-marine environment, far from any detrital source. This sequence developed above >3000 Ma felsic basement that, at the currently exposed crustal level, is now preserved only as an isotopic signature, and as detrital and inherited zircons in younger granitic and sedimentary rocks (Wyche et al., 2012). At the same time, in the western portion of the EGST, the Kalgoorlie Terrane records the development of a >300 km-wide segment of granitic crust that later became the basement of the 2730–2660 Ma komatiite-bearing greenstone sequence that characterizes this terrane. Overall, the available data suggest that the Ida Fault represents a long-lived structure that accommodated large displacements during the orogeny, juxtaposing crustal domains characterized by contrasting pre- and syn-orogenic tectono-magmatic evolution. Data discussed here have significant implications for our understanding of Archean orogenic processes.



## References

- Bédard, JH 2010, Falsification of the plate tectonic hypothesis for genesis of Archaean volcanic and plutonic rocks, and an outline of possible alternative mechanisms, *in* Yilgarn–Superior workshop — Abstracts edited by IM Tyler and CM Knox-Robinson: Geological Survey of Western Australia; Fifth International Archean symposium, Perth, 5 September 2010; Record 2010/18, p. 151–152.
- Czarnota, K, Champion, DC, Cassidy, KF, Goscombe, B, Blewett, R, Henson, PA and Groenewald, PB 2010, Geodynamics of the eastern Yilgarn Craton: *Precambrian Research*, v. 183, p. 175–202.
- de Joux, A, Thordarson, T, Fitton, JG and Hastie, AR 2014, The Cosmos greenstone succession, Agnew–Wiluna greenstone belt, Yilgarn craton, Western Australia: Geochemistry of an enriched Neoarchaeal volcanic arc succession: *Lithos*, v. 205, p. 148–167.
- Krapež, B and Barley, ME 2008, Late Archaean synorogenic basins of the Eastern Goldfields Superterrane, Yilgarn Craton, Western Australia: Part III. Signatures of tectonic escape in an arc–continent collision zone: *Precambrian Research*, v. 161, no. 1–2, p. 183–199.
- Labrosse, S and Jaupart, C 2007, Thermal evolution of the Earth: secular changes and fluctuations of plate characteristics: *Earth and Planetary Science Letters*, v. 260, p. 465–481.
- Mole, DR, Fiorentini, ML, Cassidy, KF, Thébaud, N, McCuaig, TC, Doublier, MP, Duuring, P, Romano, SS, Maas, R, Belousova, EA, Barnes, SJ and Miller, J 2015, Crustal evolution, intra-cratonic architecture and the metallogeny of an Archaean craton: Geological Society, London, Special Publications, v. 393, p. 23–80.
- Myers, JS 1995, The generation and assembly of an Archaean supercontinent: evidence from the Yilgarn Craton, Western Australia, *in* Early Precambrian processes edited by MP Coward and AC Reis: Geological Society, London, Special Publications, v. 95, p. 143–154.
- Pawley, MJ, Wingate, MTD, Kirkland, CL, Wyche, S, Hall, CE, Romano, SS and Doublier, MP 2012, Adding pieces to the puzzle: episodic crustal growth and a new terrane in the northeast Yilgarn Craton, Western Australia: *Australian Journal of Earth Sciences*, v. 59, no. 5, p. 603–623, doi:10.1080.08120099.2012.696555.
- Smithies, RH, Champion, DC, Van Kranendonk, MJ, Howard, HM and Hickman, AH 2005, Modern-style subduction processes in the Mesoarchaeal: geochemical evidence from the 3.12 Ga Whundo intra-oceanic arc: *Earth and Planetary Science Letters*, v. 231, no. 3–4, p. 221–237.
- van Hunen, J and Moyen, J-F 2012, Archean subduction: Fact or fiction?: *Annual Review of Earth and Planetary Sciences*, v. 40, p. 195–219.
- Van Kranendonk, MJ, Collins, WJ, Hickman, AH and Pawley, MJ 2004, Critical tests of vertical vs horizontal tectonic models for the Archean East Pilbara Granite–Greenstone Terrane, Pilbara Craton, Western Australia: *Precambrian Research*, v. 131, p. 173–211.
- Van Kranendonk, MJ, Ivanic, TJ, Wingate, MTD, Kirkland, CL and Wyche, S 2013, Long-lived, autochthonous development of the Archean Murchison Domain, and implications for Yilgarn Craton tectonics: *Precambrian Research*, v. 229, p. 49–92.
- Wilde, SA, Middleton, MF and Evans, BJ 1996, Terrane accretion in the southwestern Yilgarn Craton: evidence from a deep seismic crustal profile: *Precambrian Research*, v. 78, p. 179–196.
- Wyche, S, Fiorentini, M, Miller, JL and McCuaig, TC 2012, Geology and controls on mineralisation in the Eastern Goldfields region, Yilgarn Craton, Western Australia: *Episodes*, v. 35, no. 1, p. 273–282.
- Zibra, I, Clos, F, Weinberg, RF and Peternell, M 2017a, The c. 2730 Ma onset of the Neoarchean Yilgarn Orogeny: *Tectonics*, v. 36, p. 1787–1813, doi:10.1002/2017TC004562.
- Zibra, I, Korhonen, FJ, Peternell, M, Weinberg, RF, Romano, SS, Braga, R, De Paoli, MC and Roberts, M 2017b, On thrusting, regional unconformities and exhumation of high-grade greenstones in Neoarchean orogens. The case of the Waroonga Shear Zone, Yilgarn Craton: *Tectonophysics*, v. 712–713, p. 362–395, doi:10.1016/j.tecto.2017.05.017.
- Zibra, I, Smithies, RH, Wingate, MTD and Kirkland, CL 2014, Incremental pluton emplacement during inclined transpression: *Tectonophysics*, v. 623, p. 100–122, doi:10.1016/j.tecto.2014.03.020.

# De Grey Superbasin and Fortescue Basin in the Pilbara: can they be compared with the Witwatersrand Basin?

by

IM Tyler, RH Smithies and MTD Wingate

## Introduction

In July 2017, Artemis Resources, in Joint Venture with Canadian explorer Novo Resources Corp., reported the discovery of an 11 m thick gold nugget-bearing conglomerate extending for 8 km at the base of the Mount Roe Basalt at Purdy's Reward in the northwest Pilbara (Fig. 1; Artemis Resources, 2017a). Artemis subsequently reported the discovery of gold in conglomerate at Mount Oscar 20 km to the northeast, giving rise to the current 'Pilbara gold rush' (Artemis Resources, 2017b). Considerable publicity was generated in September 2017 by a video cross from Purdy's Reward live to the Denver Gold Forum (Artemis Resources, 2017c). There are now numerous explorers and prospectors investigating the base of the Fortescue Group across the Pilbara (including De Grey Mining Ltd, Coziron Resources Ltd, Calidus Resources Ltd, and Venturex Resources Ltd, among others).

The discoveries have reignited speculation that an equivalent of the highly mineralized Mesoarchean to Neoarchean (3075–2715 Ma) Witwatersrand Basin in South Africa can be found in the Pilbara Craton. This is consistent with the concept of an Archean 'Vaalbara' continent that may have included both the Kaapvaal Craton, on which the Witwatersrand Basin sits, and the Pilbara Craton (e.g. Cheney, 1996; Zegers et al., 1998; Wingate, 1998; de Kock et al., 2009, 2012).

## De Grey Superbasin and Central Pilbara Tectonic Zone

Any reconstruction of Vaalbara, attempting to match depositional units and settings, mineralized horizons, structures and tectonic settings in the Witwatersrand Basin (e.g. Robb and Meyer, 1995; Manzi et al., 2013; Tucker et al., 2016), must take account of the well-known geology of the Pilbara Craton and the Fortescue and Hamersley Basins (e.g. Huston et al., 2000; Smithies et al., 1999, 2001; Thorne and Trendall, 2001; Hickman, 2016). The Geological Survey of Western Australia (GSWA), collaborating with Geoscience Australia, published extensive 1:100 000-scale mapping, accompanied by new SHRIMP U–Pb zircon geochronology and geochemistry, during comprehensive remapping of the Pilbara in the 1990s and early 2000s (Hickman et al., 2006, 2010; Van Kranendonk et al., 2006; Hickman and Van Kranendonk, 2012; Hickman, 2016).

During the Mesoarchean, the northwestern part of the Pilbara Craton (Fig. 1) evolved through a plate tectonic cycle of subduction, accretion and collision, leading to cratonization at c. 2900 Ma. The De Grey Superbasin represents extension and subsidence following collision of the 3270–3120 Ma West Pilbara Superterrane with the older (3525–3225 Ma) granite–greenstones of the East Pilbara Terrane during the 3070–3060 Ma Prinsep Orogeny (Fig. 2). The superbasin includes the c. 3020 Ma Gorge Creek Basin, the c. 3010 Ma Whim Creek Basin, the 2970–2940 Ma Mallina Basin and the c. 2930 Ma Mosquito Creek Basin. The Gorge Creek, Whim Creek and Mallina Basins overlie a regional unconformity and form part of the Central Pilbara Tectonic Zone. The Sholl Shear Zone is a crustal-scale structure that was active during deposition within the superbasin, and represents reactivation of a suture.

The Sholl Shear Zone (Fig. 1) may have provided the pathway for volcanism and related gold mineralization sourced from underlying subduction-modified mantle (Smithies et al. 2004, 2007). At the Mount Oscar prospect, gold-bearing conglomerates (Artemis Resources, 2017b) are interlayered with basalt and are part of the geochemically distinctive Warrambie Basalt of the c. 3010 Ma Whim Creek Group (Smithies et al., 1999; Hickman, 2002; Figs 1, 2). Deposition of the conglomerates and a subsequent 230 million year history of basin formation, volcanism, metamorphism, fluid flow, and folding and faulting were driven by movements on the adjacent shear zone (Hickman, 2016). This may represent one source for gold reworked into conglomerates in the unconformably overlying Fortescue Basin.

## Fortescue Basin

The 2775–2630 Ma Fortescue Basin was the subject of a major regional study by Thorne and Trendall (2001). It overlies a craton-wide regional unconformity and represents a rift, deepening to the south. Deposition of the Fortescue Group into this rift began with dominantly subaerial continental flood basalts and associated fluvial and lacustrine sedimentary rocks (Bellary Formation, Mount Roe Basalt, Hardey Formation; Fig. 3). Post-cratonization erosion produced a rugged landscape with up to 500 m of relief (Fig. 4). Small, high-grade, lenticular, gold-bearing conglomerates are present at the basal Fortescue Group unconformity as poorly sorted, channel-fill deposits such as at the Just-in-Time gold mine near

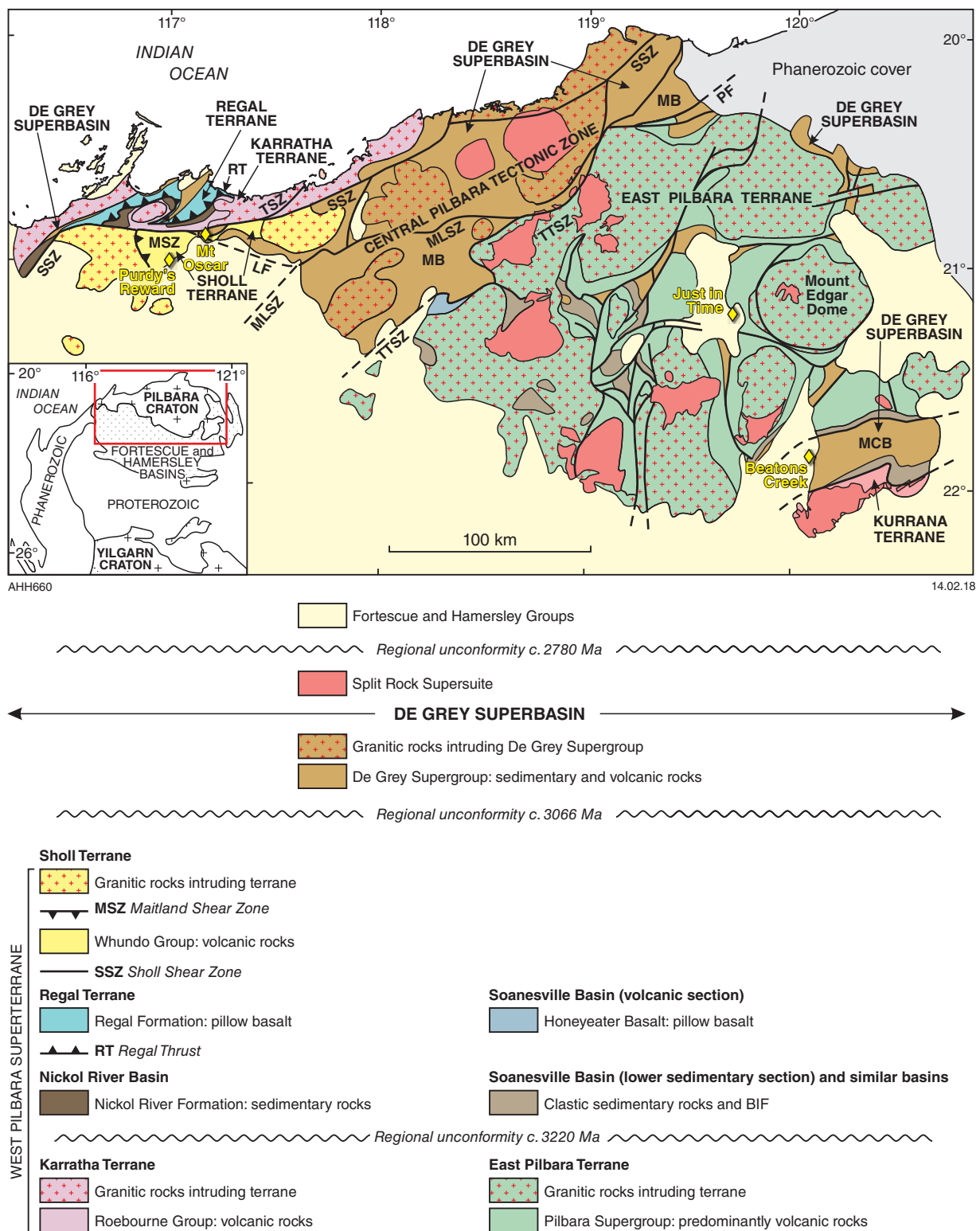


**Figure 1.** Major tectonic units of the northern Pilbara Craton (after Hickman 2016). Abbreviations: LF, Loudens Fault; MB, Mallina Basin; MCB, Mosquito Creek Basin; MLSZ, Mallina Shear Zone; MSZ, Maitland Shear Zone; PF, Pardoo Fault (part of TTSZ); SSZ, Sholl Shear Zone; TSZ, Terenar Shear Zone; TTSZ, Tappa Tappa Shear Zone



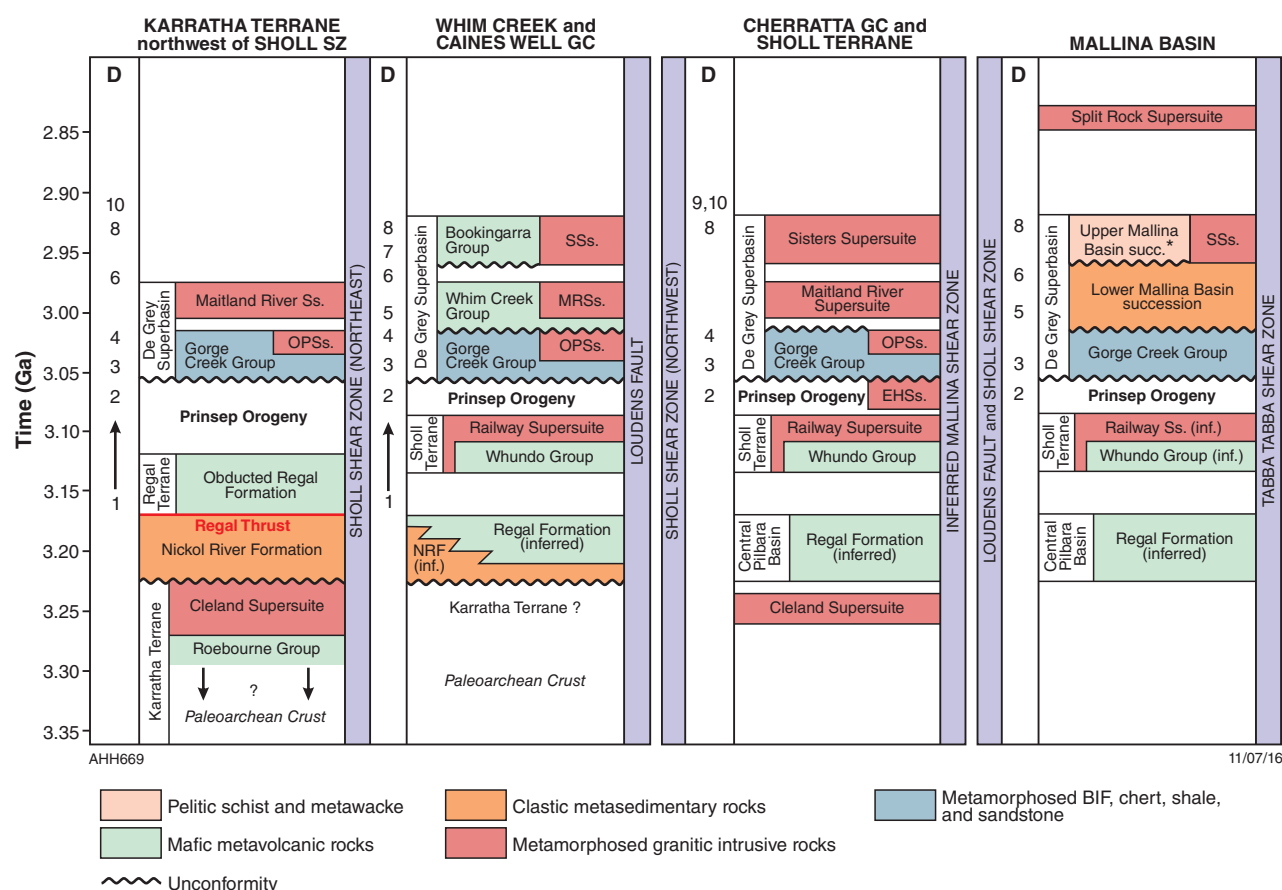


**Figure 2.** Time-space plot summarizing the stratigraphy and structural history of the four major fault-bounded terranes and basins of the northwest Pilbara Craton (from Hickman, 2016). Differences indicate significant strike-slip displacements along the major faults and regional variability of granitic intrusion, volcanism, and sedimentation following the Prinsep Orogeny (i.e. within the De Grey Superbasin). Abbreviations: GC, Granitic Complex; Ss, Supersuite; EHSs, Elizabeth Hill Supersuite; OPSs, Orpheus Supersuite; MRSs, Maitland River Supersuite; SSs, Sisters Supersuite; D, deformation event; SZ, shear zone (\* = succession)

Marble Bar (Fig. 1). In the 1980s CRA drilled eight deep holes through the Fortescue Group testing a Witwatersrand model. These cores are held in the GSWA core library.

## Discussion

The Witwatersrand Basin includes the 3086–3074 Ma Dominion Group, with the unconformably overlying Witwatersrand Supergroup comprising the lower 2970–2914 Ma West Rand Group and the upper 2894–2780 Ma Central Rand Group (Fig. 5; Robb and Meyer, 1995; de Kock, 2012; Tucker et al., 2016). Although the De Grey Superbasin in the Pilbara is a time equivalent of the lower part of the Witwatersrand Basin, there appears to be little direct correlation between the two, possibly reflecting different geodynamic histories and tectonic settings. There is no equivalent of the Prinsop Orogeny in the Kaapvaal Craton, and no equivalent of the Gorge

Creek or Whim Creek Basins. The West Rand Group may be the time equivalent of the Mallina Basin but there appears to be no equivalent in the Pilbara Craton of the Central Rand Group, which contains the vast majority of the gold deposits in the Witswatersrand Basin.

The base of the Fortescue Group and the base of the Klipriviersberg Group (Ventersdorp Supergroup) both occur at a post-cratonization unconformity at a similar time (c. 2780 Ma; Wingate, 1998; de Kock, 2009, 2012), compatible with the idea of the Vaalbara continent and with the potential for the continuation of the Ventersdorp Contact Reef onto the Pilbara Craton. But, again, the sedimentary environments appear to represent different settings and there is no evidence as yet that the conglomerate-hosted gold deposits at the base of the Fortescue Basin on the Pilbara are anything other than localized channel-fill deposits.

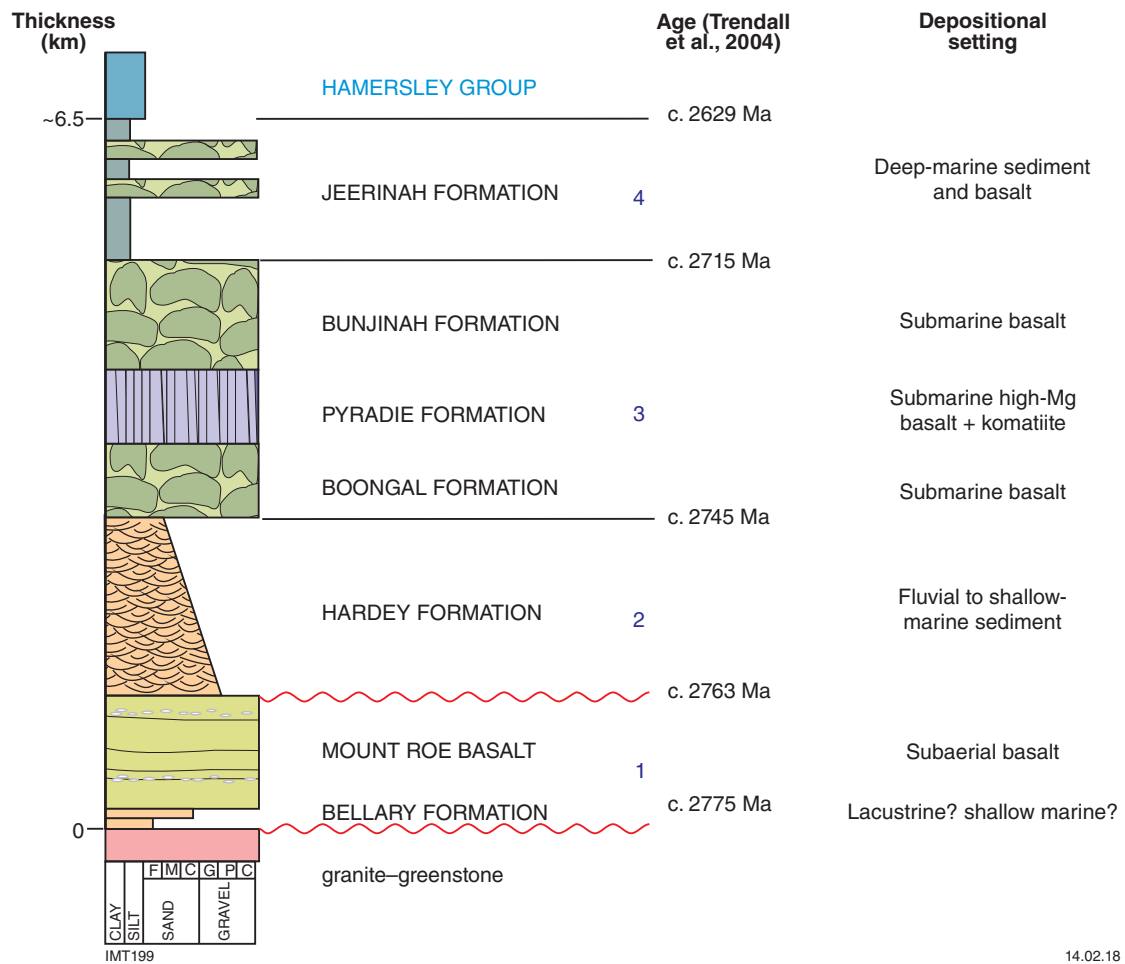


Figure 3. Stratigraphy of southern Fortescue Group (from Thorne et al., 2011)

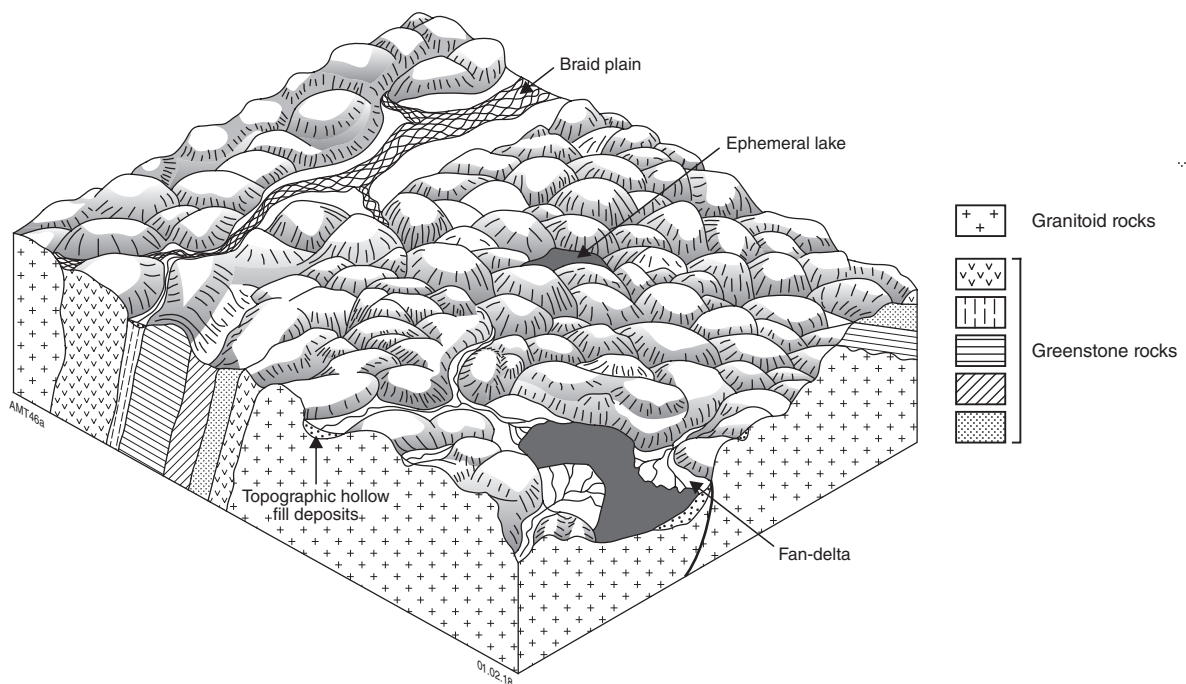


Figure 4. Depositional model for the pre-Mount Roe Basalt sedimentary units of the Fortescue Group (from Thorne and Trendall, 2001)

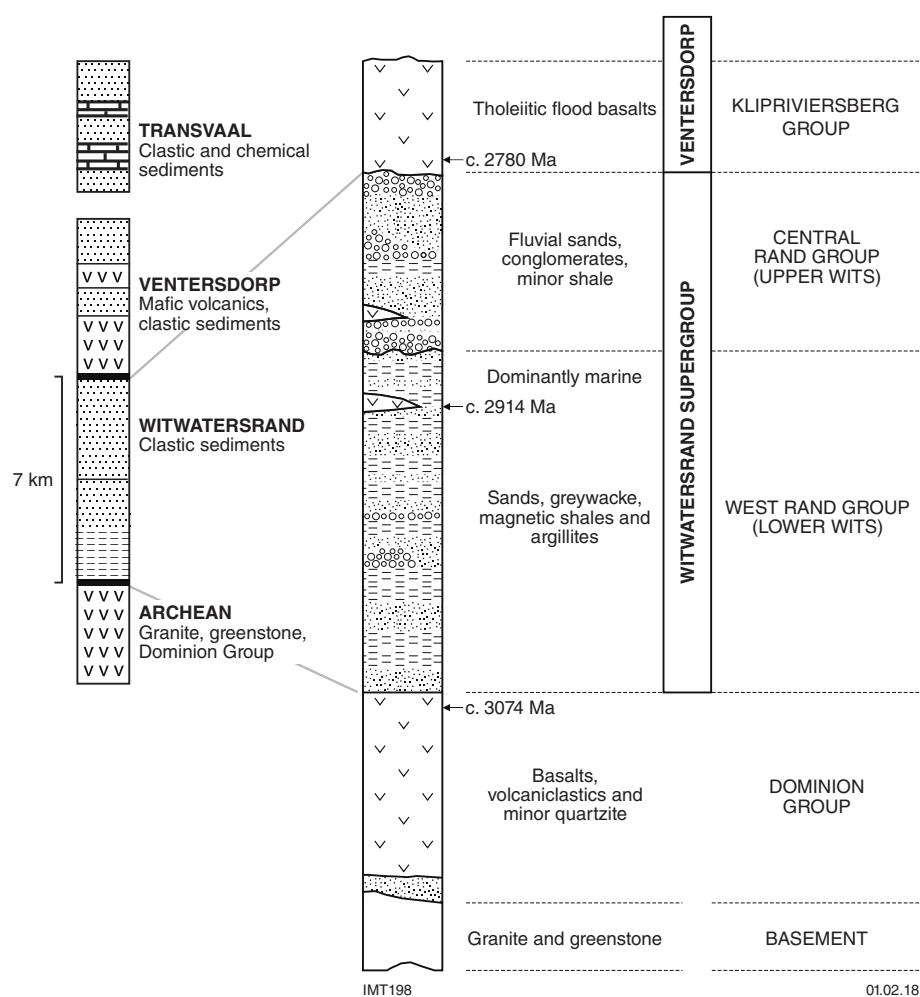


Figure 5. Stratigraphy of the Witwatersrand Basin (modified from Phillips and Powell, 2015)

## References

- Artemis Resources 2017a, Gold nuggets recovered from first bulk sample at Purdey's Reward JV with Novo Resources: Artemis Resources ASX/Media Announcement, 13 July 2017.
- Artemis Resources 2017b, 14 km of new gold-bearing conglomerate discovered at 100% owned Mt Oscar Wits gold project, Karratha, WA: Artemis Resources ASX/Media Announcement, 2 August 2017.
- Artemis Resources, 2017c, Novo Resources presenting at Denver Gold Forum 2017: Artemis Resources ASX/Media Announcement, 25 September 2017.
- Cheney, ES 1996, Sequence stratigraphy and plate tectonic significance of the Transvaal succession of southern Africa and its equivalent in Western Australia: *Precambrian Research*, v. 79, p. 3–24.
- de Kock, MO, Beukes, NJ and Armstrong, RA 2012, New SHRIMP U–Pb zircon ages from the Hartswater Group, South Africa: Implications for correlations of the Neoproterozoic Ventersdorp Supergroup on the Kaapvaal craton and with the Fortescue Group on the Pilbara craton: *Precambrian Research*, v. 204–205, p. 66–74.
- de Kock, MO, Evans, DAD and Beukes, NJ 2009, Validating the existence of Vaalbara in the Neoproterozoic: *Precambrian Research*, v. 174, p. 145–154.
- Hickman, AH 2002, Geology of the Roebourne 1:100 000 sheet: Geological Survey of Western Australia, 1:100 000 Geological Series Explanatory Notes, 35p.
- Hickman, AH 2016, Northwest Pilbara Craton: a record of 450 million years in the growth of Archean continental crust: Geological Survey of Western Australia, Report 160, 104p.
- Hickman, AH, Huston, DL, Van Kranendonk, MJ and Smithies, RH 2006, Geology and mineralization of the west Pilbara — a field guide: Geological Survey of Western Australia, Record 2006/17, 50p.
- Hickman, AH, Smithies, RH and Tyler, IM 2010, Evolution of active plate margins: West Pilbara Superterrane, De Grey Superbasin, and the Fortescue and Hamersley Basins — a field guide: Geological Survey of Western Australia, Record 2010/3, 74p.
- Hickman, AH and Kranendonk, MJ 2012, A billion years of Earth history: a geological transect through the Pilbara Craton and the Mount Bruce Supergroup — a field guide to accompany 34th IGC Excursion WA-2: Geological Survey of Western Australia, Record 2012/10, 66p.
- Huston, DL, Smithies, RH and Sun, S-S 2000, Correlation of the Archean Mallina – Whim Creek Basin: implications for base-metal potential of the central part of the Pilbara granite–greenstone terrane: *Australian Journal of Earth Sciences*, v. 47, p. 217–230.
- Manzi, MSD, Hein, KAA, King, N and Durrheim, RJ 2013, Neoproterozoic tectonic history of the Witwatersrand Basin and Ventersdorp Supergroup: new constraints from high-resolution 3D seismic reflection data: *Tectonophysics*, v. 590, p. 94–105.
- Phillips, GN and Powell, R 2015, Hydrothermal alteration in the Witwatersrand goldfields: *Ore Geology Reviews*, v. 65, p. 245–273.

- Robb, LJ and Meyer, FM 1995, The Witwatersrand Basin, South Africa: Geological framework and mineralization processes: *Ore Geology Reviews*, v. 10, p. 67–94.
- Smithies, RH, Champion, DC and Sun, S-S 2004, Evidence for Early LREE-enriched mantle source regions: diverse magmas from the ca. 3.0 Ga Mallina Basin, Pilbara Craton, NW Australia: *Journal of Petrology*, v. 45, p. 1515–1537.
- Smithies, RH, Hickman, AH and Nelson, DR 1999, New constraints on the evolution of the Mallina Basin, and their bearing on relationships between the contrasting eastern and western granite–greenstone terranes of the Archaean Pilbara Craton, Western Australia: *Precambrian Research*, v. 94, p. 11–28.
- Smithies, RH, Nelson, DR and Pike, G 2001 Development of the Archaean Mallina Basin, Pilbara Craton, northwestern Australia; a study of detrital and inherited zircon ages: *Sedimentary Geology*, v. 141–142, p. 79–94.
- Smithies, RH, Van Kranendonk, MJ and Champion, DC 2007, The Mesoarchaean emergence of modern style subduction, *in* *Island Arcs: Past and Present* edited by S Maruyama and M Santosh: *Gondwana Research*, v. 11, p. 50–68.
- Thorne, AM and Trendall, AF 2001, The geology of the Fortescue Group, Pilbara Craton, Western Australia: Geological Survey of Western Australia, Bulletin 144, 249p.
- Thorne, AM, Johnson, SP, Tyler, Cutten, HN and Blay, O 2011, Geology of the northern Capricorn Orogen *in* Capricorn Orogen seismic and magnetotelluric (MT) workshop 2011: extended abstracts edited by SP Johnson, AM Thorne and IM Tyler: Geological Survey of Western Australia, Record 2011/25, p. 7–17.
- Trendall, AF, Compston, W, Nelson, DR, de Laeter, JR and Bennett, VC 2004, SHRIMP zircon ages constraining the depositional chronology of the Hamersley Group, Western Australia: *Australian Journal of Earth Sciences*, v. 51, no. 5, p. 621–644.
- Tucker, RF, Viljoen, RP and Viljoen, MJ 2016, A review of the Witwatersrand Basin — The world's greatest goldfield: Episodes, v. 39, p. 105–133.
- Van Kranendonk, MJ, Hickman, AH and Huston DL 2006, Geology and mineralization of the east Pilbara — a field guide: Geological Survey of Western Australia, Record 2006/16, 90p.
- Wingate, MTD 1998, A palaeomagnetic test of the Kaapvaal–Pilbara (Vaalbara) connection at 2.78 Ga: *South African Journal of Geology*, v. 101, p. 257–274.
- Zegers, TE, de Wit, MJ, Dann J and White, SH 1998, Vaalbara, Earth's oldest assembled continent? A combined structural, geochronological, and palaeomagnetic test: *Terra Nova*, v. 10, p. 250–259.

# Focusing on the Fortescue and Hamersley Basins

by

HM Howard and DMcB Martin

An integrated geochemical, isotopic and geochronological study of igneous and sedimentary rocks is currently being undertaken in the Fortescue and Hamersley Basins of the southern Pilbara region (Fig. 1). The 2775–2629 Ma volcano-sedimentary Fortescue Group is conformably overlain by the 2629–2420 Ma Hamersley Group and the 2445–2208 Ma Turee Creek Group, all three of which constitute the Mount Bruce Supergroup (Fig. 2). The Mount Bruce Supergroup unconformably overlies the granite–greenstones of the Pilbara Craton in Western Australia.

A digital 1:250 000 scale interpreted bedrock geological map of the southern Pilbara Craton is planned for release in 2018. The digital map, combined with legacy data and up-to-date imagery, will form the basis of a regional dataset that will be updated as new data and insights into the geological evolution of the area arise.

Targeted field validation in support of the new geological map has identified a number of potential stratigraphic revisions. One of the most significant revisions is in the upper part of the Mount Bruce Supergroup, where a regional paraconformity to local low-angle unconformity has been recognized at the base of the Turee Creek Group. The regional lithostratigraphic relationships between the Woongarra Rhyolite and overlying Boolgeeda Iron Formation in the Hamersley Group, combined with a critical appraisal of the currently available geochronology, suggest that a similar paraconformable to unconformable relationship may also be present at the base of the Boolgeeda Iron Formation. These relationships suggest that the predominantly epiclastic sedimentary unit currently considered to be the uppermost division of the Woongarra Rhyolite should instead be included in the Boolgeeda Iron Formation, which calls into question the current definition of the upper limit of the Mount Bruce Supergroup.

The Turee Creek Group is an important stratigraphic unit that records the Great Oxidation Event and Huronian-age glaciations, but much of the stratigraphic nomenclature of the Turee Group has yet to be formalized. Recent fieldwork has identified new occurrences of known glacial horizons, as well as a potentially new horizon. In order to assist the description and correlation of this globally important succession, new formalized stratigraphic names have been introduced for all the previously unnamed units, as well as for each of the recognized glacial horizons.

Preliminary, high-precision geochemical and isotopic data, obtained from a detailed sampling traverse in the Paraburdoo area (Fig. 1), reveal significant geochemical variations in the mafic units of the Fortescue Group. In the southern Pilbara region, Thorne and Trendall (2001) proposed four tectonic packages in the Fortescue Group (Fig. 2), deposited in progressively deeper marine environments interpreted to reflect changing tectonic settings up stratigraphy, from rift to passive margin. However, geochemical data from Paraburdoo do not show progressively increasing or decreasing element trends through tectonic packages 1 to 3 in the lower part of the Fortescue Group. Rather, the Mount Roe Basalt and Boongal, Pyradie and Bunjinah Formations contain at least two (A and B) or three (A, B, and C) geochemical subgroups (Fig. 3), within which geochemical trends are evident. The geochemical subgroups display variations in Th/TiO<sub>2</sub> ratios (Fig. 3) akin to the high-, intermediate- or low-Th groups described by Barnes et al. (2012) in basalts of the Eastern Goldfields Superterrane. The geochemical variation evident in the lower part of the Fortescue Group can be explained by a komatiitic magma source modified by assimilation and fractional crystallization processes. Thorne and Trendall (2001) assigned deep-marine sedimentary rocks and basalt of the Jeerinah Formation to tectonic package 4, and suggested a passive margin setting. Geochemically the basalts of the Jeerinah Formation are more primitive than the lower parts of the volcanic succession and could not have been generated from the same komatiitic magma source.

Further outcrop and diamond drillcore sampling will be used to systematically and laterally assess the geochemical variation of magmatic units across the Fortescue Basin. The geochemical relationship between felsic and associated mafic and ultramafic igneous rocks will also be used to establish which of the mafic intrusive rocks of the region are related to the Fortescue and Hamersley Groups.

A review of the geochronology of the southern Pilbara Craton suggests that there is scope for significant improvement in coverage and accuracy. Most notably, the majority of ages available for the region are external to GSWA, and pre-date the use of modern analytical techniques such as stable isotope analyses of zircon, which provide valuable additional information regarding tectonic setting. A suite of over 17 new samples has already been collected for zircon geochronology, including a number of samples from previously undated stratigraphic horizons. These results should significantly improve the geochronological framework and understanding of the tectonic setting and evolution of the region.



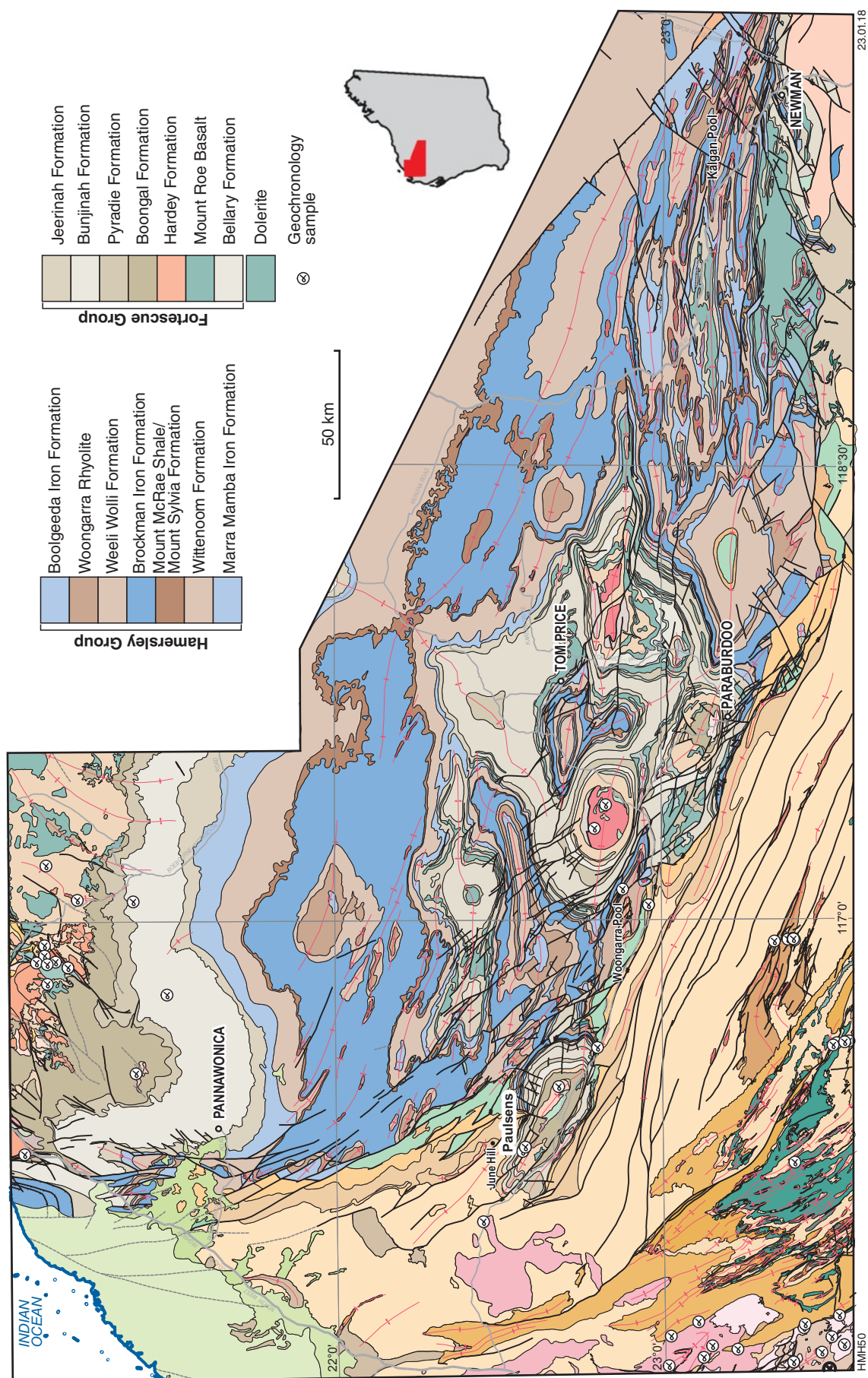
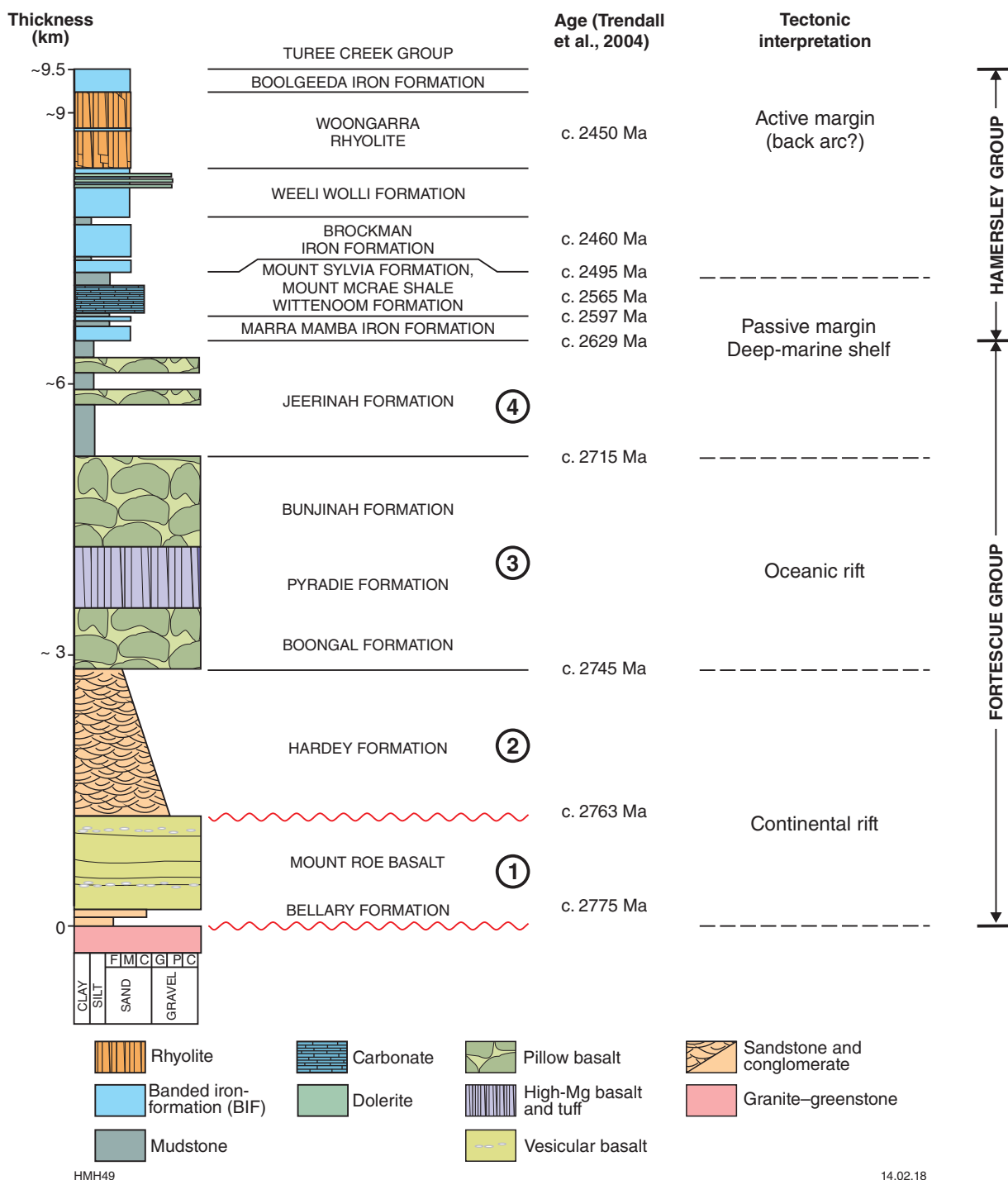
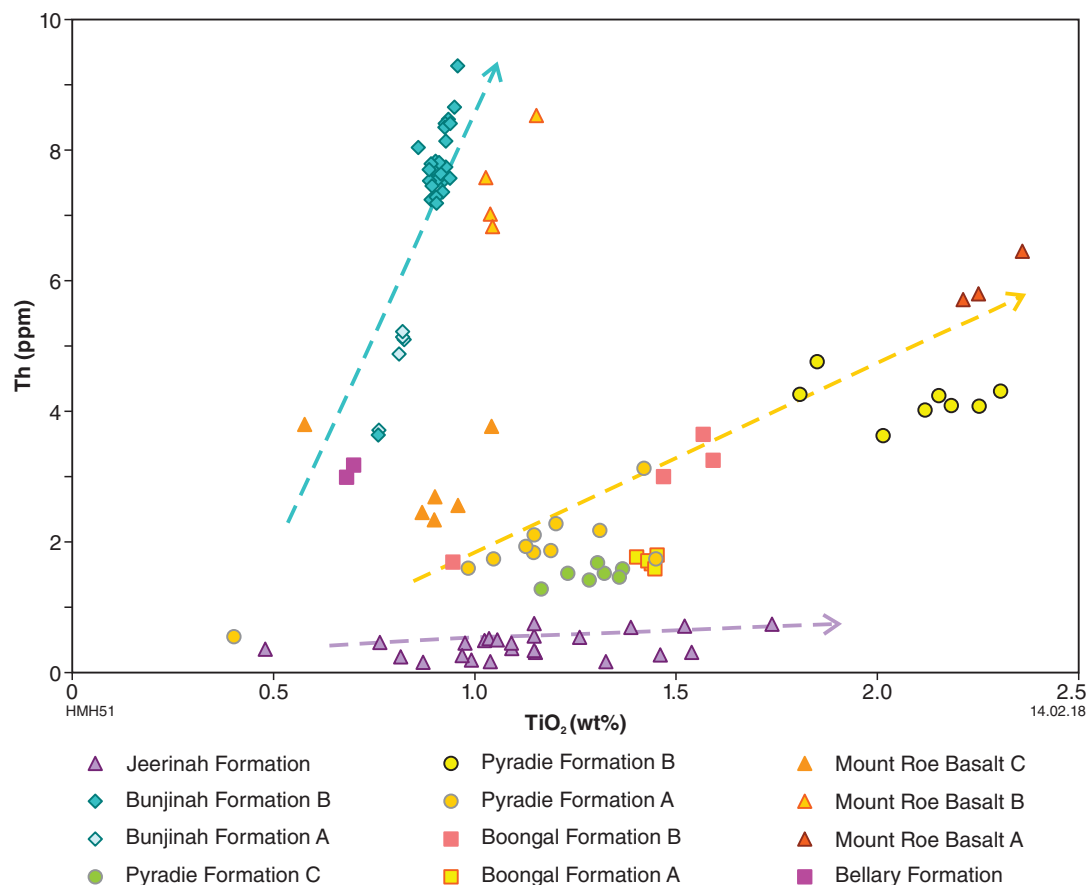


Figure 1. Geological map of the Fortescue and Hamersley Basins in the southern Pilbara



**Figure 2.** The stratigraphy of the Fortescue and Hamersley Groups in the southern Pilbara. Tectonic interpretations from Martin and Morris (2010) and Thorne et al. (2011); ages after Trendall et al. (2004). Tectonic packages of the Fortescue Group are numbered 1–4



**Figure 3.** Th vs TiO<sub>2</sub> plot showing high-, intermediate- and low-Th groups within the Fortescue Group (after Barnes et al., 2012)

Another important aspect of this project is to better understand the structural and tectonic framework of the region. The extent and timing of various fold events that constitute the northern margin of the Capricorn Orogen are poorly constrained. Furthermore, fault architecture and kinematics have not previously been systematically mapped across the southern Pilbara Craton. With the benefit of recent geophysical imagery, preliminary work has already identified a number of new regional faults, and aided systematic mapping of previously known fault systems. Future work will focus on discriminating the effects of the Ophthalmia (2215–2145 Ma) and Capricorn (1817–1772 Ma) Orogenies on the southern Pilbara Craton margin, recognizing that deformation was driven by events in the central and southern Capricorn Orogen.

## References

- Barnes SJ, Van Kranendonk, MJ and Sonntag, I 2012, Geochemistry and tectonic setting of basalts from the Eastern Goldfields Superterrane, *Australian Journal of Earth Sciences*, v. 59, no. 5, p. 707–735, doi:10.1080/08120099.2012.6873982012.
- Martin, DMcB and Morris, PA 2010, Tectonic setting and regional implications of ca. 2.2 Ga mafic magmatism in the southern Hamersley Province, Western Australia: *Australian Journal of Earth Sciences*, v. 57, no. 7, p. 911–931, doi:10.1080/08120099.2010.510172.
- Thorne, AM, Tyler, IM, Korsch, RJ, Johnson, SP, Brett, JW, Cutten, HN, Blay, OA, Kennett, BLN, Blewett, RS, Joly, A, Dentith, MC, Aitken, ARA, Holzschuh, J, Goodwin, JA, Salmon, M, Reading, A and Boren, G 2011, Preliminary interpretation of deep seismic reflection line 10GA-CP1: crustal architecture of the northern Capricorn Orogen, in *Capricorn Orogen seismic and magnetotelluric (MT) workshop 2011: extended abstracts edited by SP Johnson, AM Thorne and IM Tyler*: Geological Survey of Western Australia, Record 2011/25, p. 19–26.
- Thorne, AM and Trendall, AF 2001, *Geology of the Fortescue Group, Pilbara Craton, Western Australia*: Geological Survey of Western Australia, Bulletin 144, 249p.
- Trendall, AF, Compston, W, Nelson, DR, De Laeter, JR and Bennett, VC 2004, SHRIMP zircon ages constraining the depositional chronology of the Hamersley Group, Western Australia: *Australian Journal of Earth Sciences*, v. 51, no. 5, p. 621–644.

# Zircon composition as a fertility indicator of Archean granites

by

Y-J Lu, RH Smithies, MTD Wingate, NJ Evans<sup>1</sup>, PA Morris, DC Champion<sup>2</sup> and TC McCuaig<sup>3,4</sup>

Porphyry Cu deposits are major sources of Cu and Mo. They range in age from Archean to modern, although most are Jurassic and younger, and porphyry deposits in Precambrian terranes are rare. Nevertheless, several porphyry-type Cu or Au deposits occur in the Superior Craton of Canada (Fayol and Jebrak, 2017), and in the South West Terrane of the Yilgarn Craton (McCuaig et al., 2001; Outhwaite, 2018), suggesting that their potential in Archean cratons may not be fully recognized. Chemical fingerprinting and assessment of potential targets from terrane to deposit scale are needed by industry (e.g. Ballard et al., 2002; Loucks, 2014; McCuaig and Hronsky, 2014; Agnew, 2015; Lu et al., 2016).

In Phanerozoic porphyry Cu systems, mineralized magmatic rocks have distinctive chemical compositions, including high Sr/Y, V/Sc, Eu/Eu\*, and (Eu/Eu\*)/Y ratios (e.g. Chiaradia et al., 2012; Loucks, 2014; Lu et al., 2017). Zircon in these rocks also have distinctive compositions, such as higher Eu/Eu\* ratios (Ballard et al., 2002; Lu et al., 2016). These signatures can be attributed to high magmatic water and sulfur contents, and high oxidation states, and can be used as ore fertility indicators.

## Archean granites in the Yilgarn Craton

To test whether these fertility indicators can be applied to Archean granites across the Yilgarn Craton, we have compiled Geological Survey of Western Australia (GSWA) geochronology and geochemistry data for 230 unaltered and non-mineralized granites. The granites are divided into four groups (Fig. 1), based on their K<sub>2</sub>O/Na<sub>2</sub>O and Sr/Y ratios:

- **potassic high Sr/Y granites** have K<sub>2</sub>O/Na<sub>2</sub>O ≥ 1 and Sr/Y ≥ 40
- **sodic high Sr/Y granites** have K<sub>2</sub>O/Na<sub>2</sub>O < 1 and Sr/Y ≥ 40

- **sodic low Sr/Y granites** have K<sub>2</sub>O/Na<sub>2</sub>O < 1 and Sr/Y < 40
- **potassic low Sr/Y granites** have K<sub>2</sub>O/Na<sub>2</sub>O ≥ 1 and Sr/Y < 40.

A K<sub>2</sub>O/Na<sub>2</sub>O ratio of 1 separates potassic and sodic groups. A Sr/Y ratio of 40 is used to distinguish between high and low Sr/Y groups because porphyry Cu deposits are associated with granites that have Sr/Y ≥ 40 (Chiaradia et al., 2012; Loucks, 2014), and average Archean tonalite–trondhjemite–granodiorite (TTG) has Sr/Y > 40 (Moyen and Martin, 2012). We also examined >2000 trace element analyses for zircons from 42 Yilgarn granite samples, although screening out alteration and mineral inclusions leaves 220 analyses from 30 samples (Fig. 1).

## Fertility of Yilgarn granites revealed by whole-rock geochemistry

We compared Yilgarn granites with well-characterized hydrous and oxidized Miocene Cu-mineralized granites associated with porphyry Cu mineralization in the Lhasa Terrane of southern Tibet (Lu et al., 2015). The Tibetan granites crystallized from very hydrous magmas with >10 wt% water contents at depth, resulting mainly from high-pressure differentiation of hydrous mafic melts of sub-Tibetan mantle (Lu et al., 2015).

Figure 2a shows that neither hydrous melting nor dehydration melting of mafic lower crust can produce melts with Mg# > 50. Tibetan granites typically have Mg# > 50, some of which plot within the high-Mg diorite (HMD) field at 55–65 wt% SiO<sub>2</sub> (Fig. 2a), consistent with input of primary mafic magmas through magma mixing. In contrast, most Yilgarn granites have Mg# < 50, suggesting derivation mainly through crustal melting with limited mantle input. This interpretation is supported by the observation that few mafic microgranular enclaves (MME, mantle-derived melts) are present in Yilgarn granites, whereas MME are common in Tibetan Cu-mineralized granites.

Based on Fe<sub>2</sub>O<sub>3</sub>/FeO ratios, Yilgarn high Sr/Y granites are moderately to strongly oxidized, whereas low Sr/Y granites are moderately reduced to strongly oxidized (Fig. 2b). Tibetan Cu-mineralized granites are mainly strongly oxidized and tend to have higher Fe<sub>2</sub>O<sub>3</sub>/FeO

1 John de Laeter Centre and Department of Applied Geology, Curtin University, Bentley, WA 6845, Australia

2 Geoscience Australia, GPO Box 378, Canberra, ACT 2601, Australia

3 BHP, 125 St Georges Terrace, Perth, WA 6000, Australia

4 Centre for Exploration Targeting and ARC Centre of Excellence for Core to Crust Fluid Systems, School of Earth Sciences, The University of Western Australia, Crawley, WA 6009, Australia



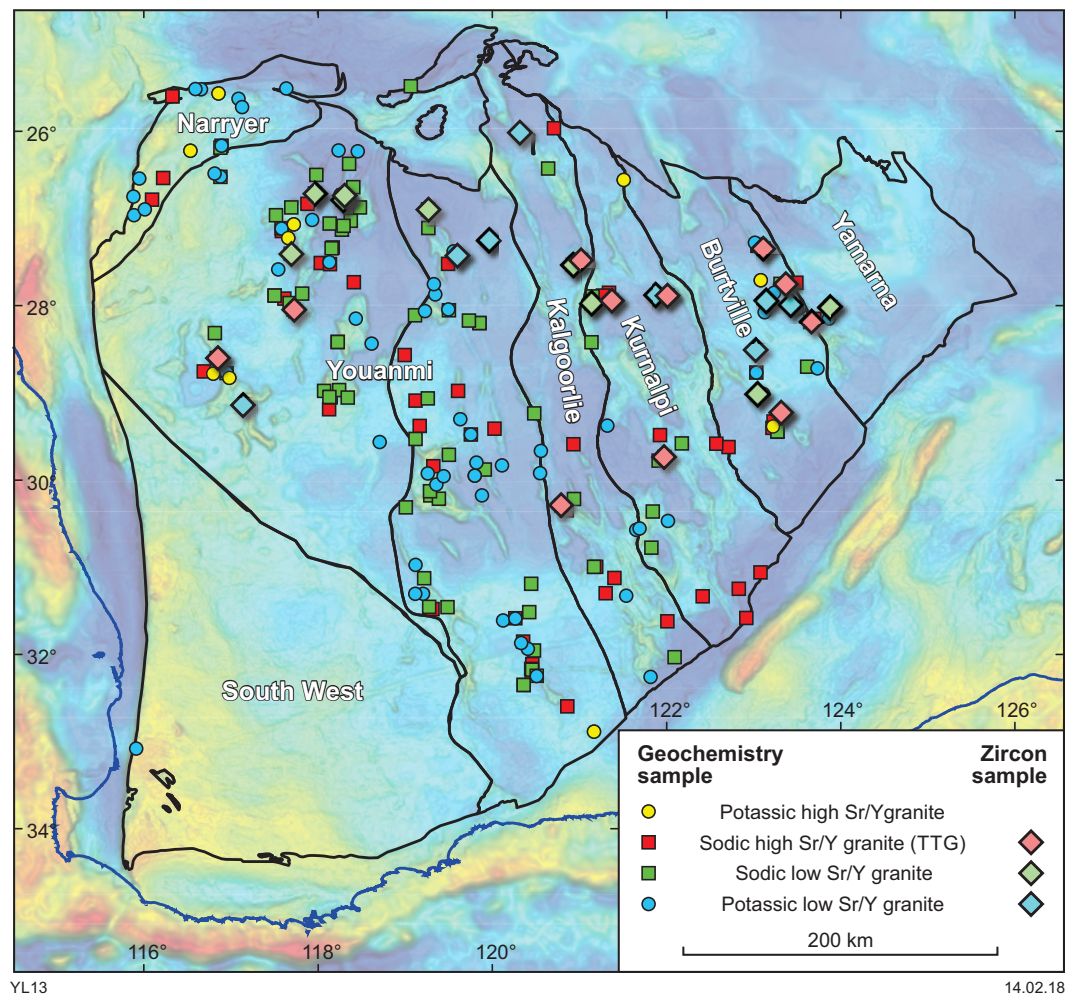


**Figure 1.** Granite whole-rock and zircon sample locations superimposed on a gravity image of the Yilgarn Craton, labelled by terrane

at a given  $\text{FeO}_{\text{total}}$ , suggesting that Tibetan granites are generally more oxidized (Fig. 2b). Note that, for samples with  $\text{FeO}_{\text{total}} < 2$  wt%, criteria other than whole-rock  $\text{Fe}_2\text{O}_3$  and  $\text{FeO}$  data should be used to assess oxidation state (Blevin, 2004).

Most Yilgarn granites plot in the Cu-infertile field in a V/Sc vs  $\text{SiO}_2$  diagram (Fig. 2c; Loucks, 2014), whereas all Tibetan Cu-mineralized granites plot in the Cu-fertile field (Table 1). High V/Sc is caused by amphibole fractionation, which removes Sc, and by suppression of magnetite fractionation, which increases V in an oxidized and hydrous melt (Loucks, 2014). The average V/Sc ratio for each group of Yilgarn granites is significantly lower, suggesting that Yilgarn granites are less fertile than Tibetan granites because the former are generally less oxidized and less hydrous. Zircon saturation temperatures (Watson and Harrison, 1983) indicate that Yilgarn granites crystallized at higher temperatures than Tibetan granites (Fig. 2d), which also suggests they are less hydrous.

The trace element patterns of Yilgarn high Sr/Y and low Sr/Y granites are distinctly different (Fig. 2e). High Sr/Y granites are characterized by an absence of Sr and Eu anomalies, and depletion in heavy rare earth elements (HREE), with an average Yb of about 0.5 ppm. Yilgarn low Sr/Y granites have significant negative Sr and Eu anomalies and elevated HREE concentrations, with an

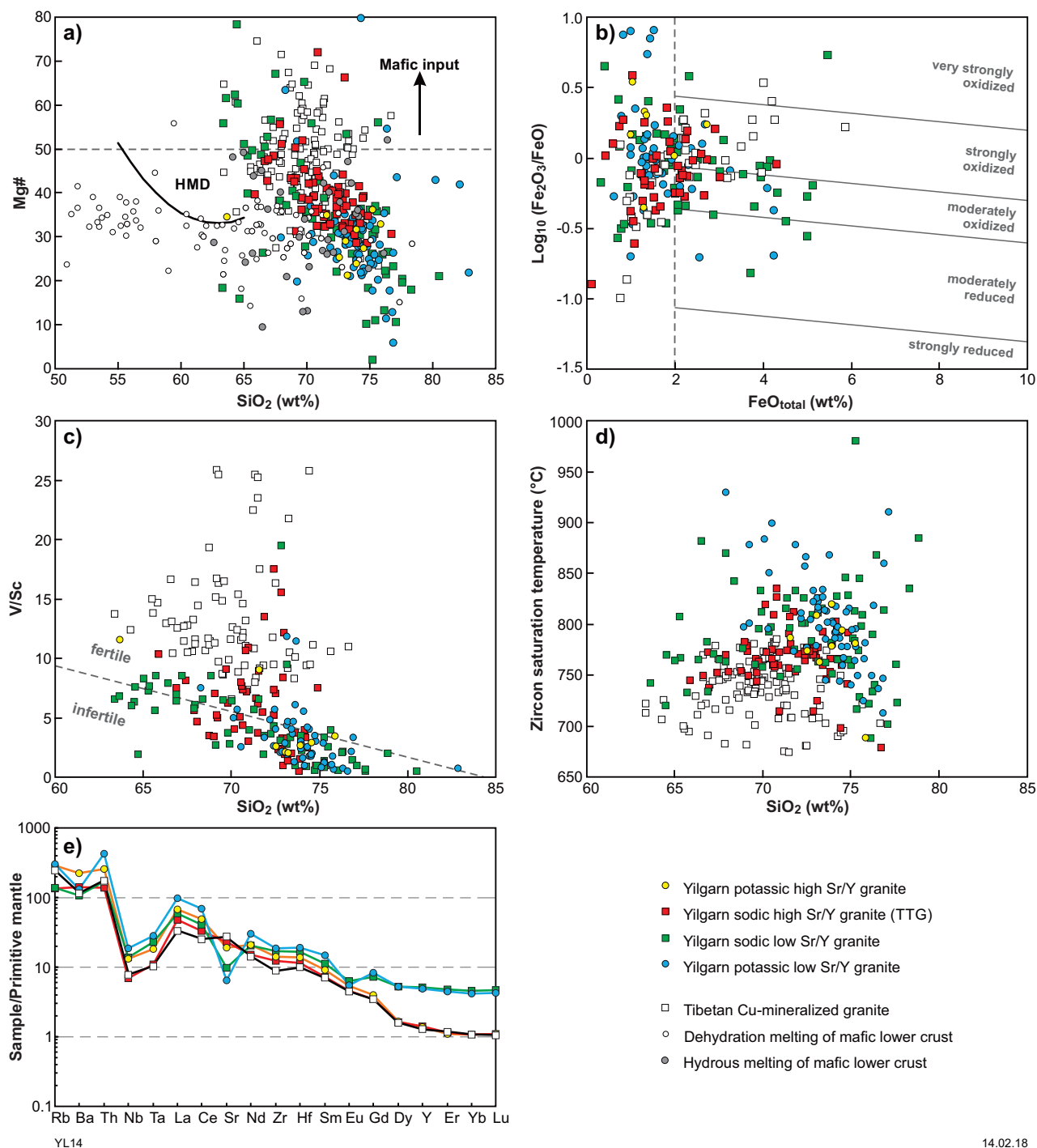
average Yb of about 2 ppm (Table 1; Fig. 2e). These features suggest that Yilgarn high Sr/Y granites were derived from high-pressure melting of mafic crust within the garnet stability field, whereas low Sr/Y granites originated mainly from low-pressure melting of crust within the plagioclase stability field (Moyen and Martin, 2012). Tibetan Cu-mineralized granites have similar HREE patterns to the Yilgarn high Sr/Y granites, but are more enriched in Sr and depleted in Zr (Fig. 2e), consistent with their derivation from high-pressure differentiation of more hydrous melts.

## Fertility of Yilgarn granites revealed by zircon compositions

We also compared zircon trace element compositions of Yilgarn granites with those of reference suites of infertile and fertile granites. The zircon REE patterns of Yilgarn granites are similar to both Phanerozoic fertile and infertile suites (Lu et al., 2016), with positive Ce anomalies, negative Eu anomalies, and steep REE patterns with low La/Yb (Fig. 3a). However, Yilgarn granites have consistently lower zircon  $\text{Ce}/\text{Ce}^*$  and  $\text{Eu}/\text{Eu}^*$  than Phanerozoic fertile suites (Table 2; Fig. 3b,c), suggesting they are less hydrous than fertile suites (Lu et al., 2016).

Zircon  $Ce/\sqrt{(U \times Ti)}$  was recently proposed as a proxy for magma oxidation state (Loucks and Fiorentini, 2018). Values for Yilgarn granites are lower than those for Phanerozoic fertile suites and similar to those of infertile

suites. This also suggests that Yilgarn granites are less oxidized than Cu-fertile granites (Table 2; Fig. 3c), and this is consistent with interpretations from whole-rock  $Fe_2O_3/FeO$  data (Fig. 2b).



14.02.18

**Figure 2.** Whole-rock compositions of Yilgarn granites. Experimental melts from hydrous and dehydration melting of mafic lower crust are plotted for comparison (see Lu et al., 2015 for full references). HMD, high-Mg diorite field, from Lee and Bachmann (2014); Cu-fertile/infertile boundary from Loucks (2014); trace element patterns in e) are normalized to primitive mantle (Sun and McDonough, 1989)

**Table 1. Average compositions of Yilgarn granites and Tibetan Cu-mineralized granites**

	<i>Yilgarn potassic high Sr/Y granite</i>		<i>Yilgarn sodic high Sr/Y granite</i>		<i>Yilgarn sodic low Sr/Y granite</i>		<i>Yilgarn potassic low Sr/Y granite</i>		<i>Tibetan Cu- mineralized granite</i>	
	<i>sd</i>		<i>sd</i>		<i>sd</i>		<i>sd</i>		<i>sd</i>	
<i>N</i>	10		65		79		76		117	
<i>Oxides (wt%)</i>										
SiO <sub>2</sub>	72.79	3.44	71.50	2.29	71.66	4.37	74.12	2.76	69.78	2.49
TiO <sub>2</sub>	0.19	0.06	0.28	0.10	0.35	0.21	0.25	0.13	0.39	0.11
Al <sub>2</sub> O <sub>3</sub>	14.53	0.98	15.38	0.74	14.32	1.32	13.70	1.16	15.49	1.05
Fe <sub>2</sub> O <sub>3</sub> T	1.62	0.70	2.09	0.92	2.88	1.57	2.16	1.46	2.46	1.07
MnO	0.03	0.02	0.04	0.03	0.05	0.03	0.03	0.02	0.04	0.02
MgO	0.37	0.23	0.74	0.45	1.07	1.10	0.66	0.95	1.12	0.40
CaO	1.31	0.72	2.33	0.90	2.57	1.92	1.35	1.10	2.29	1.14
Na <sub>2</sub> O	3.98	0.61	4.92	0.62	4.59	1.28	3.15	1.10	4.07	0.87
K <sub>2</sub> O	5.09	0.86	2.64	1.01	2.42	1.26	4.50	1.07	4.27	1.51
P <sub>2</sub> O <sub>5</sub>	0.09	0.10	0.09	0.04	0.10	0.07	0.07	0.05	0.14	0.06
<i>Trace elements (ppm)</i>										
Sr	403.0	163.2	480.6	259.5	204.7	122.4	134.7	86.0	579.0	215.7
Zr	155.8	55.9	135.9	42.9	188.1	120.8	207.5	124.4	98.4	29.5
Y	6.2	3.5	6.4	2.9	23.2	28.5	22.4	19.3	5.8	1.7
Yb	0.52	0.29	0.52	0.28	2.23	3.10	2.06	2.03	0.53	0.14
<i>Ratios</i>										
K <sub>2</sub> O/Na <sub>2</sub> O	1.28	0.13	0.55	0.23	0.56	0.31	2.46	4.42	1.26	1.25
Mg#	29.60	5.14	39.52	7.84	36.16	15.71	30.87	12.10	48.38	9.80
Sr/Y	77.50	36.40	89.80	61.20	14.90	11.30	10.00	9.00	106.40	42.80
La/Yb	114.66	88.74	77.19	56.43	32.02	31.18	52.54	47.26	43.80	13.75
Eu/Eu*	0.96	0.23	0.97	0.20	0.76	0.28	0.56	0.26	0.93	0.12
Nb/Ta	14.07	5.04	14.60	8.38	11.94	4.11	14.05	7.85	13.84	4.01
Dy/Yb	2.43	0.35	2.50	0.82	1.95	0.53	2.10	0.67	2.22	0.33
V/Sc	3.14	4.31	5.88	3.71	4.38	3.33	3.24	2.37	13.59	5.42
T <sub>zircon</sub> (°C)	777	38	767	27	788	48	803	44	736	27

**NOTES:** *N*, number of samples averaged; *sd*, standard deviation; T<sub>zircon</sub>, zircon saturation temperature (Watson and Harrison, 1983). Only samples with LOI <3.5 wt%, SiO<sub>2</sub> >63 wt% and Al<sub>2</sub>O<sub>3</sub> <20 wt% are included

**Table 2. Average zircon compositions for Yilgarn granites and Phanerozoic reference suites**

<i>Granite suite</i>	<i>N</i>	<i>Eu/Eu*</i>	<i>sd</i>	<i>Ce/(U × Ti)</i>	<i>sd</i>	<i>Ce/Ce*</i>	<i>sd</i>
<i>Yilgarn sodic high Sr/Y granite (TTG)</i>							
Yamarna Terrane	30	0.30	0.08	0.42	0.08	23	15
Burtville Terrane	3	0.41	0.26	0.13	-	5	2
Kalgoorlie–Kurnalpi Terranes	16	0.38	0.17	0.42	0.20	35	19
Murchison Domain, Youanmi Terrane	3	0.42	0.16	0.36	0.07	24	3
Yilgarn sodic low Sr/Y granite	108	0.29	0.09	0.36	0.21	29	35
Yilgarn potassic low Sr/Y granite	41	0.24	0.13	0.34	0.19	49	90
Phanerozoic infertile reference suite	80	0.08	0.07	0.33	0.27	142	215
Phanerozoic fertile reference suite	337	0.59	0.15	0.67	0.39	292	359

**NOTES:** Phanerozoic reference suites are from Lu et al. (2016). *N*, number of analyses averaged; *sd*, standard deviation

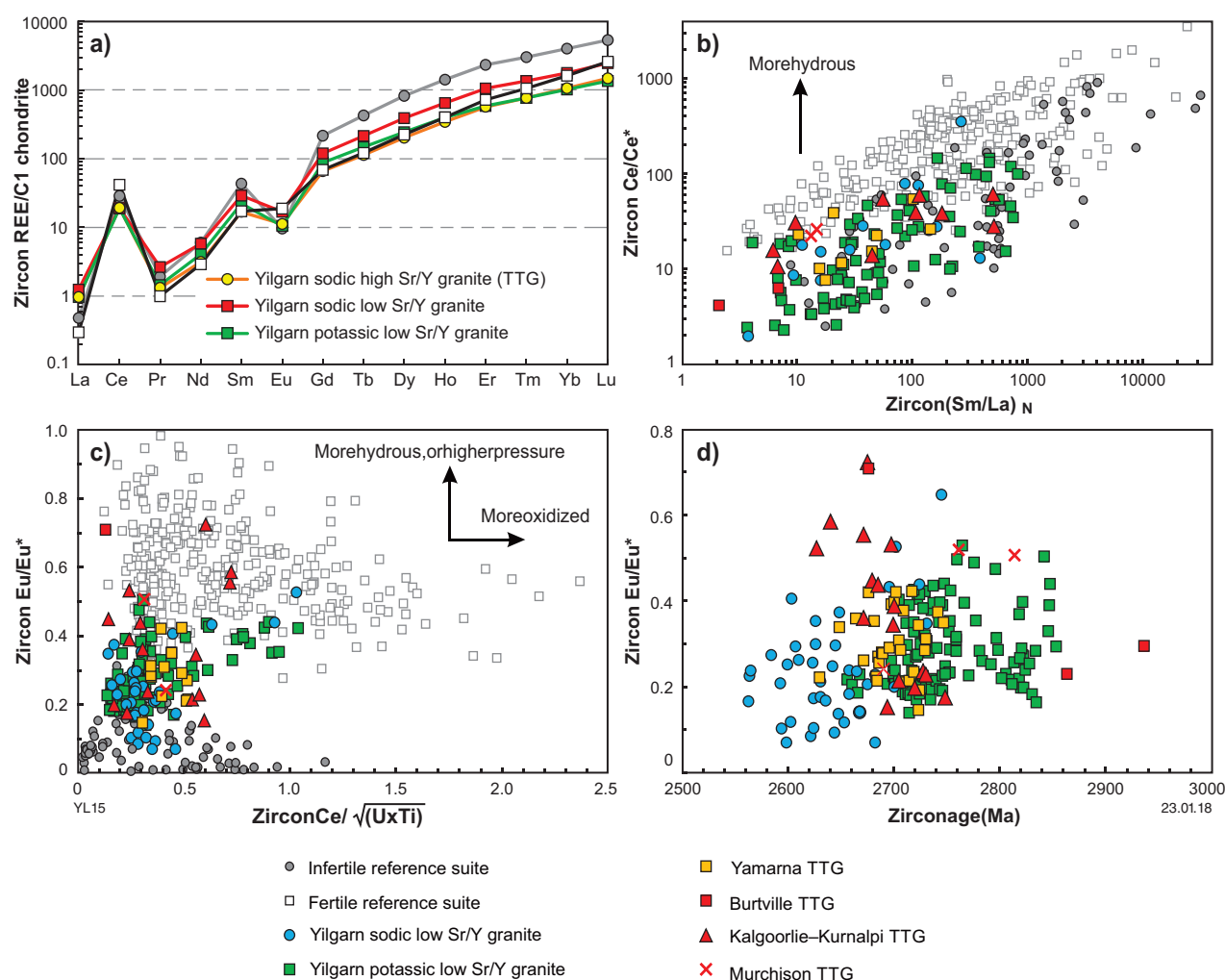


**Figure 3. Compositions of zircons from Yilgarn granites.** In b), the N subscript indicates values normalized to chondritic values (Sun and McDonough, 1989). Phanerozoic Cu-fertile and Cu-infertile reference suites are from Lu et al. (2016)

## Conclusion

Both whole-rock and zircon compositions indicate that many Yilgarn granites are less hydrous and less oxidized than Phanerozoic Cu-mineralized granites. The systematic difference in zircon chemistry between Archean granites and Phanerozoic fertile and infertile suites suggests that different processes were involved in forming Archean granites. We argue that Archean high Sr/Y granites were formed mainly through intracrustal partial melting of mafic lower crust in the garnet stability field, whereas Phanerozoic fertile suites were formed by intracrustal amphibole-dominated fractionation of mafic magmas. Granites formed by the former process have lower potential for porphyry Cu mineralization due to insufficient water and the lack of copper and sulfur accumulation in the melt.

This study employed Yilgarn granite samples currently available in the GSWA database, and did not include granites associated with mineralization. Future work will extend analyses to porphyry-style mineralized Archean granites such as those at Boddington (McCuaig et al., 2001) and at the Calingiri prospect (Outhwaite, 2018).

This will assess potential differences between mineralized and non-mineralized Archean granites, and hopefully lead to ways of identifying additional granites that have potential for porphyry-style mineralization.

## References

- Agnew, P 2015, What industry wants from research: Society of Economic Geologists Annual Conference, World-Class Ore Deposits: Discovery to Recovery, 27–30 September 2015, Hobart, Tasmania, Australia, p. 1–2.
- Ballard, JR, Palin, JM and Campbell, IH 2002, Relative oxidation states of magmas inferred from Ce(IV)/Ce(III) in zircon: Application to porphyry copper deposits of northern Chile: Contributions to Mineralogy and Petrology, v. 144, p. 347–364.
- Blevin, PL 2004, Redox and compositional parameters for interpreting granitoid metallogeny of eastern Australia: implications for gold-rich ore systems: Resource Geology, v. 54, p. 241–252.
- Chiaradia, M, Ulianov, A, Kouzmanov, K and Beate, B 2012, Why large porphyry Cu deposits like high Sr/Y magmas?: Nature, Scientific Reports 2, no. 685, doi:10.1038/srep00685.



- Fayol, N and Jebrak, M 2017, Archean sanukitoid gold porphyry deposits: A new understanding and genetic model from the Lac Bachelor gold deposit, Abitibi, Canada: *Economic Geology*, v. 112, p. 1913–1936.
- Lee, C-TA and Bachmann, O 2014, How important is the role of crystal fractionation in making intermediate magmas? Insights from Zr and P systematics: *Earth and Planetary Science Letters*, v. 393, p. 266–274.
- Loucks, RR 2014, Distinctive composition of copper-ore-forming arc magmas: *Australian Journal of Earth Sciences*, v. 61, p. 5–16.
- Loucks, RR and Fiorentini, ML 2018, New magmatic oxybarometer using trace elements in zircon reveals oxidation states of Hadean and Eoarchean lithosphere in four cratons: *Geochimica et Cosmochimica Acta*.
- Lu, Y-J, Hou, Z-Q, Yang, Z-M, Parra-Avila, LA, Fiorentini, ML, McCuaig, TC and Loucks, RR 2017, Terrane-scale porphyry Cu fertility in the Lhasa Terrane, southern Tibet, *in* TARGET 2017, Perth, Australia, abstracts *edited by* S Wyche and WK Witt: Geological Survey of Western Australia, Record 2017/6, p. 95–100.
- Lu, Y-J, Loucks, RR, Fiorentini, ML, Yang, ZM and Hou, ZQ 2015, Fluid flux melting generated post-collisional high-Sr/Y copper-ore-forming water-rich magmas in Tibet: *Geology*, v. 43, p. 583–586.
- Lu, Y-J, Loucks, RR, Fiorentini, ML, McCuaig, TC, Evans, NJ, Yang, ZM, Hou, ZQ, Kirkland, CL, Parra-Avila, LA and Kobussen, A 2016, Zircon compositions as a pathfinder for porphyry Cu  $\pm$  Mo  $\pm$  Au deposits: Society of Economic Geologists Special Publication, v. 19, p. 329–347.
- McCuaig, TC, Behn, M, Stein, S, Hagemann, SG, McNaughton, NJ, Cassidy, KF, Champion, DC and Wyborn, LAI 2001, The Boddington gold mine: A new style of Archean Au–Cu deposit, *in* International Archean Symposium, Extended Abstracts *edited by* KF Cassidy, JM Dunphy and MJ Van Kranendonk: AGSO Record 2001/37, p. 453–455.
- McCuaig, TC and Hronsky, JMA 2014, The mineral system concept: The key to exploration targeting: Society of Economic Geologists Special Publication, v. 18, p. 153–175.
- Moyen, J-F and Martin, H 2012, Forty years of TTG research: *Lithos*, v. 148, p. 312–336.
- Outhwaite, MD 2018 Metamorphosed Mesoarchean Cu–Mo–Ag mineralization: Evidence from the Calingiri deposits, southwest Yilgarn Craton: Geological Survey of Western Australia, Report 183, 216p.
- Sun, S-S and McDonough, WF 1989, Chemical and isotopic systematics of oceanic basalts: implications for mantle compositions and processes, *in* Magmatism in ocean basins *edited by* AD Saunders and MJ Norry: Geological Society of London, Special Publications, v. 42, p. 313–345.
- Watson, EB and Harrison, TM 1983, Zircon saturation revisited: Temperature and composition effects in a variety of crustal magma types: *Earth and Planetary Science Letters*, v. 64, p. 295–304.

# Putting the horse in front of the cart: why exploration geoscience needs drilling

by

D Giles<sup>1,2</sup>

Let's start with a pat on the back to 150+ years of effective mineral exploration in Australia. We are good at finding mineral deposits, and our continent is well endowed with them. Global giants of the minerals industry were born and have thrived in Australia. Innovation is a calling card of the Australian minerals industry — and is a significant export industry in its own right. Exploration geoscience is strong (world leading!) in our research institutions and government organizations. Our surveys provide abundant, high-quality pre-competitive data. So why has Australia's share of the global mineral exploration budget halved (from ~1/4 to ~1/8) since the early to mid-1990s (Schodde, 2017), and why has the value:cost ratio of our exploration (Schodde, 2015) more than halved over the same period?

In addressing these questions I am going to play an old tune (you may have heard it before) but try to add a few embellishments that I hope will provide new insights into the problem and how we should address it. To summarize: 'cover' is the perceived problem, but our approach to exploring under cover has been the real problem. The limitations of that approach are psychological (we tend to be overly optimistic in our ability to *predict* the location of ore deposits), statistical (we have insufficient data to *detect* the location of ore deposits) and technical (we do not have the tools to efficiently sample the deep cover search space). My contention is that cost-efficient drilling and sampling (and the sense to know how to use it) provides the key to overcoming these limitations.

## Detection vs prediction

The distribution of exposed prospective rocks, drillholes, and known mineral deposits on the Australian continent (Fig. 1) is a graphic illustration of: 1) our exploration success when prospective rocks are exposed; 2) the relationship between drilling and discovery, and 3) the fact that we have barely scratched the surface in the covered search space. These plots underline the importance of *detection* in mineral exploration. The most densely sampled areas have benefited from a virtuous cycle of increasing data, improving understanding and reducing risk, which has led to efficient and effective exploration.

We know these areas well, they are data rich, we can recognize patterns, construct sophisticated models of the mineralizing systems, and make informed decisions about where to invest our exploration efforts and what tools to deploy. Detection in this sense is not restricted to direct detection of ore bodies. It includes measurement of any and all components of the system that influence decisions on where to explore (or indeed where not to explore) and what to do next. Based on this approach we have become confident (I would argue overconfident, perhaps better expressed as overly optimistic) that, if economic mineralization is present, we can find it.

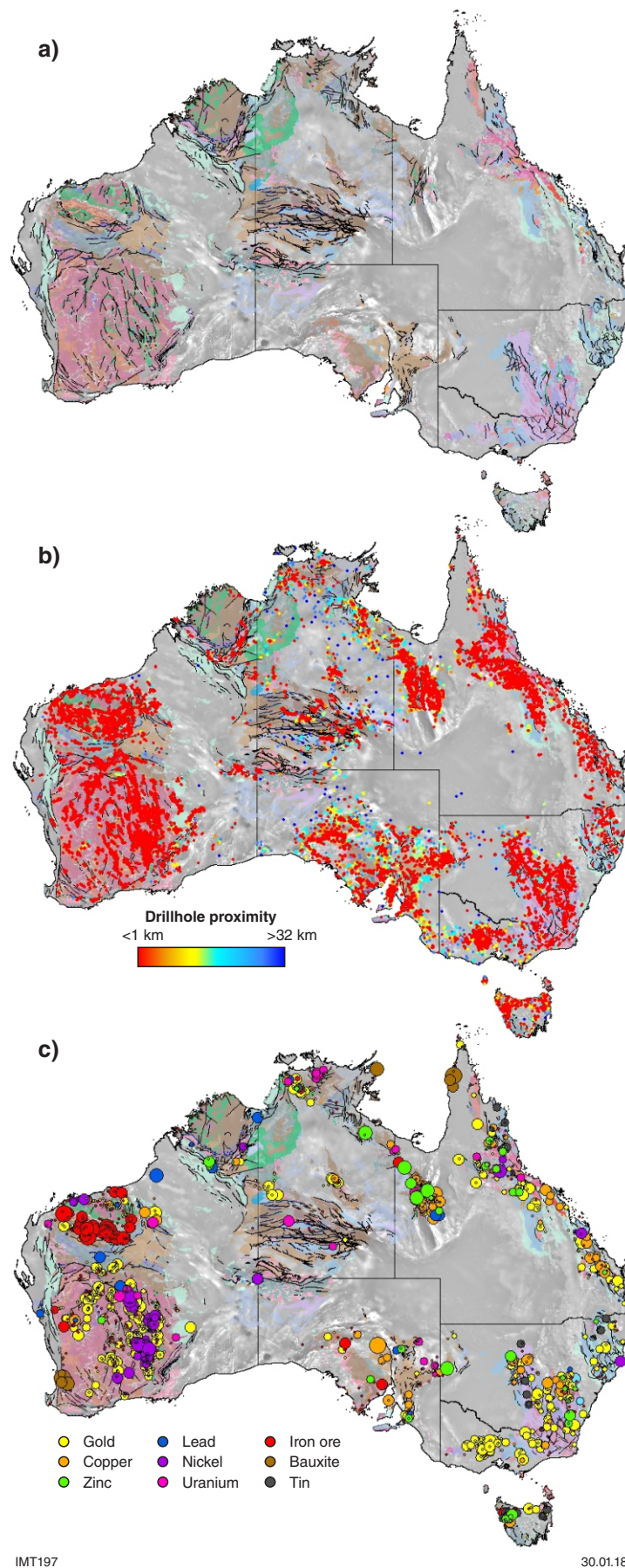
One expression of our overconfidence is the idea that *prediction* is an important component of discovery. It is an attractive idea. It adds an element of scientific mystery and places geoscientists in a position of rare influence in the exploration cycle. But it does not stack up. Prediction in its true form is a misnomer in mineral exploration — there are always some data informing exploration decisions — and, with analogies to seismology, prediction in complex geological systems is practically unfeasible. There may be different levels of data in terms of quantity or quality, and there may be different approaches to assessing and interpreting those data. Some operators have better systems in place to turn data into effective decisions and some of the decisions made may be based on little data and poor decision making, and thus be inherently speculative. They are not, however, predictive.

The mineral exploration community should move away from the language of prediction in the same way that the seismology community has done. Rather than attempting to predict the time, size and location of individual earthquakes, the seismologists focus on probabilistic 'forecasting' of earthquake risk. The latter is specifically designed to inform practical decisions (e.g. building standards, disaster plans) which can mitigate the hazard. The nature of earthquake forecasting (looking for spatial and temporal patterns in highly variable data, albeit backed by a sound understanding of the underlying scientific principles) brings attention to the importance of quantifying variability in complex systems.

---

1 Future Industries Institute, University of South Australia, Mawson Lakes, SA 5095, Australia

2 Deep Exploration Technologies Cooperative Research Centre, Adelaide Airport, SA 5950, Australia



IMT197

30.01.18

Figure 1. a) Simplified geology of the Australian continent. Exposed rocks of Paleozoic age and older are superimposed on greyscale total magnetic intensity; b) open-file drillholes extracted from the respective state geological survey online datasets overlain on simplified geology and magnetics. Drillholes are coloured by proximity to their nearest neighbour; red <1 km ranging to dark blue >32 km; c) known mineral deposits scaled roughly by size and coloured by major commodity

## Variability and sampling in under-cover exploration

Complex, inherently unpredictable spatial variability is a feature of mineral systems. Variability coupled with sparse sampling is a major source of uncertainty. The only way to decrease the uncertainty is to increase the frequency of sampling. The key question of relevance is: what frequency of sampling is required to reduce the uncertainty so as to adequately inform the next important decision? In under-cover exploration, faced with uncertainty and with inadequate tools (expensive drilling), to reduce uncertainty our tendency has been to fall back on a style of exploration towards the speculative end of the spectrum. For example: 1) build an exploration model based on known occurrences (that may or may not be relevant to the covered exploration space), 2) translate the model into an expression in one or more of the datasets that you have or can cheaply acquire (commonly aeromagnetics or gravity) to identify targets, 3) corroborate and prioritize with an independent dataset if possible, 4) drill with a view to collecting as much high-quality, detailed information from the hole as possible.

It would be unfair to ignore that this approach has led to discoveries — it has. But our declining rates of discovery and the displacement of exploration spending to better-exposed provinces argue that it is a flawed approach. Targets are limited to analogues of existing deposits; thus, we are not exposed to variations on a theme or new styles of mineralization. Targeting is very often based on proxies for mineralization rather than on mineralization itself and thus is beset with false positives, and the financially constrained ‘one-shot-in-the-chamber’ approach to drilling too often does not effectively inform the next level of decision making. The idea of capturing as much detailed information from the drillhole as possible is laudable but misplaced. It is an overinvestment to very precisely collect information that does not influence decision making. The ‘cart’ of targeting (one of the most important decisions in the exploration cycle) is being put before the ‘horse’ of data collection.

## It begins with more drilling

This brings us to a conundrum — better drillhole targeting requires reduced uncertainty, reduced uncertainty requires more sampling, more sampling requires drilling. But where do I drill? Three related concepts at the heart of our work in the Deep Exploration Technologies CRC (DET CRC) are that:

1. drilling should be a primary means of data collection in areas of deep cover, whereby the exact location of each drillhole is not as important as the overall drill pattern and spatial density of drilling
2. the density of drilling and the detail of data collected during drilling need only be sufficient to drive the next level of decision making (e.g. where to drill next)
3. the cost and speed of drilling and sampling is the single most important technical barrier to overcome.

The hope of DET CRC is that, having spent eight years developing technology (the RoXplorer® CT drilling rig and associated sensing platforms) designed to reduce the cost of drilling and sampling (horse before cart), we can engage with the exploration geoscience community (not least the geological surveys) to determine the required drilling and sampling parameters in various geological scenarios, and thus drive a fundamental change in our approach to under-cover exploration.

Why does exploration geoscience need (cost-efficient) drilling (as a reconnaissance exploration tool)? Without drilling, vast tracts of potentially prospective geology will remain largely unknown and will attract only sporadic and inefficient exploration. With it, we can facilitate the same virtuous cycle of data acquisition, systems understanding, and risk reduction that has underpinned exploration success in our exposed mineral provinces.

## References

- Schodde, 2015, Review of Australia's discovery performance of the last 40 years: Presentation to Australian Institute of Geoscientists Seminar on Value Creation via Exploration, Perth, 13 July 2015, <[www.minexconsulting.com/publications.html](http://www.minexconsulting.com/publications.html)>.
- Schodde, 2017, Recent trends and outlook for global exploration: Presentation to Prospectors and Developers Association Canada, Toronto, 6 March 2017, <[www.minexconsulting.com/publications.html](http://www.minexconsulting.com/publications.html)>.



# Compatibility of ground and airborne gravity data in the Western Australia ‘Generation 2’ reconnaissance gravity mapping project

by

SHD Howard

## Introduction

The first Gravity Map of Australia published in 1976 by the then Australian Bureau of Mineral Resources, Geology and Geophysics (BMR) was a seminal product in Australia and the world (Anfiloff et al., 1976; BMR, 1976). More than 40 years later, the underlying ‘first generation’ data — mostly at 11 km station spacing — still provided the best coverage available over a substantial part of the continent.

It was not until the late 1990s that advances in technology served to bring down gravity survey costs substantially and heralded a ‘second generation’ of regional ground gravity surveys by Australian geological surveys at a quasi-standard station spacing of 4 km. In 2005, the Geological Survey of Western Australia (GSWA) adopted a nominal 2.5 km station spacing for its own systematic program of second-generation ground gravity surveys. Working together with Geoscience Australia (GA), coverage of the southwestern half of the state was complete by 2016.

With ground access in the north and east of the State becoming increasingly difficult, GSWA turned to the use of airborne gravity surveys after an assessment of existing datasets led to the conclusion that airborne surveys at a line spacing of 2.5 km should provide ‘interpretability equivalence’ with regional ground surveys on a 2.5 km grid of stations.

In June 2016, GSWA and GA contracted Sander Geophysics Limited (SGL) to conduct an airborne gravity survey with its AIRGrav system over approximately 84 000 km<sup>2</sup> in the east Kimberley region of Western Australia. All data and the survey operations and processing reports are contained in the GSWA data delivery package (Fig. 1; Sander Geophysics Ltd, 2017).

Further results and interpretation from that survey, and assessment of the suitability of airborne gravimetry for capturing regional gravity data, were presented at the Australian Exploration Geoscience Conference, Sydney, 18–21 February 2018.

## Compatibility of airborne and ground data

Comparisons of two airborne Bouguer anomaly profiles with coincident profiles of ground data at 1 km spacing from a 2007 survey show a match to within 1%. Grids made from both datasets demonstrate equally good correspondence.

From 18 passes during the course of the survey over a 50 km test line, the linear precision of the Bouguer gravity data after filtering with a 100-second low-pass filter is about 0.5 mGal (Fig. 2). A similar figure is obtained for the overall survey precision based on traverse tie-line intersections after final 2D spatial filtering to smooth the data to the nominal target survey spatial resolution of 5 km. This is about the same as the ‘sampling precision’ of regional ground surveys at 2.5 km station spacing demonstrated in an analysis of ground data from the Kauring gravity test range (Elieff, 2017).

The mean values from the test line were used to check along-line spatial resolution of the airborne data in comparison with two well-defined anomalies from ground measurements (‘N’ and ‘B’ in road data, Fig. 2a). As expected, the airborne data after filtering cannot fully resolve features less than the nominal 5 km full-wavelength resolution of the filter (Fig. 2b). This implies that apparent anomalies in the airborne data with wavelengths about 5 km must be regarded with caution if the amplitude is less than about 2.0 mGal (4 standard deviations of the precision measure of 0.5 mGal). Anomalies of amplitude greater than this are likely to be real; however, they may be the attenuated response of a narrow anomalous density contrast rather than the ‘true’ ground amplitude response of a broader feature. Features wider than 5 km appear to be well resolved in both amplitude (within the limits of the data precision) and wavelength. At a whole-of-survey level, the new data incorporate seamlessly into the Western Australia State gravity 400 m-cell compilation grid (Brett, 2017).

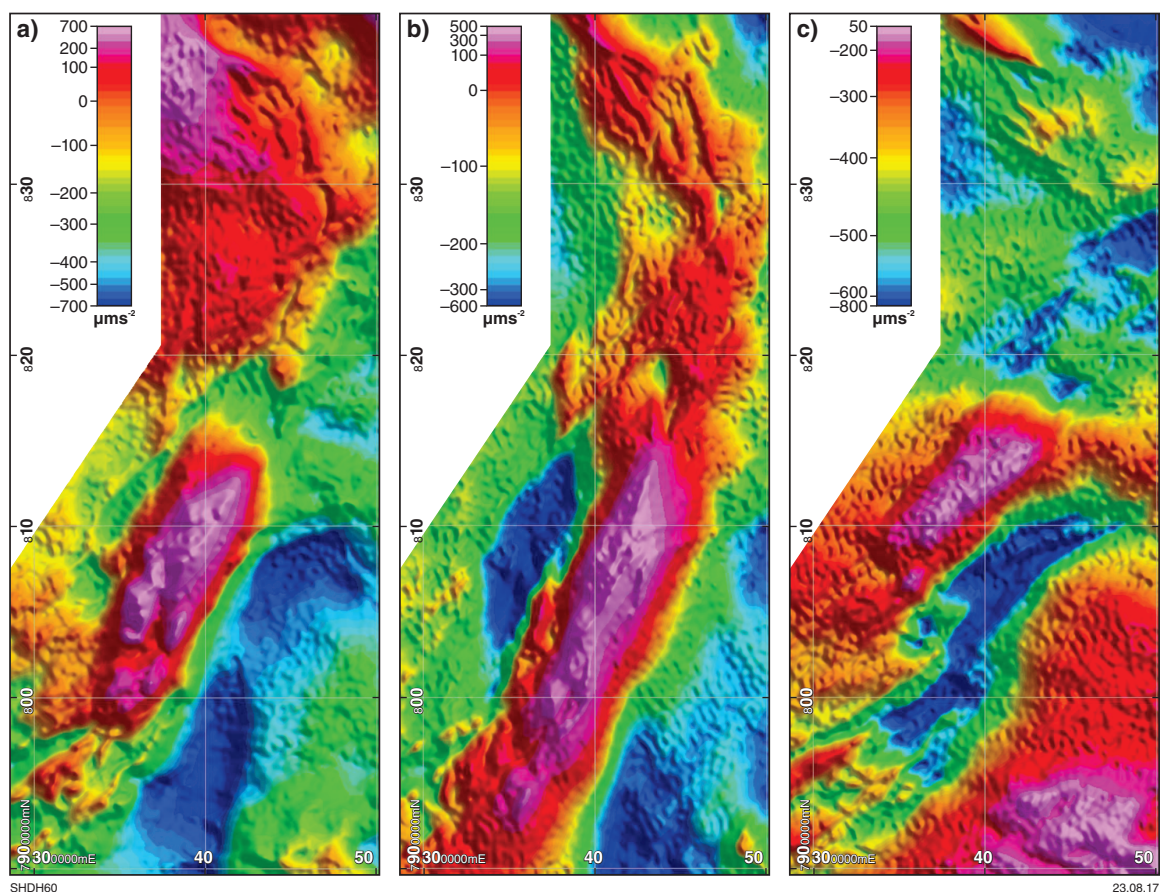


Figure 1. East Kimberley Bouguer anomaly vector components: a) vertical; b) east; c) north. Coordinates in MGA Zone 52

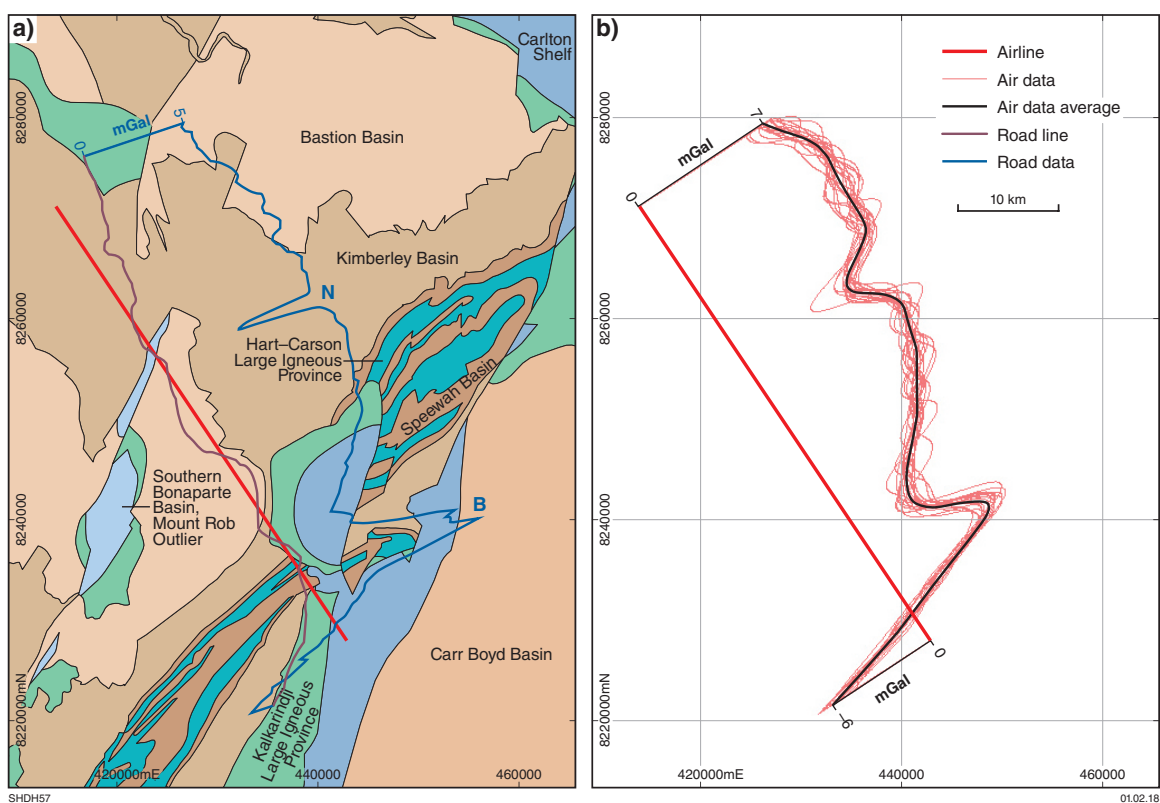


Figure 2. a) Location of airborne test line in relation to ground traverse on local geology (for geology detail and legend see GSWA, 2016). Ground Bouguer anomaly profile with 400 m stations; b) airborne Bouguer anomaly profiles after 100 s (5000 m) filter from 18 passes (red) and average (black)

## Conclusions

By all measures, the east Kimberley survey met the expectations of both GSWA and GA to the extent that they commissioned two new aerogravity surveys in 2017: a Falcon gravity gradiometer survey over the Kidson Sub-basin for the delivery of computed vertical gravity, and a GT-2A survey over the Tanami and northeast Canning Basin. Additional surveys in the Paterson Orogen, and over the Kimberley, Gunbarrel and Officer Basins, are presently under consideration for 2018–19.

The responses tendered for the 2017 and 2018 surveys indicate that prices for large aerogravity surveys are trending downwards, so that they are becoming increasingly cost-competitive with ground surveys at this scale. If present funding levels remain, GSWA would hope to complete second-generation gravity coverage of Western Australia by 2020.

## References

- Anfiloff, W, Barlow, BC, Murray, A, Denham, D and Sandford, R 1976, Compilation and production of the 1976 1:5 000 000 Gravity Map of Australia: BMR Journal of Australian Geology and Geophysics, v. 1, p. 273–276.
- Bureau of Mineral Resources (BMR) 1976, Gravity Map of Australia, 1:5 000 000: Australian Bureau of Mineral Resources (Geoscience Australia), Canberra, <<https://data.gov.au/dataset/compilation-and-production-of-the-1976-1-5-000-000-gravity-map-of-australia>>.
- Brett, JW 2017, 400 m gravity merged grid of Western Australia 2017 version 1: Geological Survey of Western Australia, <[www.dmp.wa.gov.au/geophysics](http://www.dmp.wa.gov.au/geophysics)>.
- Elieff, S 2017, An illustration of the impact of sampling on precision: Australian Society of Exploration Geophysics, Preview 2017, v. 190, p. 55–56.
- Geological Survey of Western Australia (GSWA) 2016, 1:500 000 State interpreted bedrock geology of Western Australia, 2016: Geological Survey of Western Australia, <[www.dmp.wa.gov.au/geoview](http://www.dmp.wa.gov.au/geoview)>.
- Sander Geophysics Ltd, 2017, Technical report, east Kimberley airborne gravity survey, Western Australia 2016 for Geoscience Australia: [Dataset and Report], in Geological Survey of Western Australia airborne geophysics database, MAGIX registration no. 71156, <[www.dmp.wa.gov.au/magix](http://www.dmp.wa.gov.au/magix)>.



# Looking beneath the Canning Basin: new insights from geochronology, seismic and potential-field data

by

PW Haines, MTD Wingate, Y Zhan and DW Maidment

The onshore Phanerozoic Canning Basin covers an extensive area of northern Western Australia. Although there has been some mineral exploration under thin cover around the margins of the Canning Basin, mainly near Telfer, the nature and age of basement beneath the deeper parts of the Canning Basin is speculative. A few deep petroleum exploration wells do penetrate basement, mainly on the Lennard Shelf, Broome Platform and Barrow Terrace. Recent advances in knowledge of the

basement include new geochronology from selected wells, and new deep crustal seismic data, with further seismic acquisition planned. Extensive coverage by new airborne gravity surveys will be available early in 2018. Currently available data have been used to update the Canning Basin SEEBASE (Structurally Enhanced view of Economic BASEment) model including basement topography (depth to basement) and interpretations of basement composition and structure (Fig. 1).

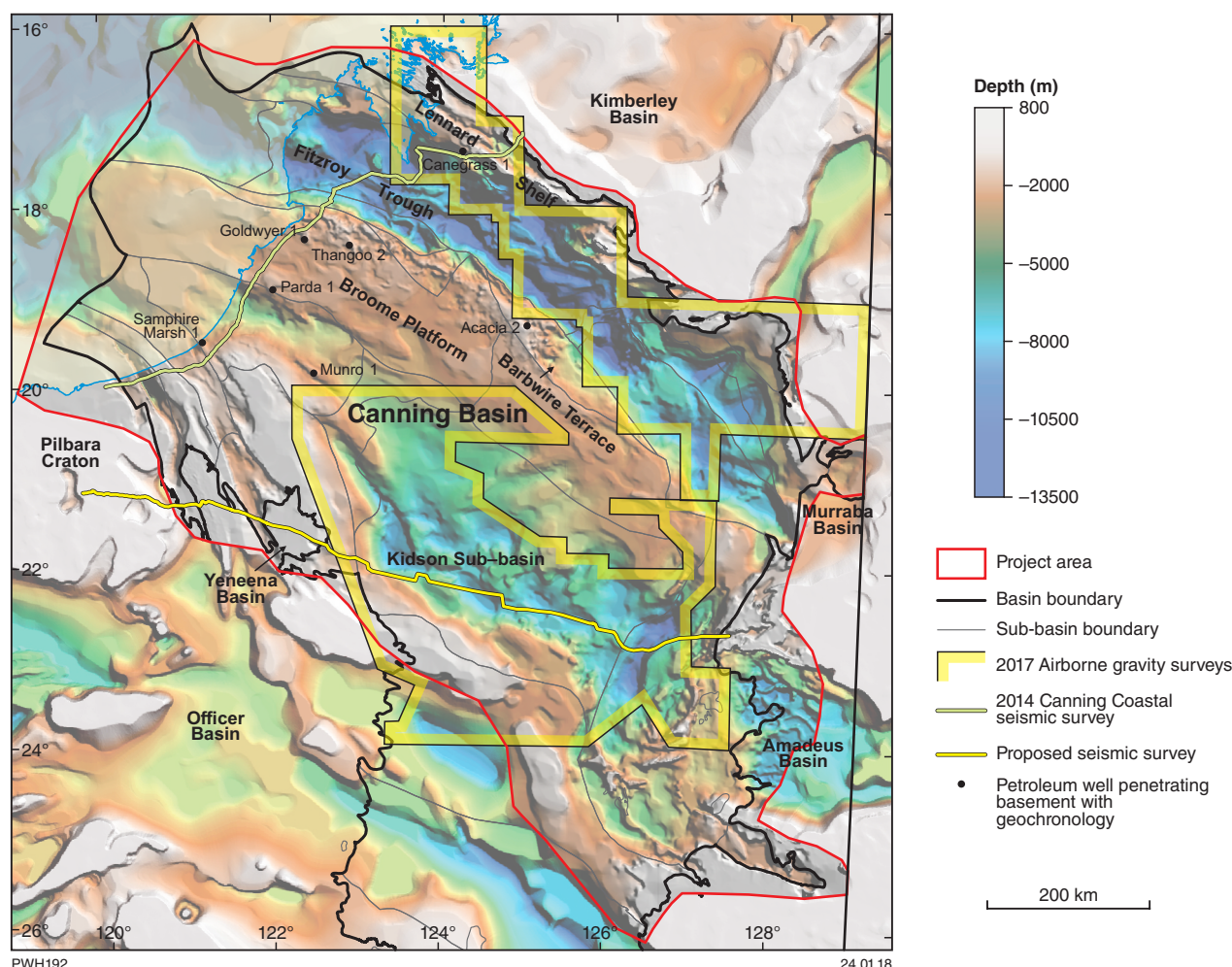


**Figure 1.** 2017 SEEBASE image for the Canning Basin project area with 2005 SEEBASE image as background. The image is coloured for modelled basement depth (sediment thickness). Thin extensions of the Canning Basin over older sedimentary successions in the south were excluded from the study. Map includes outline of 2017 airborne gravity surveys, the 2014 Canning Coastal seismic survey, the proposed survey across the southern Canning Basin, and locations of petroleum wells with basement geochronology

## Basement geochronology

Although mineral exploration drillholes locally intersect relatively shallow basement near the edge of the Canning Basin, only petroleum exploration wells intersect deeper basement farther inboard. Recent SHRIMP U–Pb zircon geochronology on magmatic and metasedimentary basement rocks penetrated in selected petroleum wells near the Canning Coastal seismic survey (Fig. 1) provides new insight into the age of the basement directly below the basal unconformity (Figs 2, 3; Table 1). An igneous crystallization age of  $654 \pm 3$  Ma (Fig. 2b) for granitic rock in Goldwyer 1 is within the age range reported for granitic rocks of the O’Callaghans Supersuite (678–607 Ma; Maidment, 2017) in the Telfer area of the Paterson Orogen. However, this well is more than 300 km north of the northernmost outcrops of O’Callaghans Supersuite along the southwestern edge of the Canning Basin. Granitic rock in Samphire Marsh 1 has an igneous crystallization age of  $505 \pm 4$  Ma (Fig. 2a), whereas the dominant group of inherited zircons in the same rock yields a weighted mean age of  $653 \pm 7$  Ma, similar to the age of the granitic rock in Goldwyer 1. A pegmatite vein intruding schist in Parda 1 yields a  $^{207}\text{Pb}/^{206}\text{Pb}$  age of  $537 \pm 13$  Ma (Fig. 2c).

These Cambrian ages are significantly younger than previously known felsic igneous events in the region, with the possible exception of the  $512.5 \pm 4.3$  Ma U–Pb baddeleyite date reported by Jourdan et al. (2014) for granodiorite basement in Munro 1. The baddeleyite is presumably hosted within the abundant mafic enclaves in this rock, and Jourdan et al. (2014) suggested a connection with the  $510.7 \pm 0.6$  Ma mafic Kalkarindji Large Igneous Province. Subsidence associated with the Samphire Marsh Extension, which resulted in the initial formation of the Canning Basin, is no younger than early Ordovician (Tremadocian; 485–478 Ma), the biostratigraphic age of the oldest marine sedimentary unit in the Nambeet Formation (Nicoll, 1993). The relatively short period separating mafic–felsic magmatism and sedimentation might indicate that Cambrian magmatism reflects an early phase of extension related to initiation of the basin. In central Australia, bimodal magmatism at c. 520 Ma is interpreted to be related to an early stage of rifting focused between the Amadeus and Georgina Basins that also culminated in the early Ordovician, possibly reflecting a continent-scale extensional event (Maidment et al., 2013).

The age of the youngest detrital zircon in metasedimentary rocks in Thangoo 2,  $953 \pm 21$  Ma ( $1\sigma$ ), is similar to the youngest date of  $961 \pm 29$  Ma ( $1\sigma$ ) previously reported from Acacia 2 (Wingate and Haines, 2009; Fig. 3a,b). Both samples show detrital zircon age spectra similar to those of sedimentary successions of the lower Yeneena Basin (Bagas and Nelson, 2007) and lower Murraba Basin (Haines and Allen, 2017) exposed along the southern and eastern margin of the Canning Basin, respectively. Both are components of the Neoproterozoic–Paleozoic Centralian Superbasin. The granitic rock in Samphire Marsh 1 and pegmatite in Parda 1 contain early Neoproterozoic inherited zircons (Fig. 2a,c) presumably derived from the terrane they intrude. These observations suggest that tectonized components of the Centralian Superbasin may be widespread beneath the Canning Basin, at least south of the Fitzroy Trough. In contrast,

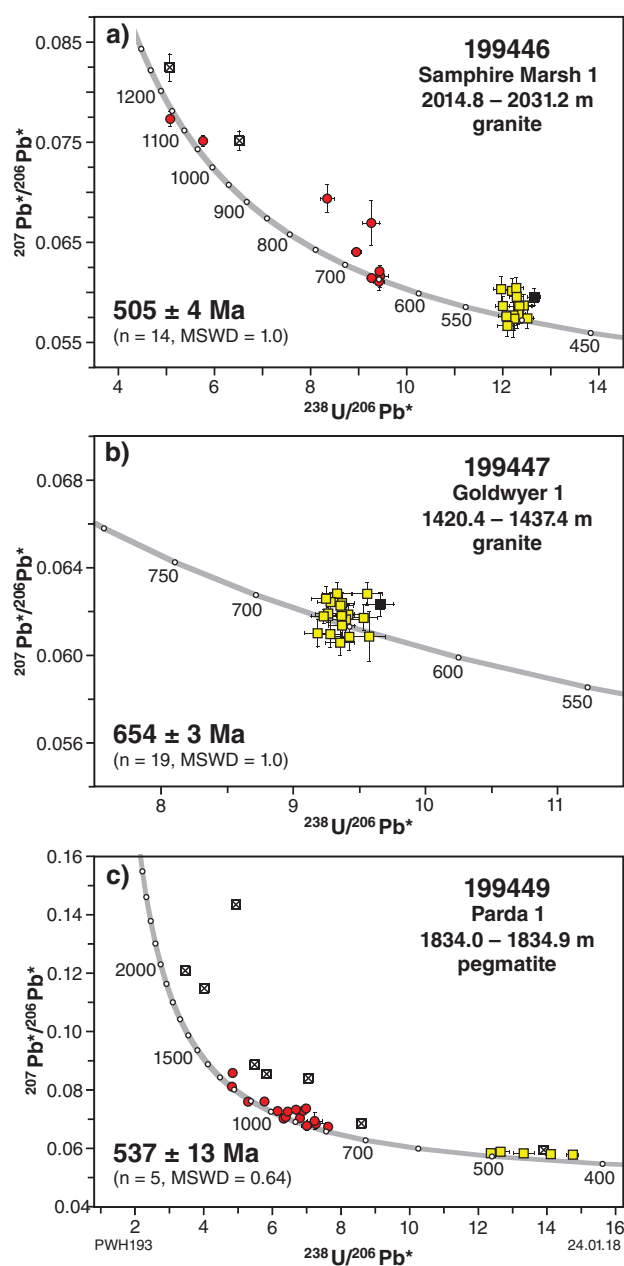


**Figure 2.** U–Pb analytical data for magmatic zircons (yellow squares) and inherited zircons (red circles) in igneous basement rocks from Canning Basin petroleum wells. Black squares indicate analyses affected by Pb loss and crossed squares indicate data with discordance >5%. Weighted mean ages are quoted with 95% uncertainties; Pb\*, radiogenic Pb

a basement metasedimentary breccia from Canegrass 1 on the Lennard Shelf of the northern Canning Basin has no zircons younger than  $1791 \pm 13$  Ma ( $1\sigma$ ; Fig. 3c) and an age spectrum similar to those for samples from the Paleoproterozoic Kimberley Basin reported by Phillips et al. (2017). This suggests that the Kimberley Basin directly underlies the Canning Basin in this area and that sedimentary rocks of the Centralian Superbasin were either not deposited there, or were uplifted and eroded prior to the Paleozoic.



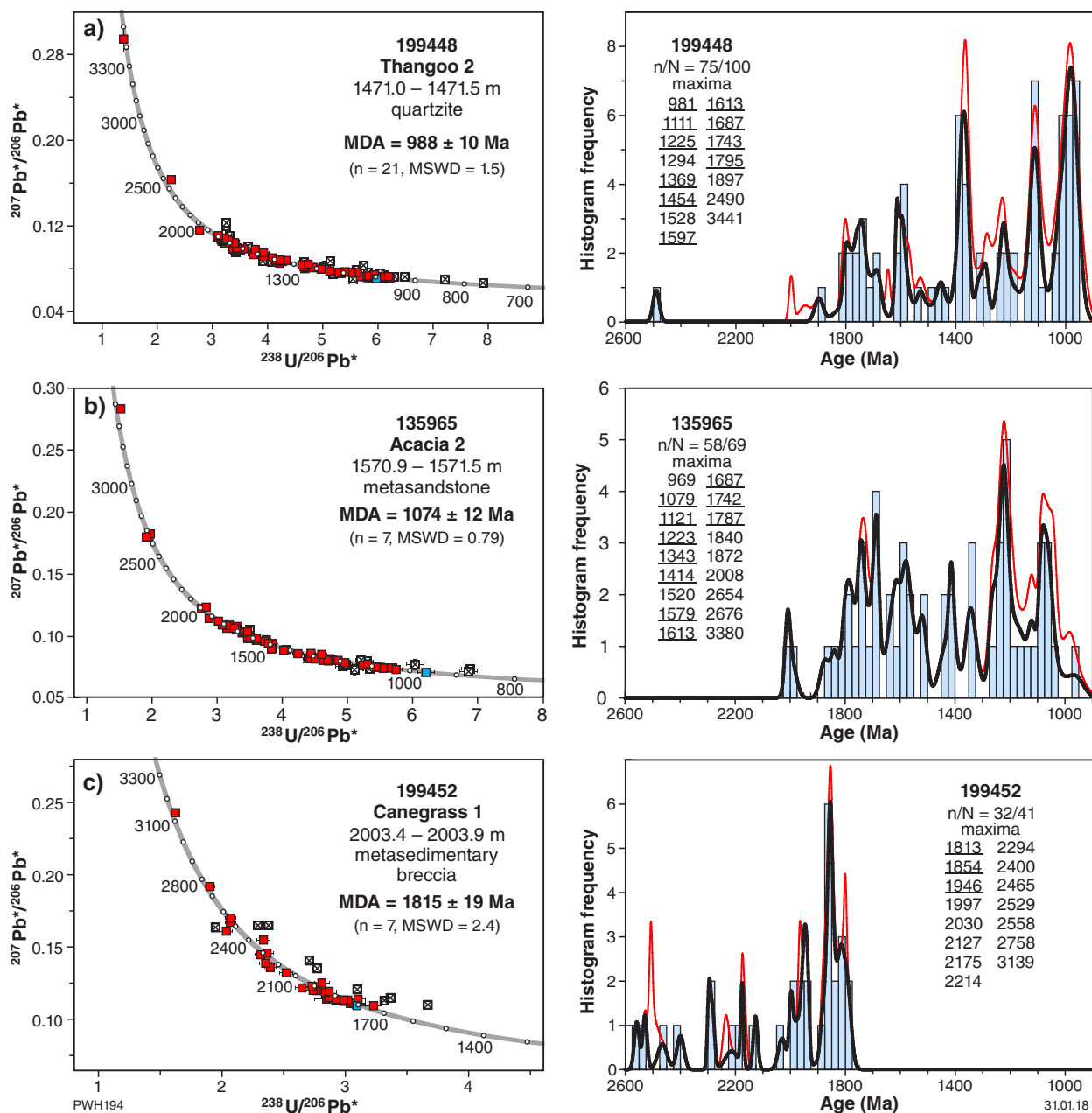


**Figure 3.** U–Pb analytical data (left) with corresponding probability density diagrams and histograms (right) for detrital zircons in metasedimentary basement rocks from Canning Basin petroleum wells. Crossed squares indicate data with discordance >5%. MDA is maximum depositional age expressed as weighted mean age of the youngest group (uncertainties are 95%, n = number of zircons in youngest group). Thick black probability curve, maxima values, and frequency histograms include only data <5% discordant; thin red curve includes all data (n/N = number of analyses <5% discordant/total number analyses). Significant age components (based on three or more dates) are underlined

## New Canning Basin SEEBASE study

During 2017, Frogtech Geoscience produced an updated SEEBASE study and ArcGIS package of the Canning Basin recently released as Geological Survey of Western Australia (GSWA) Report 182 (Frogtech Geoscience, 2017). SEEBASE is a map of the depth to economic basement (from a petroleum perspective), and this update is based on the latest potential-field, seismic, and other datasets. The result is a substantial increase in the resolution of the Canning Basin depth-to-basement

model (Fig. 1) compared to the 2005 OZ SEEBASE (Frog Tech, 2005). The revised SEEBASE basement topography model provides a new view of basin geometry as a foundation upon which to build basin, petroleum systems, and exploration models. The study also provides an interpretation of underlying basement terranes, their structure and tectonic evolution. This includes maps of basement composition, crustal thickness, depth to Moho, and basement-derived heat flow. The SEEBASE product is designed to be easily reviewed and updated as new data, such as the current and future gravity and seismic survey data discussed below, become available.

**Table 1. U–Pb ages from Canning Basin basement in petroleum exploration wells**

GSWA sample ID	Well name	Sample depth	Lithology	Age	Reference
<b>Igneous crystallization zircon ages</b>					
199446	Samphire Marsh 1	2014.7 – 2031.2 m cuttings	granite	505 ± 4 Ma	GSWA, in prep.
199447	Goldwyer 1	1420.4 – 1437.4 m cuttings	granite	654 ± 3 Ma	GSWA, in prep.
199449	Parda 1	1834.0 – 1834.9 m	pegmatite	537 ± 13 Ma	GSWA, in prep.
<b>Detrital zircon ages</b>					
199448	Thangoo 2	1471.0 – 1471.5 m	quartzite	953 ± 21 Ma <sup>1</sup> 988 ± 10 Ma <sup>2</sup>	GSWA, in prep.
135965	Acacia 2	1570.9 – 1571.5 m	metasandstone	961 ± 29 Ma <sup>1</sup> 1074 ± 12 Ma <sup>2</sup>	Wingate and Haines, 2009
199452	Canegrass 1	2003.4 – 2003.85 m	metasedimentary breccia	1791 ± 13 Ma <sup>1</sup> 1815 ± 19 Ma <sup>2</sup>	GSWA, in prep.
<b>Igneous crystallization baddeleyite age</b>					
135990 (= B01)	Munro 1	2113.5 – 2115.6 m	granodiorite	512.5 ± 4.3 Ma	Jourdan et al., 2014

NOTES: 1. Age of youngest detrital zircon (1 $\sigma$ )

2. Weighted mean age of youngest detrital age component; all mean ages are quoted with 95% confidence intervals

## Deep crustal seismic and airborne gravity

A collaboration between Geoscience Australia and GSWA to acquire a deep crustal reflection seismic survey across the southern Canning Basin and surrounding basement terranes is currently in the planning stage. The survey will ideally extend west from the western edge of the Arunta Orogen, across the southern Canning Basin (mainly Kidson Sub-basin) and Paterson Orogen near Telfer, to the Pilbara Craton (Fig. 1). The proposed survey would use an existing east–west road corridor across central Western Australia, which is well located to investigate southern Canning Basin depocentres interpreted by the new SEEBASE model. Apart from providing an unprecedented transect across the southern Canning Basin, the survey should be capable of imaging major basement structures and provide new insights into the nature of basement through this area. Passive seismic monitoring stations along the line are also proposed. An earlier deep crustal reflection survey was acquired in 2014, also in collaboration with Geoscience Australia. Referred to as the Canning Coastal seismic survey (Fig. 1), it provides a transect normal to major basement structures across the western Canning Basin (Zhan, 2017). In-progress reprocessing of part of this line aims to enhance imaging of basement structure. A passive seismic survey along the same route is currently underway in collaboration with the Institute of Geology and Geophysics of the Chinese Academy of Sciences, Macquarie University, and The University of Western Australia. The survey will yield valuable data about the deep structure of the crust beneath the Canning Basin, and the nature of fundamental terrane boundaries. Data from 2017 airborne gravity surveys over major depocentres of the Canning Basin (Fig. 1) are scheduled for release in early 2018. These should provide further insights into deep crustal terrains beneath the Canning Basin.

## References

- Bagas, L and Nelson, DR 2007, Provenance of Neoproterozoic sedimentary rocks in the northwest Paterson Orogen, Western Australia, *in* Proceedings of the Central Australian Basins Symposium (CABS), Alice Springs, Northern Territory, 16–18 August 2005 *edited by* TJ Munson and GJ Ambrose: Northern Territory Geological Survey, Special Publication 2, p. 1–10.
- FrOG Tech Pty Ltd 2005, OZ SEEBASE™ Study 2005 — Public Domain Report to Shell Development Australia, 174p.
- Frogtech Geoscience, 2017, 2017 Canning Basin SEEBASE study and GIS data package: Geological Survey of Western Australia, Report 182, 297p.
- Haines, PW and Allen, HJ 2017, Geological reconnaissance of the southern Murraba Basin, Western Australia: Geological Survey of Western Australia, Record 2017/4, 38p.
- Jourdan, F, Hodges, K, Sell, B, Schaltegger, U, Wingate, MTD, Evins, LZ, Söderlund, U, Haines, PW, Phillips, D and Blenkinsop, T 2014, High-precision dating of the Kalkarindji large igneous province, Australia, and synchrony with the Early–Middle Cambrian (Stage 4–5) extinction: *Geology*, v. 42, no. 6, p. 543–546, doi:10.1130/G35434.1.
- Maidment, DW, Hand, M and Williams, IS 2013, High grade metamorphism of sedimentary rocks during Palaeozoic rift basin formation in central Australia: *Gondwana Research*, v. 24, no. 3–4, p. 865–885.
- Maidment, DW 2017, Geochronology from the Rudall Province, Western Australia: implications for the amalgamation of the West and North Australian Cratons: Geological Survey of Western Australia, Report 161, 95p.
- Nicoll, RS 1993, Ordovician conodont distribution in selected petroleum exploration wells, Canning Basin, Western Australia: Australian Geological Survey Organisation, Record 1993/17, 136p.
- Phillips, C, Maidment, DW and Lu, Y-J 2017, Revised tectono-stratigraphy of the Kimberley Basin, northern Western Australia, *in* GSWA 2017 Extended abstracts: promoting the prospectivity of Western Australia: Geological Survey of Western Australia, Record 2017/2, p. 33–37.
- Wingate, MTD and Haines, PW 2009, 135965: phyllitic metasandstone, Acacia 2; Geochronology Record 780: Geological Survey of Western Australia, 5p.
- Zhan, Y 2017, Canning Coastal seismic survey — an overview of the Canning Basin: Geological Survey of Western Australia, Record 2017/5, 29p.

# Western Australia: a battery metal powerhouse

by  
TJ Beardsmore

## Driving the battery-world economy

The generally improving individual wealth and living standards of the world's population are creating ever greater demands for energy, mobility and consumer goods, but there is also an increased awareness of anthropogenic pollution in the natural environment, and a desire to significantly mitigate this. Society is consequently moving towards greater use of renewable energy sources to power residential, retail and industrial centres, the global transportation network that connects these, and the burgeoning constellation of portable electronics.

Renewable energy sources are commonly periodic or transient in nature, which necessarily requires the use of rechargeable batteries to store and regulate the distribution of this energy. A battery comprises two electrodes (anode and cathode) made of different materials (single elements or multi-element compounds), connected by a cation-conducting fluid or gel electrolyte, but insulated against direct electron flow between electrodes, all contained in a casing (Fig. 1a). Battery component materials and architecture optimize application-specific characteristics such as terminal voltage, mass, energy density (amount of stored energy per unit mass or volume), durability, cost and safety, within constraints imposed by cost of raw materials and manufacturing, stability of component mixes, reversibility of electrochemical reactions (rechargeability), and operating temperature ranges. The variety of possible battery chemistries is enormous, and continually expanding, collectively using a significant proportion of the periodic table (notably aluminium, antimony, arsenic, barium, cadmium, carbon, calcium, cobalt, iron, lanthanum, lead, lithium, manganese, nickel, phosphorus, selenium, sodium, sulfur, tin, titanium, vanadium and zinc).

There has been widespread use of so-called lithium-ion batteries because there is no practical constraint on their size, they are comparatively light, have voltages, energy densities and recharge rates generally exceeding those of other battery types, and their cost of manufacture is falling. Lithium is used as the charge-transport cation because it is efficiently released from and absorbed into the structure of the electrodes during discharge and recharge. However, the bulk of any Li-ion battery comprises many other materials. Those batteries with the highest energy density — suitable for large-scale

grid power storage, and powering hybrid petrol–electric and fully electric vehicles — use significant amounts of nickel, cobalt, manganese, aluminium and graphite (Table 1; Fig. 1b).

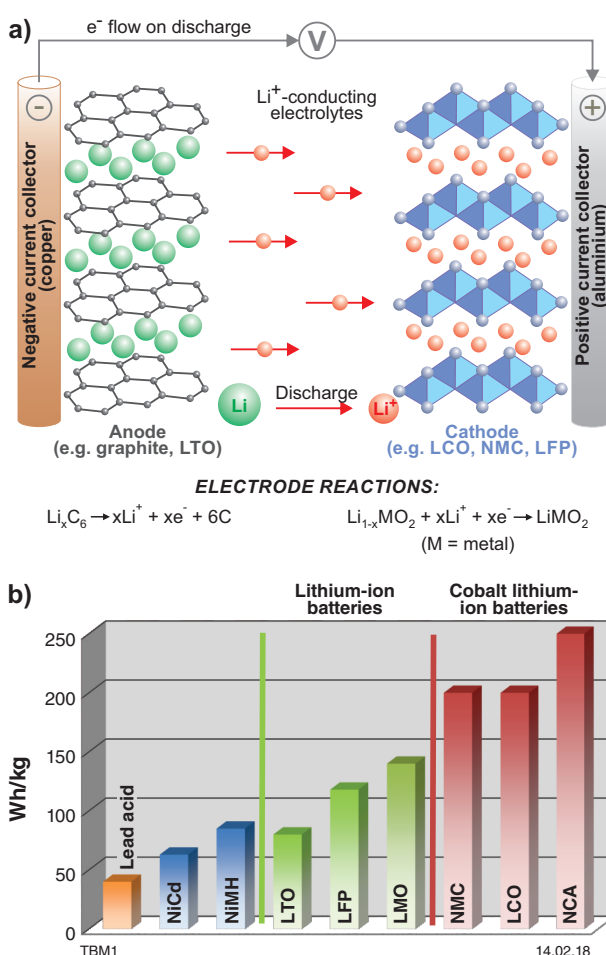


**Figure 1.** A synopsis of selected characteristics of (Li-ion) batteries: a) schematic architecture and electrode reactions (modified after Wiaux and Chanson, 2013); b) typical specific energies for common battery types. Abbreviations: NiCd, nickel–cadmium; NiMH, nickel–metal hydride; other abbreviations as per Table 1; modified after Battery University (2017, fig. 15)

**Table 1. Common Li-ion battery types, listing cathode composition and typical applications (compiled from Battery University, 2017). High-capacity types currently favoured for mobile devices, electric vehicles and grid power storage in bold**

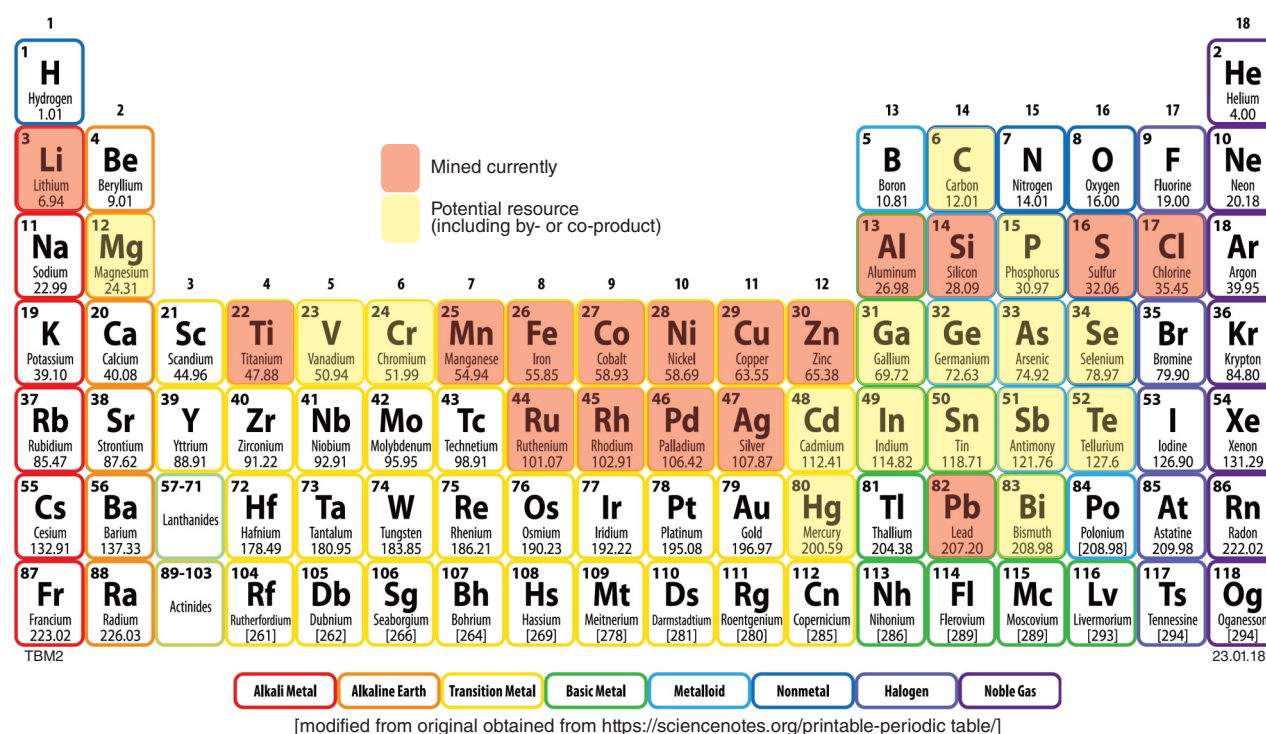
Chemical name (abbreviation)	Cathode material	Anode material	Nominal voltage per cell (V)	Specific energy (Wh/kg)	Applications
<b>Lithium cobalt oxide (LCO)</b>	<b>LiCoO<sub>2</sub></b>	<b>graphite</b>	<b>3.60</b>	<b>150–200</b>	<b>Mobile phones, tablets, laptops, cameras</b>
Lithium manganese oxide (LMO)	LiMn <sub>2</sub> O <sub>4</sub>	graphite	3.70, 3.80	100–150	Power tools, electric vehicles, medical devices, hobbyist
Lithium iron phosphate (LFP)	LiFePO <sub>4</sub>	graphite	3.20, 3.30	90–120	Power tools, electric vehicles, medical devices, hobbyist
<b>Lithium nickel manganese cobalt oxide (NMC)</b>	<b>LiNiMnCoO<sub>2</sub></b>	<b>graphite</b>	<b>3.60, 3.70</b>	<b>150–220</b>	<b>Power tools, electric vehicles, medical devices, hobbyist</b>
<b>Lithium nickel cobalt aluminium oxide (NCA)</b>	<b>LiNiCoAlO<sub>2</sub></b>	<b>graphite</b>	<b>3.60</b>	<b>200–260</b>	<b>Electric vehicles, grid storage, medical devices</b>
Lithium titanate (LTO)	LMO or NMC cathode	Li <sub>4</sub> Ti <sub>5</sub> O <sub>12</sub>	2.40	50–80	Electric vehicles, grid storage, solar street lighting

## Battery metal contributions from Western Australia

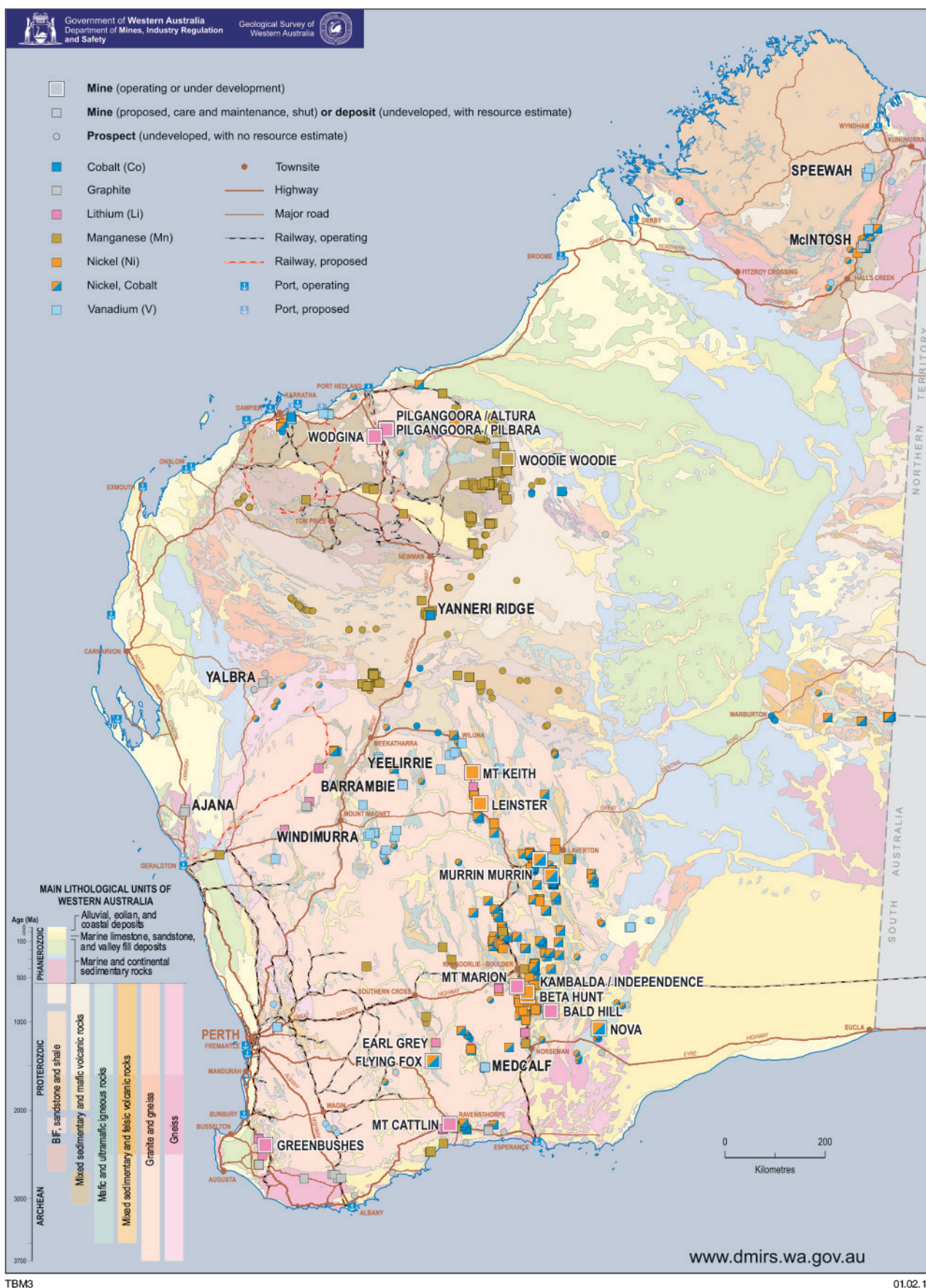
Western Australia can now, or could in the future, supply many if not most commodities required by the battery manufacturing industry (Figs 2, 3). In light of recent commercial emphasis on the development of Li-ion battery technology, Western Australia's actual or potential contribution is herein illustrated for six currently prominent metals used in such batteries — lithium, graphite (though not technically a metal), nickel, cobalt, manganese and vanadium (Table 2).

**Lithium** is primarily sourced from pegmatites and evaporitic lake brines (Dill, 2010). Western Australia has no known brine deposits, but is well endowed with

lithian pegmatites (Fig. 3), including the world's largest single deposit (at Greenbushes). The State has four operating lithium mines at Greenbushes (Talison Lithium Pty Ltd), Mt Marion (Reed Industrial Minerals Pty Ltd), Mt Cattlin (Galaxy Resources Ltd), and Wodgina (Mineral Resources Ltd), and has been the world's largest lithium producer since 2013 (ahead of Chile, Argentina and China), contributing 41% (14.3 kt) of global supply in 2016 (Jaskula, 2017). Rising demand and projected consumption for lithium have driven prices upwards and impelled a surge in lithium exploration and development that, in Western Australia, has yielded significantly increased resources (11.6 Mt at the end of 2017; Fig. 4a; Table 2), ranking fourth globally in 2016 (behind Argentina, Chile, and China; Jaskula, 2017).

**Figure 2. Periodic table of the elements (sans lanthanides and actinides), highlighting those commonly used in batteries, and that now are, or may in the future be, mined in Western Australia**





TBM3

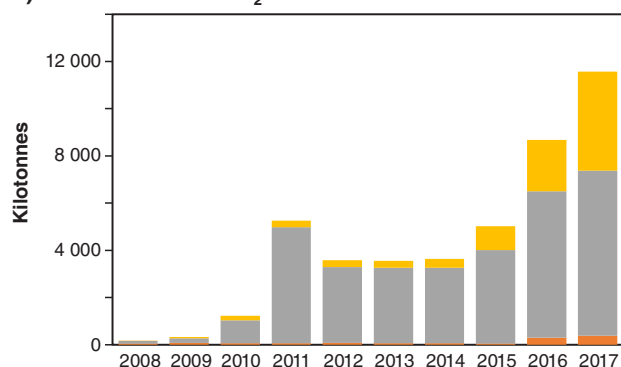
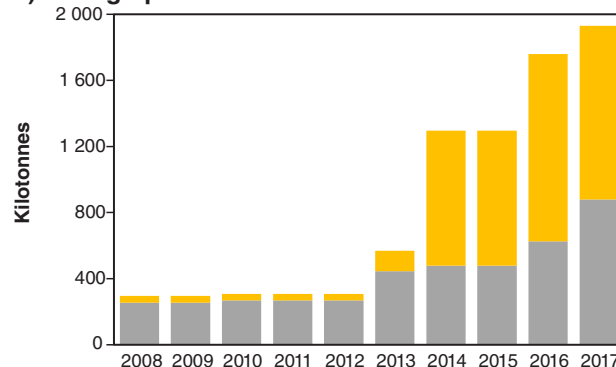
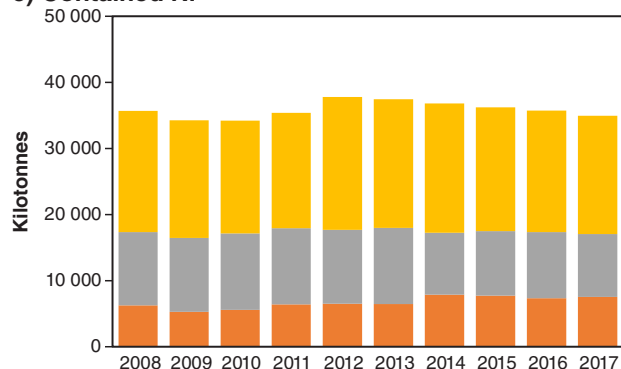
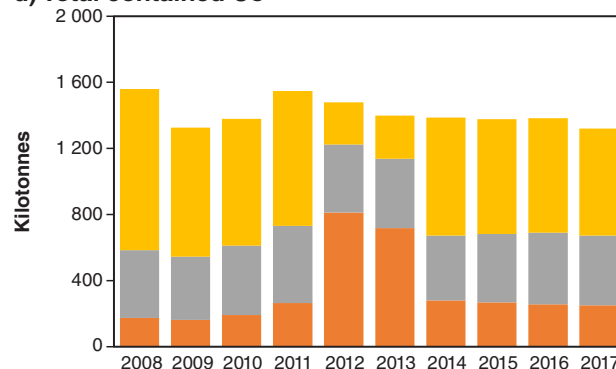
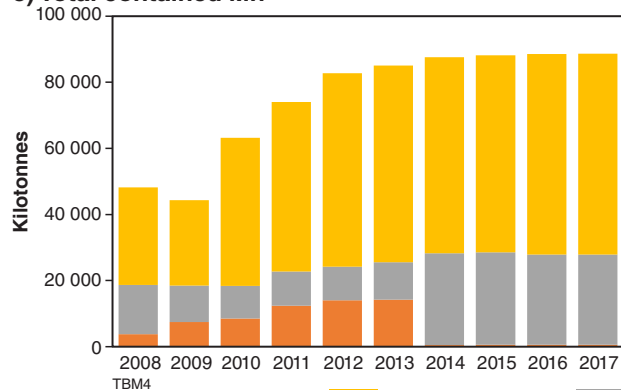
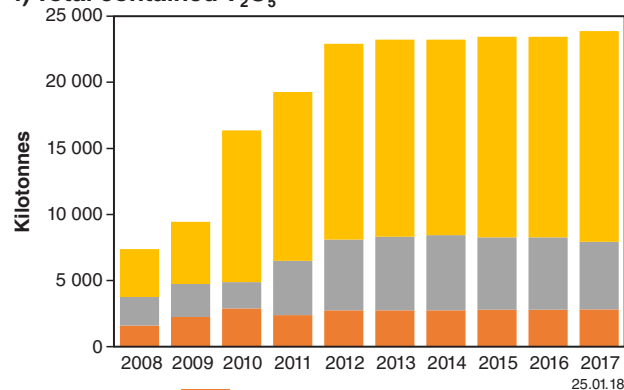
01.02.18

**Figure 3. Significant Western Australian deposits and other occurrences of the six prominent 'battery metals': cobalt, graphite, lithium, manganese, nickel and vanadium**

**Table 2. Western Australia's resource and production estimates and global ranking for six important 'battery metals'**

Commodity	Resources (kt) <sup>(a)</sup>	% of global resources <sup>(b)</sup>	Global resource ranking <sup>(b)</sup>	Production 2016 (kt) <sup>(b)</sup>	% of global production <sup>(b)</sup>	Global production ranking <sup>(b)</sup>
Lithium (Li <sub>2</sub> O)	11 572.1	11.4	4	14.3 <sup>(c)</sup>	41	1
Graphite (TGC) <sup>(d)</sup>	1 931.0	negligible	—	0	0	—
Nickel (Ni)	34 945.8	26.9	1	206 <sup>(e)</sup>	9.1	4
Cobalt (Co)	1 319.5	14.3	2	5.1	4.2	5
Manganese (Mn)	88 687.1	6.4 <sup>(f)</sup>	4	0 <sup>(g)</sup>	0	—
Vanadium (V <sub>2</sub> O <sub>5</sub> )	23 867.8	9.5 <sup>(h)</sup>	4	0	0	—

**NOTES:** (a) Total contained metal or oxide resources as at 31 December 2017. Source: DMIRS MINEDEX database <www.dmp.wa.gov.au/minedex>  
 (b) Estimates are based on resource and production figures from the USGS Mineral Commodity Summaries for 2016, unless otherwise indicated: Lithium – Jaskula (2017); Nickel – Schnebele (2017); Cobalt – Shedd (2017); Manganese – Corathers (2017); Vanadium – Polyak (2017)  
 (c) Western Australia accounted for all Australian lithium production in 2016 (Britt et al., 2016)  
 (d) TGC – Total graphitic carbon  
 (e) Nickel production and global percentage estimates are for Australia, but in 2016 Western Australia accounted for all of these  
 (f) Estimate is for 2015, determined using Western Australia resources from DMIRS MINEDEX database <www.dmp.wa.gov.au/minedex>, total Australia resources from Britt et al. (2016) and global estimates from Corathers (2016)  
 (g) Western Australia's only operating Mn mine at Woodie Woodie went into care and maintenance in January 2016, and recommenced mining in late 2017  
 (h) Australian V<sub>2</sub>O<sub>5</sub> resources are predominantly in Western Australia, but the estimate by Polyak (2017) is likely to be significantly understated

**a) Total contained Li<sub>2</sub>O****b) Total graphitic carbon****c) Contained Ni****d) Total contained Co****e) Total contained Mn****f) Total contained V<sub>2</sub>O<sub>5</sub>**

Legend: Inferred resources (yellow), Indicated resources (grey), Measured resources (orange)

**Figure 4. Cumulative total Western Australian resources by year for: a) lithium; b) total graphitic carbon; c) nickel; d) cobalt; e) manganese; f) vanadium (source: <www.dmp.wa.gov.au/minedex>)**

Talison Lithium Pty Ltd will soon double spodumene production at Greenbushes (to ~800 ktpa), and several other projects are rapidly advancing towards mining at Pilgangoora (Pilbara Minerals; Altura Mining), Bald Hill (Tawana Resources NL/Alliance Mineral Assets Ltd), and Earl Grey (Kidman Resources Ltd/Sociedad Quimica y Minera de Chile SA).

**Graphite** is a significant component of many battery types (typically for the anode), but the raw material must be of high purity and appropriate grain size. Western Australia's more than 100 graphite occurrences are overwhelmingly in Archean to Mesoproterozoic graphitic schists or gneisses (metamorphosed carbonaceous sedimentary rocks), although sporadic hydrothermal vein- and pegmatite-hosted deposits are known (e.g. Ajana – Anson Resources Ltd; and near Katanning). Defined graphite resources of ~2 Mt (Fig. 4b; Table 2) are contained in four of Western Australia's 13 'active' graphite projects, all in graphitic schists and gneisses, but the state is not yet a graphite producer. The two most advanced projects are McIntosh, in the east Kimberley (Hexagon Resources Ltd), and Yalbra, in the Gascoyne (Buxton Resources Ltd/Montezuma Mining Ltd). The state's graphite resources are negligible on the global scale, but can potentially yield high-purity, coarse (large and jumbo flake) graphite suitable for production of spherical graphite, and graphene, the new wonder material!

**Nickel** is found predominantly in sulfides in ultramafic (komatiitic) volcanic and mafic intrusive rocks, and in oxides in supergene-enriched laterites developed over originally sulfidic host rocks (Dill, 2010). Western Australia is well endowed with all these mineral deposit types, and has the world's largest nickel resources (~27% of the total, or ~35 Mt contained Ni in 87 deposits; Fig. 4c; Table 2). The state is currently Australia's only nickel producer, supplied from just eight mines while nickel prices are depressed (currently about US\$13 000 per tonne, well down from about US\$20 000/tonne in 2014; <[www.kitcometals.com/charts/nickel\\_historical\\_large.html](http://www.kitcometals.com/charts/nickel_historical_large.html)>, accessed 17 January 2018). Mining yielded ~206 kt of Ni in 2016, or 9.1% of the global total, ranking Western Australia fourth in the world (after Canada, the Philippines and Russia). Twenty-five other mines remain under care and maintenance, but many of these could reopen if nickel prices increase sufficiently.

**Cobalt** is a critical component in many battery designs, and perceptions of susceptibility to supply restriction have driven prices upwards — 47% in 2016, and a further ~57% in 2017 (to about US\$51 000/t in March 2017). Cobalt principally occurs as a trace element associated with copper in mafic or ultramafic magmatic Ni–Cu deposits and stratabound, sediment-hosted Cu deposits (Dill, 2010). Known Co resources in Western Australia rank second globally after the Democratic Republic of the Congo (DRC), totalling ~1.32 Mt in Ni–Cu sulfide and Ni laterite ores in 37 mafic and ultramafic magmatic deposits (Fig. 4d; Table 2). All cobalt production to date from Western Australian operations has been as a byproduct in Ni sulfide and laterite ores (5140 t in 2016; <[www.dmp.wa.gov.au/minedex](http://www.dmp.wa.gov.au/minedex)>), representing 4.1% of global production (fourth globally after China, Canada and the Democratic Republic of the Congo). Cobalt grades rarely approach economic in their own right unless subsequently enriched by supergene processes. Despite this, interest has recently turned to defining standalone resources in Western Australia, although prospective deposits are mostly at prefeasibility stage.

**Manganese** deposits may originally be magmatic hydrothermal (volcanic exhalative, epithermal, skarn), structurally controlled hydrothermal, or marine sedimentary exhalative or clastic (including black shale-hosted, carbonate-hosted, and deep-marine nodules). All of these might also show subsequent (commonly economically necessary) supergene enrichment (Dill, 2010). Western Australia's significant known Mn deposits are conventionally considered to be supergene-enriched exhalative or clastic sedimentary deposits in marine shales, carbonates, and iron formations, although Jones (2011) suggested that supergene-enriched carbonate-hosted deposits in the Woodie Woodie camp may instead have a structurally controlled hydrothermal primary origin. Western Australia's Mn inventory is largely in the Pilbara–Capricorn region, and exceeds 88 Mt (Fig. 4e), the bulk contained in just 14 of the 39 defined resources. This represents ~6.4% of the global inventory, and is the fourth largest after Brazil, South Africa and the Ukraine (Table 2). Western Australia has been producing Mn for more than 50 years, almost exclusively for metallurgical use in the steel industry (its principal application), although the only presently active mine is at Woodie Woodie (Consolidated Minerals Pty Ltd), which recently reopened as Mn economics have improved. Global demand for Mn has doubled over the past decade (to ~20 Mt in 2017), driven in part by increasing demand for high-purity electrolytic Mn-dioxide for use in several high-capacity lithium-ion battery types used in grid storage, electric vehicles and medical devices. Some Western Australia-based companies are therefore evaluating their projects specifically as sources of electrolytic Mn-dioxide (e.g. Yanneri Ridge, Montezuma Mining Ltd).

**Vanadium** resources in Western Australia are currently ~24 Mt V<sub>2</sub>O<sub>5</sub>, the fourth highest globally (after China, Russia and South Africa), at ~9.5% of the total (Fig. 4f; Table 2). They occur predominantly in vanadiferous titanomagnetite in orthomagmatic mafic–ultramafic intrusions (e.g. Windimurra, Speewah, Barrambie). The Speewah deposit (King River Copper Ltd) in the east Kimberley region is Australia's largest titanomagnetite deposit, containing more than half of Western Australia's known resources, but total V<sub>2</sub>O<sub>5</sub> production in this state since 2000 is just 14 100 t, and the only developed vanadium deposit — at Windimurra (Atlantic Ltd) — remains under care and maintenance. Vanadium resources in Western Australia are also known in lateritic regolith over pyroxenite (Medcalf, Audalia Resources Ltd), and associated with sandstone- and calcrete-hosted uranium (Yeelirrie, Cameco Australia Pty Ltd). Other possible vanadium resources include heavy mineral placers and hydrothermal base metal vein deposits, though none is yet known or defined in Western Australia.

**Many other metals** are also used in particular battery designs, such as aluminium, antimony, arsenic, barium, cadmium, calcium, copper, iron, lead, phosphorus, some rare earth elements, selenium, sodium, sulfur, tin, titanium and zinc. Western Australia has defined resources for many of these metals, and is already a significant supplier of several from particular deposit types (e.g. Al, Cu, Fe, Na, Pb, REE, S, Ti, Zn). Several of these also occur in deposits that cannot yet be developed economically (e.g. Ti in titanomagnetite in layered mafic intrusions; high-purity Al in kaolin clays), as do several of the less abundant battery metals (e.g. P in sedimentary phosphates; Sn in pegmatites), though some of these are already being



exported as beneficial or deleterious byproducts in other ores (e.g. Se in Cu ores and coal; Cd in Zn ores).

## Local processing of Western Australian battery metals?

All ‘battery metals’ presently exported from Western Australia are in raw mineral concentrates, for secondary processing and value-adding by third parties in foreign plants. However, many current and potential battery metal miners are working to develop in-house or co-invested processing of their product to maximize returns to shareholders.

Tianqi Lithium Australia PL (51% owner of Talison Lithium Pty Ltd and the Greenbushes mine) is constructing a lithium hydroxide processing plant (LHPP) at Kwinana, south of Perth, to process its share of spodumene concentrate from the Greenbushes mine (announced 5 November 2016). The LHPP will reputedly be the largest of its kind and produce the highest quality lithium hydroxide in the world. In November 2017, Greenbushes partner Albermarle Ltd proposed to build its own Li-hydroxide plant at Kemerton. BHP announced in August 2017 that it would build the world’s largest Ni-sulfate plant at Kwinana, to produce 100 000 tonnes of electrolytic nickel per year, and Northern Minerals will soon commission a pilot hydrometallurgical plant (at the mine site) to produce mixed rare earth carbonates from its Browns Range ores.

Lithium-focused companies such as Lepidico Ltd, Lithium Australia Ltd and NeoMetals Ltd are developing several novel, proprietary hydrometallurgical processes that promise to allow production of Li-carbonate, Li-hydroxide and Li-titanate from a wider variety of ‘hardrock’ Li-bearing silicate minerals. This will potentially make many other pegmatitic lithium deposits economically viable (the L-max, SiLeach and ‘LiOH acid-leach’ processes, respectively). Other companies are attempting to develop and commercialize alternative, more cost-effective hydrometallurgical and/or electrochemical processes to extract Co and Ni from lateritic deposits (e.g. atmospheric pressure HCl leaching – Ardea Resources Ltd), V, Ti and Fe from titanomagnetite ores (e.g. NEOMET process – NeoMetals Ltd), and high-purity alumina from kaolin (Altech Chemicals Ltd). Montezuma Mining has commissioned CSIRO to develop a process to produce electrolytic Mn-dioxide from the Butcherbird (Yanneri Ridge) Mn deposits. Given appropriate economics, some of these novel processing plants might be established in Western Australia, though it seems likely that many will be located interstate or offshore.

## Western Australia — future battery powerhouse

Battery research and development are dynamic fields that have produced an enormous and continually expanding variety of chemistries and architectures that directly influence global demand for a considerable proportion of the periodic table. Such work also continually improves existing battery performances, potentially allowing previously less-competitive designs to challenge the pre-eminence of other battery types

(e.g. Black, 2017, following Wei et al., 2017). Global environmental concerns and national interest priorities — such as the European Union’s METGROW+ initiative <<http://metgrowplus.eu/>> — are also influencing raw material resource economics by driving the development of technologies to profitably extract all potentially valuable or otherwise ‘critical’ elements from low-grade mineralization, metallurgical waste (slags, slimes, etc.), and discarded manufactured items (‘e-waste’).

Western Australia’s high-ranking status as a resource investment destination (Jackson and Green, 2017) and expansive resource inventory will probably ensure this State’s position as a supplier of raw materials to the battery manufacturing industry into the future, regardless of technological and economic developments. With appropriate market conditions, government policies and infrastructure development, the State could also reap significant extra economic benefits from further expansion of the domestic downstream battery material processing and manufacturing sector.

## References

- Battery University 2017, BU-205: Types of lithium battery; <[http://batteryuniversity.com/index.php/learn/article/types\\_of\\_lithium\\_ion](http://batteryuniversity.com/index.php/learn/article/types_of_lithium_ion)>, accessed 18 January 2018.
- Black, H 2017, Battery breakthrough – in zinc: Premium Mining News, 21 August 2017; <[www.miningnews.net/insight/feature-stories/battery-breakthrough-in-zinc](http://www.miningnews.net/insight/feature-stories/battery-breakthrough-in-zinc)>, accessed 18 January 2018.
- Britt, A, Summerfield, D, Senior, A, Roberts, D, Kay, P, Hitchman, A, Champion, D, Huston, D, Simpson, R, Smith, M, Sexton, M and Schofield, A 2016, Australia’s Identified Mineral Resources 2016: Geoscience Australia, Canberra, 16p., doi:10.11636/1327-1466.2016.
- Corathers, LA 2016, Manganese *in* USGS Mineral Commodity Summaries, January 2016, p. 106–107, doi:10.3133/70194932.
- Corathers, LA 2017, Manganese *in* USGS Mineral Commodity Summaries, January 2017, p. 106–107, doi:10.3133/70194932.
- Dill, HG 2010, The ‘chessboard’ classification scheme of mineral deposits: Mineralogy and geology from aluminum to zirconium: *Earth Science Reviews*, v. 100, p. 1–420.
- Jackson, T and Green, KP 2017, Fraser Institute Annual Survey of Mining Companies 2016: Fraser Institute, 70p., <[www.fraserinstitute.org](http://www.fraserinstitute.org)>.
- Jaskula, BWJ 2017, Lithium *in* USGS Mineral Commodity Summaries, p. 100–101, doi:10.3133/70194932.
- Jones, S 2011, Proterozoic deformation in the east Pilbara Craton and tectonic setting of fault-hosted manganese at the Woodie Woodie mine: *Australian Journal of Earth Sciences*, v. 58, p. 639–673.
- Polyak, DE 2017, Vanadium *in* USGS Mineral Commodity Summaries, January 2017, p. 182–183, doi:10.3133/70194932.
- Schnebele, EK 2017, Nickel *in* USGS Mineral Commodity Summaries, January 2017, p. 114–115, doi:10.3133/70194932.
- Shedd, KB 2017, Cobalt *in* USGS Mineral Commodity Summaries, January 2017, p. 52–53, doi:10.3133/70194932.
- Wei, L, Karahan, HE, Zhai, S, Liu, H, Chen, X, Zhou, Z, Lei, Y, Liu, Z and Chen, Y 2017, Amorphous bimetallic oxide–graphene hybrids as bifunctional oxygen electrocatalysts for rechargeable Zn-air batteries: *Advanced Materials*, v. 29, no. 38, 10p., doi:10.1002/adma.201701410.
- Wiaux, JP and Chanson, C 2013, The lithium-ion battery service life parameters: Presentation to the UN Informal Working Group on Electric Vehicles and the Environment, Session 6, Geneva, 3 June 2013, <[www2.unece.org/wiki/download/attachments/8126481/EVE-06-05-Rev1e.pdf](http://www2.unece.org/wiki/download/attachments/8126481/EVE-06-05-Rev1e.pdf)>, accessed 21 January 2018.



# Provenance fingerprinting of gold from the Kurnalpi Goldfield

by

EA Hancock and TJ Beardsmore

## Introduction

Many alluvial gold nuggets are believed to be liberated fragments of primary hypogene mineralization (e.g. Liversidge, 1893; Petrovskaya, 1973; Hough et al., 2007; Butt and Timms, 2011). Their morphology, internal crystal structure, chemistry, and accessory inclusions provide important information on mineralizing fluid composition, physical and chemical depositional conditions, proximity to primary source, primary mineral deposit type, and post-mineralization modification, and therefore prospectivity for undiscovered bedrock gold deposits (e.g. Chapman et al., 2002; Nikolaeva et al., 2004; Hancock et al., 2009; Nikiforova et al., 2013; Hancock and Thorne, 2016).

The Geological Survey of Western Australia (GSWA) has undertaken a pilot study of provenance, metallogenesis and prospectivity for placer gold in the Kurnalpi Goldfield, approximately 85 km east-northeast of Kalgoorlie (Fig. 1). The study uses a suite of alluvial gold nuggets generously provided by mineral exploration company KalNorth Gold Mines Limited, and sourced from 36 widely distributed sites over an area of ~80 km<sup>2</sup> (Fig. 1). These nuggets were originally collected by local prospectors from thin gravels at the base of Quaternary channels buried 1–2 m beneath surficial loams; however, gold nuggets have also been discovered in Cenozoic laterite and calcrete deposits, and pre- or early Cenozoic deep leads in buried paleochannels (Schupp, 1985).

Known bedrock-hosted gold mineralization occurs at the Scottish Lass and Brilliant sub-economic prospects (Fig. 1). Gold occurs mainly as microscopic grains in moderately dipping quartz veins with associated silica–pyrite ± carbonate ± hematite alteration in metabasalt and north-northwesterly striking, magnetite-bearing, granophyric quartz dolerite dykes that cut ultramafic rocks (Gunther, 2004). The mineralization style at Scottish Lass and Brilliant appears to be similar to other quartz-vein stockwork deposits in the Eastern Goldfields (e.g. Darlot–Centenary; Beardsmore and Gardner, 2003), but does not seem a likely source for the coarse, nuggetty placer gold at Kurnalpi.

GSWA therefore sought to determine the nature and origin of the bedrock source for the gold nugget samples from the Kurnalpi Goldfield, using techniques that included visual morphometry, acid etching, reflectance microscopy, scanning electron microscopy with energy dispersive X-ray analysis (SEM-EDX), and laser ablation inductively coupled plasma mass spectrometry (LA-ICP-MS).

## Gold nugget characteristics

Seventy-five representative gold nuggets, from a total of 274 specimens provided, were selected for detailed analysis. Degree of roundness was used as the main criterion to distinguish proximity of gold nuggets to a potential primary bedrock source. About 30% of nuggets have irregular, angular shapes and are intergrown with vein quartz (Fig. 2a), hence they appear to have been collected from very close to their primary sources. These gold nuggets were used as a baseline reference for the mineralogical characteristics of primary bedrock gold, from which these nuggets were shed. They show:

- irregularly angular, spongy, or crystalline morphologies
- intergrowth with milky and brown quartz
- monocrystalline and polycrystalline internal microstructure, with local recrystallization and twin planes; indistinct zoning
- rounded, 10–100 µm micro-inclusions comprising assemblages of galena and gold/silver or lead tellurides, and an arsenopyrite–pyrite assemblage in one grain from the Six Mile site
- silver contents ranging from 5 to 11 wt%, and 3 wt% Ag in a grain with arsenopyrite–pyrite inclusions
- Cu contents from 30 to 300 ppm, and Hg contents from 10 to 100 ppm; traces of Sb and Pb.

The localities from which these ‘proximal’ nuggets were obtained are mostly clustered in the central eastern part of the goldfield (Camp Gully, Minters Gully, Discovery Hill, Hakes Patch, and Sparkle), but some come from the vicinity of Six Mile, in the northwest (Fig. 1).

The remaining gold specimens in the sample suite were sourced from across the goldfield (including domains of ‘proximal’ nuggets), although they preserve mineralogical characteristics similar to those of the ‘proximal’ reference specimens, such as:

- relict primary compositional microstructure
- rounded 10–200 µm inclusions of galena, chalcopyrite, and Au/Ag, Pb, and Bi tellurides
- 5–9 wt% Ag; consistent 20–600 ppm Cu and more variable 1–4000 ppm Hg

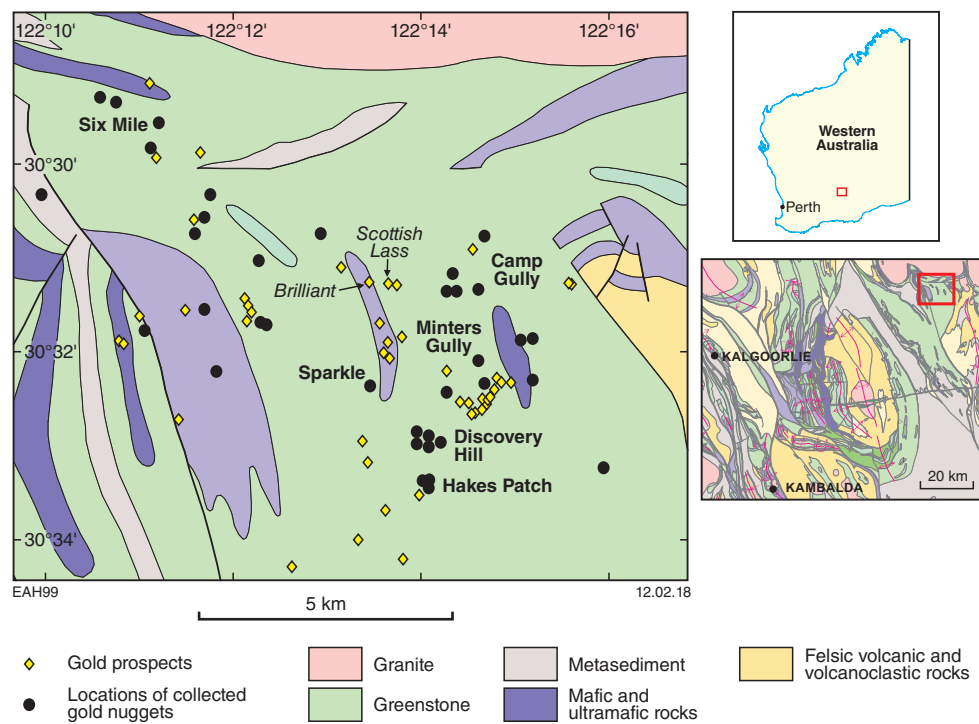


**Figure 1.** Geological setting of the Kurnalpi Goldfield (red frame in overview map) and locations of collected gold nuggets. Site names in *italics* are localities of known bedrock-hosted gold mineralization; bedrock geology from GSWA (2016)

- sporadic and universally low Sb, Te, Bi, Pb, Al, Fe, and Mg.

They also show secondary mechanical and chemical transformations indicating greater transportation from their primary source, and/or burial and in situ alteration in paleochannels for some time subsequent to erosion from the primary source. Features indicating these processes include:

- subrounded to well-rounded shapes with smooth surfaces (Fig. 2b)
- continuous to discontinuous, 5–100  $\mu\text{m}$  thick marginal rims characterized by variable silver depletion and/or incipient to complete recrystallization (due to chemical leaching and mechanical deformation; Fig. 3a)
- absence of quartz; partial leaching of primary inclusions
- local recrystallization around incorporated regolith inclusions
- Fe- and Ca-rich clay inclusions and coatings; rounded maghemite, ilmenite, and hematite inclusions
- commonly well-developed veinlets along intergranular crystal boundaries, now partly filled with mixtures of clay, silica, and fine secondary gold (Fig. 3b).

The intergranular veinlets are of particular significance as they appear to have formed by a selective dissolution–

(re)precipitation process similar to that for the supergene corrosive rims, although formation of the veinlets may have begun in the hypogene environment in response to deformation and hydrothermal fluid interaction. Acidic groundwater in the regolith environment further leached Ag from grain rims and intergranular crystal boundaries; because the latter were more protected from abrasion during placer transport, their full thicknesses were preserved, although eventual ‘cracking’ along them created channel ways that then filled with regolith minerals.

The combination of secondary features suggests placer gold grains from the Kurnalpi region are locally derived, and experienced only short periods of deformation and supergene weathering during transport from the basement to final residence in the regolith, but a more prolonged period of in situ supergene alteration.

## Implications for gold metallogenesis and prospectivity

Placer gold nuggets from the Kurnalpi Goldfield all have a hypogene origin, and appear to have been transported at most only a short distance within the goldfield from their primary bedrock source(s). Their original microstructure is largely preserved, with no evidence for subsequent regional hydrothermal or metamorphic alteration, and only relatively minor overprinting by physical and chemical alteration related to short periods of surface transportation followed by longer periods of residence in the regolith.



**Figure 2.** Morphology of gold nuggets: a) angular irregular with pitted and spongy surface, intergrowth with milky quartz; sample GSWA 201951; b) well-rounded and folded with even and smoothed pitted surface, inclusions of ferruginous clay mixture; sample GSWA 201946

The primary hypogene source for the studied alluvial gold nuggets appears to have been of the greenstone-hosted 'orogenic' quartz-vein style, possibly with two subtypes reflected by the gold–arsenopyrite–pyrite and gold–galena  $\pm$  chalcopyrite  $\pm$  Pb–Ag–Bi–telluride associations, which might indicate deeper and shallower crustal depths of formation, respectively. At the very least, these associations suggest several different, discrete sources for the nuggets. This style is distinctly different to mineralization at the Scottish Lass and Brilliant deposits, although mineralization styles at those deposits and in the placer nuggets are broadly compatible in terms of depth of formation in the crust. This suggests the Kurnalpi Goldfield remains prospective for the discovery of both these styles of orogenic gold deposits. Furthermore, placer gold nuggets are closest to their primary bedrock source in the central eastern and northwestern parts of the goldfield, indicating that these regions deserve particular scrutiny.

## References

- Beardsmore, TJ and Gardner, Y 2003, Darlot gold deposit, Yandal gold province, Yilgarn Craton, Western Australia: CSIRO Explores 1: Yandal Gold Province, *in* Geoscience and Exploration Success edited by KS Ely and GN Phillips, CSIRO Exploration and Mining, Melbourne, p. 173–219.
- Butt, CRM and Timms, NE 2011, The Liversidge nugget collection: a new look at some old gold: Australian Journal of Earth Sciences, v. 58, p. 777–791.
- Chapman, RJ, Leake, RC and Styles, MT 2002, Microchemical characterization of alluvial gold grains as an exploration tool: Gold Bulletin, v. 35, no. 2, p. 53–65.
- Geological Survey of Western Australia (GSWA) 2016, 1:500 000 State interpreted bedrock geology of Western Australia, 2016: Geological Survey of Western Australia, digital data layer, <www.dmp.wa.gov.au/geoview>.
- Gunter, L 2004, Kurnalpi Joint Venture, Annual Report for the period 12 January 2003 to 31 December 2003; Newcrest Mining Limited: Australian Securities Exchange, February 2004, 12p.



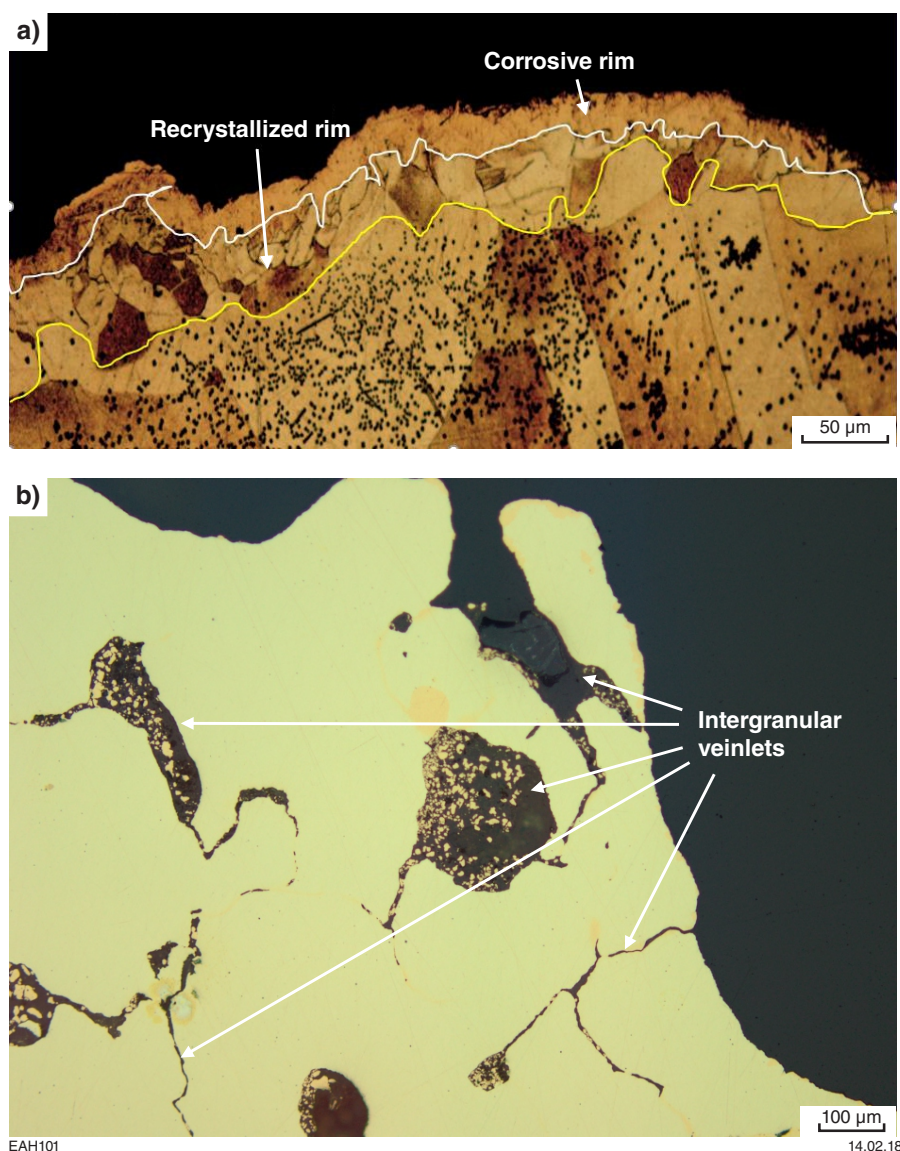


**Figure 3.** Reflected light photomicrographs of cut and polished gold nuggets showing their microstructure: a) compacted, thin, corrosive rim of pure gold overgrowing larger recrystallized marginal rim; several bent twin planes in grain's interior; silver chloride crystals (black dots) after aqua regia etching; sample GSWA 201933; b) well-developed, large, intergranular veinlets filled with mixture of clay, silica, and fine secondary gold; sample GSWA 201931

- Hancock, EA, Thorne, AM, Morris, PA, Watling, RJ and Cutten, HNC 2009, Mineralogy and trace element chemistry of lode and alluvial gold from the western Capricorn Orogen: Geological Survey of Western Australia, Record 2009/6, 30p.
- Hancock, EA and Thorne, AM 2016, Mineralogy of gold from the Paulsens and Mount Olympus deposits, northern Capricorn Orogen, Western Australia: Geological Survey of Western Australia, Record 2016/14, 16p.
- Hough, RM, Butt, CRM, Reddy, SM and Verrall, M 2007, Gold nuggets: supergene or hypogene?: Australian Journal of Earth Sciences, v. 54, p. 959–964.
- Liversidge, A 1893, On the origin of gold nuggets: Journal and Proceedings of the Royal Society of New South Wales, v. 27, p. 303–343.
- Nikiforova, ZS, Gerasimov, BB, Glushkova, EG and Kazhenkina, AG 2013, Gold resource potential of the eastern Siberian Platform: placers and their feeding sources: Geology of Ore Deposits, v. 55, no. 4, p. 265–277.
- Nikolaeva, LA, Gavrillov, AM, Nekrasova, AN, Yablokova, SV and Shatilova, LV 2004, Native gold in lode and placer deposits of Russia, in Atlas: TsNIGRI, Moscow, Russia, 176p.
- Petrovskaya, NV 1973, Native Gold: Nauka, Moscow (in Russian), 347p.
- Schupp, J 1985, Kurnalpi Project – Preliminary geological report: Metana Minerals NL: Geological Survey of Western Australia, Statutory mineral exploration report, A15630, 12p.



# Diamond prospectivity of Western Australia: a major synthesis and review

by

MT Hutchison and DJ Flint

Away from areas of thick cover, Western Australia hosts 696 000 km<sup>2</sup> of exclusively Archean rocks and 439 000 km<sup>2</sup> of Paleoproterozoic rocks. Pre-1.6 Ga rocks comprise about 45% of the onshore area of the State, constituting the West Australian Craton (WAC; incorporating the Yilgarn and Pilbara Cratons) and the western part of the North Australian Craton (NAC). Seismic tomography demonstrates that considerable remaining portions of the State are also underlain by thick mantle lithosphere (Kennett et al., 2013), hosting the conditions under which diamonds form. Most of the State is therefore prospective for diamonds and numerous diamondiferous lamproite and kimberlite fields are known. Emplacement of diamond-bearing rocks in Western Australia spans much of geological time, from the c. 1868 Ma Brockman Creek kimberlite in the Pilbara (White, 2000) to the c. 17 Ma Walgidee Hills lamproite, Noonkanbah field, West Kimberley (Phillips et al., 2012).

Australia produced approximately 11% of global rough diamond production by weight in 2015 (Kimberley Process Certification Scheme statistics), ranking it fourth in the world. All diamonds were derived from two mines, both in Western Australia. However, Western Australia's size, terrain, infrastructure, and climate mean that many areas still remain underexplored for diamonds. With the closure in 2015 of the Ellendale mine, which was responsible for a large proportion of the world's fancy yellow production, only one currently producing mine remains in Australia (at the AK1 olivine lamproite at Argyle, NAC). Hence a compelling case can be made for encouraging future diamond exploration in Western Australia. To that end, a thorough compilation of historical diamond exploration has been made (GSWA, 2018). The resulting data have subsequently been assessed in order to understand the effectiveness of prior exploration, draw attention to favourable, yet underexplored areas, and generate regional models of diamond prospectivity (Hutchison, 2018a).

## Methodology

Continuous diamond exploration since the 1970s has resulted in numerous public and previously private datasets and 4200 statutory company reports citing diamond as a commodity of interest. These data have been used to construct the Diamond Exploration Database (DED; GSWA, 2018), which follows the structure described in Hutchison (2018b) and is based on similar

structure previously applied to the Northern Territory (Hutchison, 2011). The focus has been on the primary method of exploration — that is, physical sampling. The DED incorporates the locations of over 88 000 diamond exploration samples, the overwhelming majority (~90%) having been tested for diamonds or other minerals indicating diamond potential. Associated with these samples are over 30 000 good-quality chemical analyses of mineral-separate grains. Furthermore, locations of 524 discrete in situ bodies with in-principal diamond potential (kimberlites, lamproites, ultramafic lamprophyres and carbonatites) have been compiled, of which 114 are confirmed to be diamondiferous. As a companion to the in situ occurrences, 127 determinations of emplacement age from 63 bodies have also been compiled with detailed geochronological information.

A two-fold approach to assessing diamond prospectivity has been followed. Mineral chemistry data are detailed in their coverage to the extent that statements can be made regarding the composition and thickness of the mantle lithosphere both regionally and underlying various specific locations with diamond potential. These data have been applied to four broad areas comprising the NAC, WAC, and off-craton in eastern and western parts of the State. Independently, mineral sampling data, including visual identification of diamond-prospective grains, have been detailed enough to allow prospectivity to be assessed with the State subdivided into 67 onshore tectonic units. The extent and results of sampling, in conjunction with the age of surface rocks relative to ages of diamond-prospective rocks, and of the underlying mantle structure, have been analysed to produce a prospectivity map. The methodology follows that of Hutchison (2012, 2013) for the Northern Territory (NT) and the resulting map presents a thirteen-level ranking of attractiveness for future diamond exploration.

## Mineral sampling and mineral chemistry

Indicator distributions and sampling methodologies show that programs recovering >0.3 or 0.4 mm grains from high-energy trap sites are most successful. Diamond was present in 3.5% of the indicator mineral samples, and yellow and pink diamonds responsible for much of the revenue from Western Australia's diamond mines were also recovered from exploration samples. Diamond morphology is dominated by primary octahedral forms,

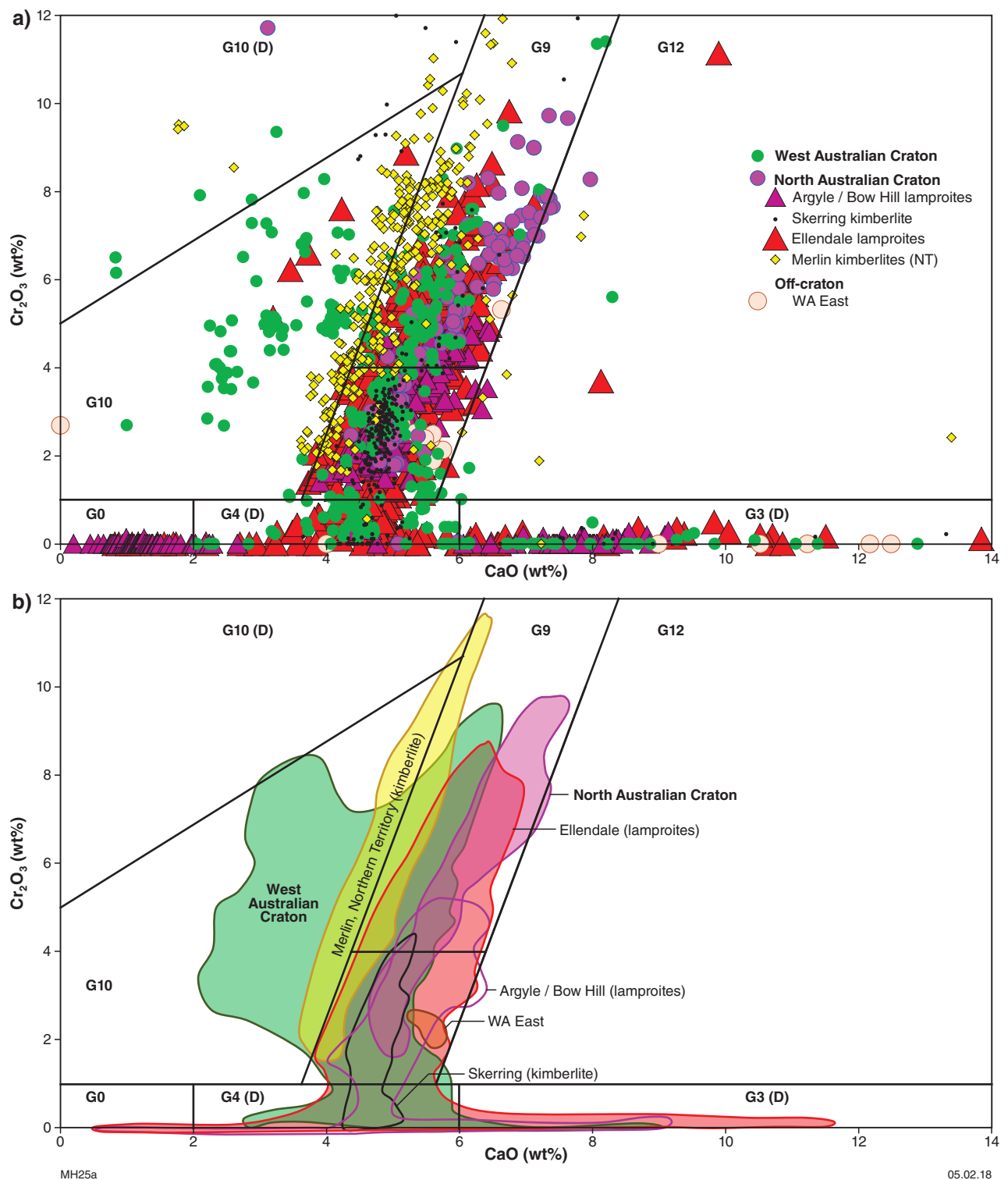


**Figure 1.** Chemical composition of pyrope–almandine–grossular garnets in terms of  $\text{CaO}$  and  $\text{Cr}_2\text{O}_3$ : a) point data from all Western Australian and Northern Territory samples, with Argyle, Bow Hill and Skerring data from Ramsay (1992) and Merlin (Northern Territory) data from Reddcliffe (1999). Argyle, Bow Hill and Ellendale all contain abundant G0 composition garnets not considered to be mantle derived according to standard criteria (Grütter et al., 2004); b) simplified diagram showing representative compositional fields encompassing about 90% of analyses from each location: Argyle, Bow Hill, Ellendale and Skerring garnets – Ramsay (1992); Merlin garnets (Northern Territory) – Reddcliffe (1999). The Iherzolite trends are increasingly Ca-depleted from the North Australian Craton of Western Australia (including Ellendale, Argyle and Bow River), through the West Australian Craton to the Merlin field (Northern Territory) samples. However, the West Australian Craton samples also show a much higher proportion of G10 (Grütter et al., 2004) garnets with an intermediate Ca-Iherzolite trend

but subsequent etching and resorption is also common. Recovered diamonds suggest that diamonds are more likely to have formed under Western Australia compared to the Northern Territory. However, in some places they are also more likely to have been damaged before reaching the surface.

Non-diamond indicators were identified by visual inspection in 28% of samples. The majority are spinels, capable of surviving Western Australia's harsh weathering environment. The Yilgarn and Pilbara Cratons and western parts of Western Australia (WA West) are particularly dominated by Al-free chromites, whereas (Mg,Fe,Ti)-bearing Al-chromites are abundant in the NAC and eastern areas of Western Australia (WA East). Increasing dominance of Al in chromites is interpreted as a sign of a shallower source than for mantle-derived Al-depleted Mg-chromites. Clinopyroxene indicators also largely show a mantle-derived garnet peridotite affinity. Kimberley Basin samples are more consistently eclogitic than other parts of the NAC. However, clinopyroxenes not classed as Cr-diopsides are associated with diamondiferous rocks in Western Australia, particularly at Argyle. For garnets, based on Grütter et al.'s (2004) methodology, the progression of garnet chemistry through G9 compositional space and into the G10 field from the NAC to the WAC (Fig. 1) suggests an incrementally increasing source depth for each of these areas. Garnet compositions, in a similar fashion to clinopyroxenes, show that despite diamond production being associated with the NAC, the WAC is particularly distinguished for its deep-mantle sourced indicators. Among ilmenites, 93% with indicator chemistry fall within the kimberlite field of Wyatt et al. (2004; Fig. 2). Samples from the Eastern Goldfields Superterrane are most kimberlitic. As with clinopyroxenes, Argyle-hosted ilmenites (Ramsay, 1992) would not be classed as indicators following the Wyatt et al. (2004) scheme, thus supporting a re-assessment of mineral chemistry exploration methodologies.

Further to regional observations, indicator mineral recovery, diamonds with un-attributed sources, and mineral chemistry anomalies also occasionally point to areas of local interest. Examples include the Hamersley Basin, the central Kimberley Basin, and the Big Spring area east of Ellendale, which has been the site of recent new lamproite discoveries.

## Regional prospectivity ranking

Figure 3 shows the results of prospectivity ranking based on the 67 geological subdivisions of the State (Martin et al., 2016). Indicator mineral occurrences and in situ bodies with diamond potential largely occupy the north (NAC) and west (WAC) of the State. These areas correspond to thick mantle lithosphere (Kennett et al., 2013) establishing the conditions for diamond growth. Clusters in Figure 3 particularly correlate with areas of significant changes in mantle thickness reflecting structures favourable for diamond emplacement. Understanding deeply penetrating crustal and mantle structures using methods such as SEEBASE (Frogtech Geoscience, 2017) can be very useful for prioritizing exploration strategies.

The NAC, location of Western Australia's diamond mines, scores well in prospectivity ranking. However, partly because of under sampling combined with good indicator recovery, results point to parts of the WAC being more prospective. This corroborates the mineral chemistry study. The Hamersley Basin scores highest in prospectivity ranking. Equal second are the Eastern Goldfields Superterrane and Goodin Inlier, both located in the Yilgarn Craton. Regions ranked third are the WAC's Ashburton Basin, Biranup Zone, Bryah and Fortescue Basins, and Pilbara Craton; the Narryer Terrane, Marymia Inlier and the Youanmi Terrane of the Yilgarn Craton; and the Lamboo Province of the NAC. Areas with lowest scores, such as the Eucla Basin, lie farthest from craton margins and contain the youngest rocks.

## Conclusions

Despite prolific diamond exploration, Western Australia is considerably underexplored and diminishing known reserves warrant a re-evaluation of diamond potential. Indicator mineral chemistries reflect mantle sources with respectable diamond tenor, consistent with diamond and visually determined indicator recovery, known diamondiferous source rocks, and mining in parts of the State. However, analysis of exploration data also draws attention to underexplored areas, particularly in the WAC. There are significant opportunities for diamond-affinity rocks being present near surface even within the large, underexplored sedimentary basins overlying thick mantle lithosphere evident through much of the State. Recent discoveries and the results of prospectivity analysis make a compelling case for renewed diamond exploration in Western Australia.

## References

- Frogtech Geoscience, 2017, 2017 Canning Basin SEEBASE study and GIS data package: Geological Survey of Western Australia, Report 182, 297p.
- Geological Survey of Western Australia (GSWA) 2018, Diamond exploration and prospectivity of Western Australia: Geological Survey of Western Australia, digital data package.
- Grütter, HS, Gurney, JJ, Menzies, AH and Winter, F 2004, An updated classification scheme for mantle-derived garnet, for use by diamond explorers: *Lithos* v. 77, p. 841–857.
- Hutchison, MT 2011, Northern Territory Diamond Exploration Database: Northern Territory Geological Survey Digital Information Package DIP-011, DVD-ROM with Explanatory Notes (vers. December 2011).
- Hutchison, MT 2012, Diamond exploration and prospectivity of the Northern Territory: Northern Territory Geological Survey, Record 2012-001, 64p., vi and one map plate.
- Hutchison, MT 2013, Diamond Exploration and Regional Prospectivity of the Northern Territory of Australia, in *Proceedings of the 10th International Kimberlite Conference, Volume 2* edited by DG Pearson, Special Issue of the *Journal of the Geological Society of India*, p. 257–280.
- Hutchison, MT 2018a, Diamond exploration and prospectivity of Western Australia: Geological Survey of Western Australia, Report 179, 70p.
- Hutchison, MT 2018b, Data methodologies applied in the Western Australian diamond exploration package: Geological Survey of Western Australia, Record 2017/16, 24p.

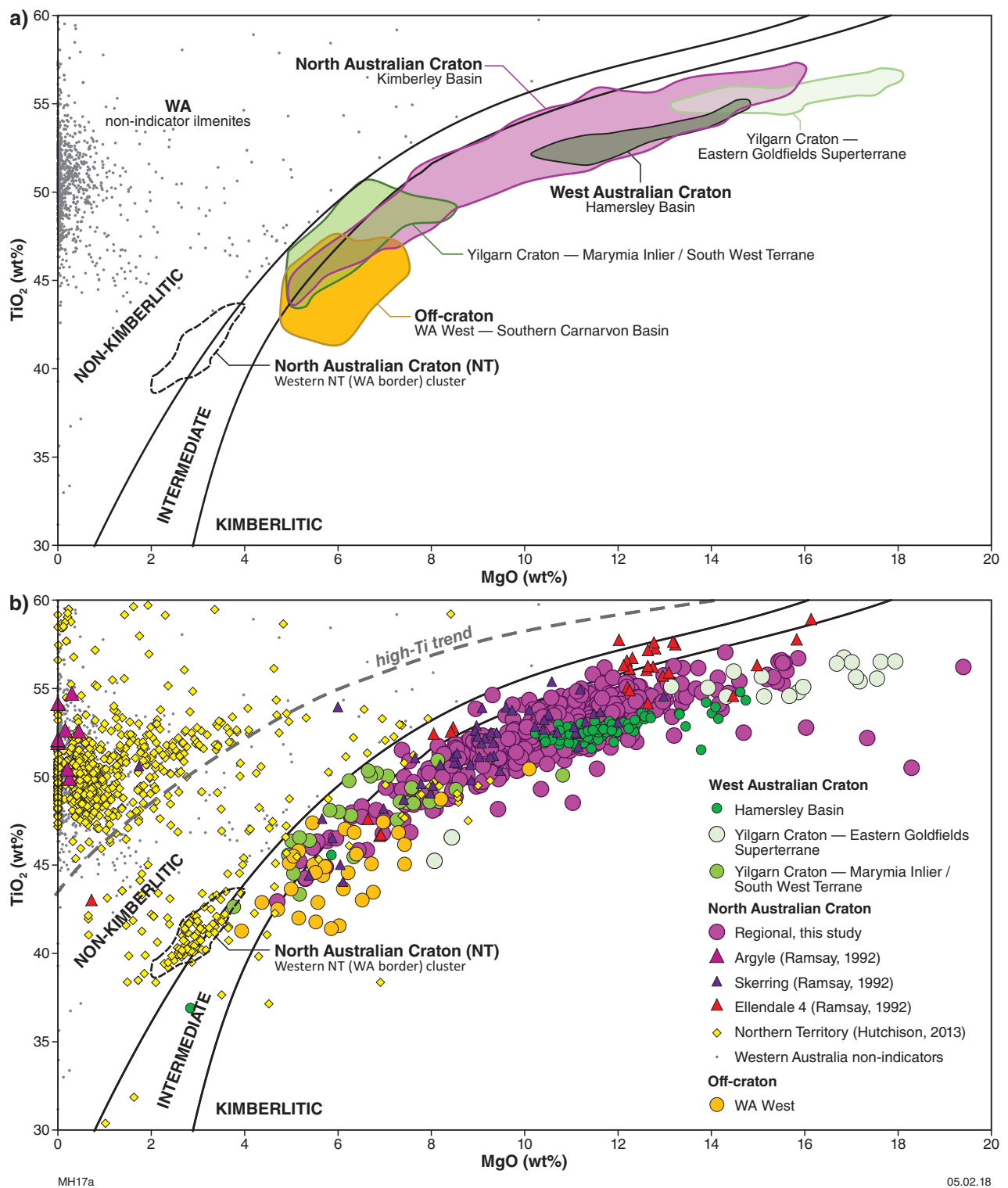
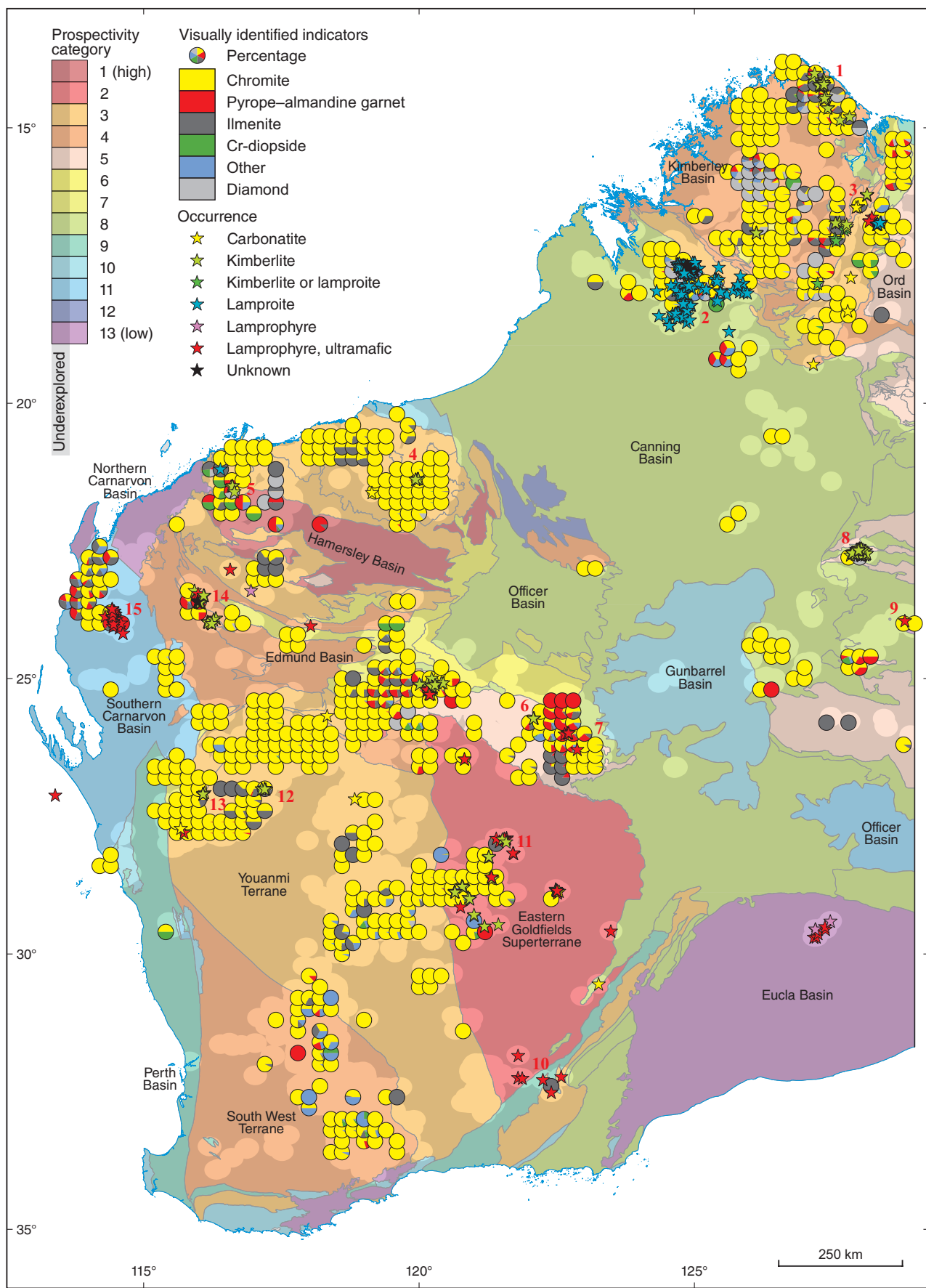


**Figure 2.** Chemical composition of ilmenites plotted as  $\text{TiO}_2$  vs  $\text{MgO}$ : a) indicator-composition ilmenites are identified by fields encompassing 90% of data excluding outliers. Non-indicator composition ilmenites (Wyatt et al., 2004) are shown by grey dots. Among the Northern Territory ilmenites, a cluster of Northern Territory – Western Australia-border ilmenite compositions are labelled; b) all data points from the DED (GSWA, 2018) for Western Australia indicator ilmenites in the context of Northern Territory compositions (Hutchison, 2013) and locality-specific compositions from the NAC (Ramsay, 1992). Different regions show distinct compositional trends whereby kimberlite-derived samples (Skerring kimberlite pipe; Ramsay, 1992) generally fall more firmly within the kimberlite compositional field than lamproite samples (Ellendale 4 and Argyle; Ramsay, 1992). Lamproite-hosted Argyle ilmenites would not be classed as having indicator mineral compositions at all. Eastern Yilgarn samples are more kimberlitic than samples from the western WAC, just as western NAC samples are more kimberlitic than those in the Northern Territory (Hutchison, 2013)





MH5a

06.02.18

**Figure 3. (opposite) Prospectivity map of Western Australia. Geological subdivisions are ranked for prospectivity (after Hutchison, 2018a) in the context of mantle structure, the age of surface rocks, the extent of sample coverage and recovery of visually determined indicators. A rank of 1 is the most prospective area and 13 is the least prospective. In situ bodies with diamond potential (tested or otherwise) are shown by stars colour coded according to the key. Notable localities numbered in red on the map are: 1 – Ashmore, 2 – Ellendale field, 3 – Argyle, 4 – Brockman Creek, 5 – Blacktop, 6 – Jewill, 7 – Bulljah Pool, 8 – Webb, 9 – JYP58, 10 – Norseman, 11 – Akbar, 12 – Cue, 13 – Mileura, 14 – Barlee, 15 – Wandagee. Sample site areas are indicated by shading such that unshaded areas lie within 20 km from an exploration sample location. Locations of recovered indicator minerals are shown within blocks of 0.2 degrees of longitude and latitude**

- Kennett, BLN, Fichtner, A, Fishwick, S and Yoshizawa, K 2013, Australian Seismological Reference Model (AuSREM): mantle component: *Geophysical Journal International* v. 192, p. 871–887.
- Martin, DMcB, Hocking, RM, Riganti, A and Tyler, IM 2016, 1:10 000 000 tectonic units of Western Australia, 2016: Geological Survey of Western Australia, digital data layer, <www.dmp.wa.gov.au/geoview>.
- Phillips, D, Clarke, W and Jaques, AL 2012, New  $^{40}\text{Ar}/^{39}\text{Ar}$  ages for the West Kimberley lamproites and implications for Australian plate geodynamics, *in* Extended Abstracts of the 10th International Kimberlite Conference: 10IKC, Bangalore, India, p. 104.
- Ramsay, RR 1992, Geochemistry of diamond indicator minerals: Department of Geology and Geophysics, The University of Western Australia, Perth, PhD thesis, 135p. and v. 2 of tables, figures and appendices (unpublished).
- Reddicliffe, TH 1999, Merlin Kimberlite Field, Batten Province, Northern Territory: Department of Geology and Geophysics, The University of Western Australia, Perth, MSc thesis (unpublished), 221p. and 3 appendices.
- White, B 2000, The geochronology and thermochronology of the Brockman Creek 01, Melita 01 and Melita 02 kimberlites, Western Australia: The University of Melbourne, Victoria, BSc (Hons) Research Report (unpublished).
- Wyatt, BA, Baumgartner, M, Anckar, E and Grütter, H 2004, Compositional classification of 'kimberlitic' and 'nonkimberlitic' ilmenite: *Lithos*, v. 77, p. 819–840.



This Record is published in digital format (PDF) and is available as a free download from the DMIRS website at <[www.dmp.wa.gov.au/GSWApublications](http://www.dmp.wa.gov.au/GSWApublications)>.

Further details of geological products produced by the Geological Survey of Western Australia can be obtained by contacting:

Information Centre  
Department of Mines, Industry Regulation and Safety  
100 Plain Street  
EAST PERTH WESTERN AUSTRALIA 6004  
Phone: (08) 9222 3459 Fax: (08) 9222 3444  
[www.dmp.wa.gov.au/GSWApublications](http://www.dmp.wa.gov.au/GSWApublications)

